Università
Ca'Foscari
Venezia

Master's Degree

in

Science and
Technologies of Bio
and Nanomaterials

Final Thesis

A Microwave Spectroscopic investigation of 2-Propene-1-Imine for Astrochemical purposes

Supervisor
Dr. Andrea Pietropolli Charmet

Assistant supervisor
Dr. Luca Bizzocchi

Graduand
Davide Alberton
837485

Academic Year
2018 / 2019

"I know that I know nothing"

Socrate

CA' FOSCARI VENEZIA

Abstract

Science and Technologies of Bio and Nanomaterials
Department of Molecular Sciences and Nanosystems

Master Degree

A Microwave Spectroscopic investigation of 2-Propene-1-Imine for Astrochemical purposes

by Davide ALBERTON

In the attempt of studying the processes that lead to the building blocks of life, in this work the microwave spectroscopic survey conducted on 2-Propene-1-Imine will be presented. This molecule, a possible intermediate in the synthesis of amino acids, would be an important tracer of the aforementioned reaction. In this regard, rotational spectroscopic measurements have been carried out in a range of frequencies ranging from 85GHz to 500GHz, in order to obtain the conformational constants of the two conformers, TA and TS, that come to form precursor pyrolysis, a process made necessary by the instability of the investigated compound. Additionally, what has been collected offers the spectroscopical fingerprints of these two conformational isomers, possibly contributing to the astrochemical evolutional search of more complex compounds from which life, as we know it, may have on Earth originated from...

Acknowledgements

Many are those people who directly or indirectly have contributed with their help or support to the completion of this work and have accompanied me along this path of study. First of all I must deeply thank Dr. Andrea Pietropolli Charmet who beyond normal institutional obligations has always been available to help me in clearing up my frequent doubts and patiently correcting my mistakes. Without his support and help I wouldn't even have had the opportunity to go to Munich, where the material on which this work was written was collected. Therefore, many thanks.
In the same way I have to thank all of those who at Max Planck für extraterrestrische Physik, in addition to the institute itself and its Director Prof. Paola Caselli, welcomed me and guided me step by step in the laboratory, dispensing advices and helping me even morally when I found myself living situations that I would have preferred to avoid. Among these I have to thank Dr. Luca Bizzocchi, who helped me by providing support and additional material as well as having constantly assisted me with Dr. Pietropolli Charmet in the drafting of the thesis itself; Domenico Prudenzano, PhD student that I pestered with abundant questions and with whom I shared the workstation and countless laughs; Elena Redaelli, another PhD student with whom with Domenico we shared climbing and barbecues in the free time and who introduced me to her partner Matteo, an exquisite person. To these must be added Jake and Valerio who helped me with the software and Michela, who kindly lend me her own books to cheat the time of hospitalization. I also want to thank my German roommates Ester and Isabel for always offering to help me when it was not possible for me to be independent and who completely welcomed me into their home last summer, sharing laughs, thoughts and beautiful moments. A heartfelt thanks to all.
I must then thank those who have become the friends who accompanied me on this university path. Among all Alberto, the main responsible for the choice of Bio and Nanomaterials Master Degree, without which I would not be where I am now; Nicola, a great reckless companion of adventures; Aurelio, trusted and loyal companion; Valeria, genuine person. To these are added all those with whom I have had the opportunity to spend wonderful years for which I thank infinitely.
I thank all the students and friends of the San Giuseppe of Cassola Study Room with whom I shared opening and closing evenings, talks and break moments; in addition to have given to me the opportunity to have a silent place where study, with their initiative they have allowed the same also to all those who otherwise would have not have had a place in which go for the exams preparation.
I have to thank Federica, who kindly corrected parts of my uncertain English.
I thank all those who have been my employers and colleagues known at Abercrombie&Fitch, at Glam&Co, at Symposio restaurant and at Biancoia chalet. Everyone allowed me to earn what it took to get here and taught me things I wouldn't have learned if I hadn't gone through such a path.
I thank Jesus (who is not the Jesus you are thinking about) who is waiting for me to load the thesis to have a beer together, spending another evening talking about science, hopes and experiences.
I thank Elias for his sincere friendship and irony, for considering me his equal and for having been able to listen to me when in difficulty I could only turn to him.
I thank my brother Luca, with whom I had and I have the privilege of sharing experiences that have inevitably led us to see the definition of brotherhood fading into that of friendship and with which I am probably linked above all others.
But most at all, I want and I must thank those who in all these years have been the

safe haven that always welcomed me when in storms, regardless of the time I was back in, the ailments I was doing and the nonsense I was saying have always welcomed me with a smile, instilled me confidence and given me hope. Those who have endured my shortcomings and with love, without ever imposing themselves, despite the difficulties of these years, have always put their person aside to give me the opportunity to define myself as an individual, my parents. To them the greatest thanks.
Finally, I thank and apologize to all those who have not been mentioned above but who have been with me in recent years, both inside and outside the university.
Thank you all.

Molte sono le persone che direttamente o indirettamente con il loro aiuto o sostegno hanno contribuito alla riuscita di questo lavoro e mi hanno accompagnato lungo questo percorso di studi. In primis devo profondamente ringraziare il Dott. Andrea Pietropolli Charmet che si è sempre reso disponibile oltre i normali obblighi istituzionali per aiutarmi a risolvere i miei frequenti dubbi e pazientemente correggere i miei errori. Senza il suo appoggio ed aiuto non avrei nemmeno avuto l'opportunità andare a Monaco di Baviera dov'è stato raccolto il materiale su cui è stato scritto questo lavoro. Un sentito grazie.
Allo stesso modo devo ringraziare coloro che la Max Planck für extraterrestrische Physik, oltre all'istituto stesso e alla sua Direttrice Prof.ssa Paola Caselli, mi hanno accolto e mi hanno guidato passo passo nel laboratorio dispensando consigli e aiutandomi anche moralmente quando mi sono ritrovato a vivere situazioni che avrei volentieri preferito evitare. Tra questi il Dott. Luca Bizzocchi, che mi ha aiutato fornendomi materiale di supporto e aiuto oltre ad aver costantemente assistitomi insieme al Dott. Pietropolli Charmet nella stesura stessa della tesi; il Dott. Domenico Prudenzano, aspirante dottorando con cui ho condiviso la postazione di lavoro e innumerevoli risate, assillandolo di domande; la Dott.ssa Elena Redaelli, altra aspirante dottoranda dell'istituto con cui assieme a Domenico abbiamo nel tempo libero condiviso arrampicate e barbecue, e che mi ha introdotto il suo compagno Matteo, persona squisita. A questi devono essere aggiunti Jake e Valerio che mi hanno aiutato con la parte del software e Michela, che mi ha prestato i suoi stessi libri per ingannare il tempo della degenza. Voglio anche ringraziare le mie coinquiline tedesche Ester e Isabel per essersi sempre offerte di aiutarmi quando non mi era possibile essere indipendente e per avermi accolto a braccia aperte nella loro casa la scorsa estate, condividendo risate, pensieri e momenti meravigliosi. A tutti un sentito grazie.
Devo poi ringraziare coloro che sono diventati gli amici che mi hanno accompagnato in questo percorso universitario. Fra tutti Alberto, vero responsabile della scelta di Bio e Nanomateriali, senza il quale non sarei dove sono ora; Nicola, grandioso scapestrato compagno di avventure; Aurelio, fidato e leale compagno; Valeria, persona genuina. A questi vanno a sommarsi tutti coloro con cui ho avuto modo di trascorrere anni meravigliosi e che per questo ringrazio infinitamente.
Ringrazio tutti i ragazzi ed amici dell'Aula Studio San Giuseppe di Cassola con cui ho condiviso aperture e chiusure serali, chiaccherate e momenti di break; oltre ad avermi dato la possibilità di avere uno spazio silenzioso dove poter studiare hanno

permesso altrettanto anche a tutti coloro che nel comprensorio non avrebbero altrimenti avuto un luogo nel quale ritirarsi per preparare gli esami.
Devo ringraziare Federica, che si è gentilmente prestata a correggere alcuni passaggi nel mio incerto inglese.
Ringrazio tutti quelli che sono stati i miei datori di lavoro e colleghi conosciuti ad Abercrombie&Fitch, al Glam&Co, al ristorante Symposio e al rifugio Biancoia. Ognuno mi ha permesso di guadagnarmi quello che mi è servito per arrivare qui e mi ha insegnato cose che non avrei appreso se non avessi fatto un percorso del genere.
Ringrazio Jesus (che non è il Gesù a cui starete pensando) che sta aspettando che carichi la tesi per andare a bere una birra in compagnia, per passare un'altra serata a parlare di scienza, speranze ed esperienze.
Ringrazio Elias per la sua sincera amicizia ed ironia, per considerarmi suo pari e per aver saputo ascoltare quando in difficoltà non avrei potuto che rivolgermi che a lui.
Ringrazio mio fratello Luca, con cui avuto ed ho il privilegio di aver condiviso esperienze che ci hanno portato inevitabilmente a veder sfumare la definizione di fratellanza in quella di amicizia e con cui probabilmente sopra ogni altro sono legato.
Ma più di tutti voglio e devo ringraziare coloro che in tutti questi anni sono stati il porto sicuro che sempre mi ha accolto quando in burrasca, senza badare all'orario nel quale rientravo, ai malanni che facevo e alle sciocchezze che dicevo mi hanno sempre accolto con il sorriso, infuso fiducia e dato speranza. Coloro che hanno sopportato le mie mancanze e con amore, senza mai imporsi, malgrado le difficoltà di questi anni hanno sempre messo in disparte la loro persona per darmi la possibilità di definirmi come singolo, i miei genitori. A loro il grazie più grande.
Ringrazio e mi scuso infine con tutti coloro che non sono stati sopra menzionati ma che mi sono stati accanto in questi anni, fuori e dentro l'università.
Grazie a tutti voi.

List of Abbreviations

KBOs	**K**uiper **B**elt **O**bjects
IDPs	**I**nterplanetary **D**ust **P**article
IOM	**I**nsoluble **O**rganic **M**atter
SOM	**S**soluble **O**rganic **M**atter
FUV	**F**ar **U**ltra **V**iolet radiation
COMs	**C**omplex **O**rganic **M**olecules
OMC	**O**rion **M**olecular **C**loud
VLA	**V**ery **L**arge **A**rray
PDRs	**P**hoton **D**ominated **R**egions
ALMA	**A**tacama **L**arge **M**illimeter/Submillimeter **A**rray
OMC	**O**rion **M**olecular **C**loud
MHD	**M**agneto **H**ydro **H**ynamics
PdBI	**P**lateau **B**ure **I**nterferometer
IRAM	**I**stitut de **RA**dioastronomie **M**illimétrique
VUV	**V**acuum **U**ltra **V**iolet
LMC	**L**arge **M**agellanic **C**loud
HITRAN	**HI**gh **TRAN**smission
CALPAM	**CAL**ifornia **P**rogr**AM** or **CAL**culation **P**rogr**AM**
CASAC	**C**enter for **A**strochemical **S**tudies **A**bsorption **C**ell
HFS	**H**yper **F**ine **S**tructure

Contents

List of Figures

List of Tables

Physical Constants

Speed of Light	$c_0 = 2.997\,924\,58 \times 10^8\,\mathrm{m\,s^{-1}}$ (exact)
Astronomical Unit	$au = 14.959\,787\,07 \times 10^{10}\,\mathrm{m}$
Parsec	$pc = 3.0857 \times 10^{16}\,\mathrm{m}$
Light-year	$ly = 9.4607 \times 10^{15}\,\mathrm{m}$

List of Symbols

a	distance	m
P	power	W (J · s)
ω	angular frequency	rad · s^{-1}

To my parents.

Chapter 1

Introduction

1.1 The dance

The world we are living in is as marvellous as the things that make it up. Its complexity and vastity has always fascinated humankind and are of such beauty that in the effort of understanding it we feel overwhelmed. The deeper we dig, the more we discover, and in the discovery of what things are made of, the same role of the man is inevitably questioned. Starting from our primordial ancestors we passed from looking at Nature as something of be scared of, to something, in the process of revealing its inaccessible mysteries, that gave us the freedom of choice. We have gone from being at the mercy of hostile environments, perishing due to lack of food and illness, to being the advocates of our own destiny.

But this process has not been as fast as we could imagine. Thousands of years and hundreds of generations passed in order to allow us to learn how to hone the tools, and once the ones that allowed us to face with imminent needs had been sufficiently sharpened, we started to shift the emphasis from the practical to the abstract. Heated, refreshed and appeased the man started to feed his mind, applying its potential in ludic activity.

An amazing example, one among the first, is constituted by the "Caves of Lascaux". Discovered by accident the 12th of September 1940 by the 18-year-old Marcel Ravidat, these caves retain a multitude of exquisite workmanship paintings depicting animals of the ice-age fauna. [1]. 6000 representation dated ~17000 years back succeed one another, leaving the visitor in a state of wonder. Animals, human figures and abstract signs are present with a number of details that in the first two cases resemble the concept of the living counterpart in an impressive way. Try to explain what these paintings represent is as risky [2] as out of topic, but undoubtely is that even a long time ago the mind of the *Homo sapiens* was fascinated by Nature to such an extent that made him want to try and imitate it, and he was not the first. Findings in the "Cueva de los Aviones", southeast Spain, are attributed to the *Homo neanderthalensis* and testify that this fascination is even older. [3].

Along the time this encoding process has constituted the most powerful way to develop more and more knowledge. It allowed us to be succeed in the systematic husbandry of plants and animals, and with this our nomadism ceased and labour division started. Accounting and writing were developed, and human civilization flourished in all its diversities, various from place to place. The same *Homo sapiens*, who has been dragged out of the caves, passed through the Antiquity. After this the Middle Ages followed, and with this the rise of Christianity, Islamic Golden Age and the Italian Renaissance, the invention of the modern printing and the Scientific Revolution, ending up being catapulted in the Early Modern Period. In the latter he was able to see first-hand, being in fact its patron, the Age of Enlightenment and the

Age of Discovery, through of the Industrial Revolution and beyond, leading up to the time in which we are right now, the Late Modern Period. [4].

Every reached step has been necessary to prepare the jump to the next one, and if we exclude some small differences, it has been made by the same genetic heritage. Approximately the same sequence of bases, anchored in its conformation by a skeleton of deoxyribose (a sugar) and a phosphate group, has been the architect of all this enrichment. Everything that made possible all the history of the humankind is enclosed in a script that, if pulled, is as long as an 1.8 m tall man, in this case its final product. The latter is nothing more than a code that try to decode, to analyse, to assimilate and reformulate, generalizing to make predictions for purposes and for having fun in the process of satisfying its intrinsic curiosity.

But how we arrived from the DNA to the human being is not straightforward. Restrained in the space of a cellar nucleus this long string, rolled up forming a double helix structure wrapped into supercoiled conformation, has to be rolled out, read by conglomerates of deputies proteins and RNAs filaments that forming complex machineries activated and attenuated by different strategies transcribe the sequence into an RNA filament. This one, properly shortened and processed in the way out of the nucleus, is translated inside the ribosomes into a sequence of amino acids that again, processed, fold up in quaternary structure in the effort of minimizing their energy in the physiological environment of the cytoplasm. To the last structure we have given the name of protein. This will be selectively developed and produced by the cell depending on where the latter is located in the organism and will give to the cell its specific functions. Specialized cells constitute a tissue, a functional agglomeration of metabolically active machines that are able to perform limited high skilled tasks. Different tissues combined forma an organ, a little "factory" that employing its dedicated employed tissues is able to face with more complex duties. The set of organs, different both in function and structure, that jointly work for a common purpose are said organ system. The overall of the latter form what we call a human being.

Anyway, even if this hierarchy is valid for the newest products of Nature, vertebrates, is not valid for all the organisms. What all the biologic entities share for sure are only DNA and proteins, even if to be precise the first is not the only way to store information. Some viruses, for example, stock their genetic information in RNA strands. At any rate, along the time, exerting pressure on the populations thermodynamics produced abnormalities in the genetic code, be them DNA or RNA. Their expression, namely their phenotype, decreed their success in dependence of the environment, a theory proposed to the world on 24th November 1859 by Charles Darwin. [5] Along the time other pieces have been added, as for example the sexual selection, but the principle that the environment shapes the direction of evolution still remain unchanged.

If we now imagine zooming in the double α helix we would see that it is formed by atoms. Even if we have seen them the first time only recently [6], their idea goes back a long time ago. The first one that made the effort to postulate their existence, even unless supported by evidence, was Leucippus from Miletus (mid-5th century BCE), master of Democritus of Abdera. In contrast with Aristotle whom believed that matter was infinitely divisible, one century before he argued that the latter was inherently grainy and that everything was formed by an enormous amount of various things, precisely the atoms (from the Greek word *atom*, 'indivisible'). The dispute continued even after 1803, when John Dalton remarked that to explain that chemical compounds always combines in certain portions there should have been hypothesized single entities merging to form unites called molecules. The first aid

in support of their existence came in one of the four articles published in 1905 by Albert Einstein, namely the one about the Brownian motion. But still they were elusive object. Several years before, J. J. Thomson had demonstrated the existence of the electron, but only with the discovery of the nucleus made in 1911 by the British physicist Ernest Rutherford, the evidence of the reality of atom became concrete. Then, in 1932 a colleague of Rutherford's at Cambridge, James Chadwick, discovered that the nucleus contained another particle, called neutron, which had almost the same mass of the proton but with no electrical charge. [7]. It took more than two millennia to agree with Leucippus.

The one of the atom has been an amazing challenge that once resolved gave us the certainty of its existence and, with the black body that served as a prelude, putted in crisis what at that time was thought as insuperable, namely Classical Physics. In the struggle to overpass the impasse Quantum Mechanics has been developed, and with its new tools mankind is now able to study system from an unprecedent point of view that give us a deeper level of knowledge. It works for atoms and for molecules, but beautiful as it may be, it merely describes the variation in probability of a wave function over time, and nothing tells us where these atoms and molecules come from. They entirely make us, from our nails to our DNA; they dance in a swing in which the change of partners keeps alive the meaning of the dance itself: ourselves, and with it our thought, our being. Life. If we think at how this twirl is vorticose the risk of losing the balance is behind the corner. Nevertheless, is what it happens, every moment of our existence. But as in every dance, there has to be a start, and here questions come out. Are these partners, the molecules, whom are mainly made of Carbon, Oxygen, Hydrogen and Nitrogen, always being here in the way that allow the whirl of life to sustain itself? Or are them arrived in some extent already pre-packaged? Do they have been formed directly here, along the eons, from scratch, or do they have come in any conformation that have made the subsequent development easier? And moreover, is possible that is this tiny dot of earth the only witness of this miracle? We need answers but search them at the same level of the questions is insane. We need to have a better prospective, from a higher point of view. So, we rise our eyes to the sky.

1.2 The formation

Even if we saw that Aristotle was not right about the idea of the finiteness of matter, he was for the shape of our planet. In his book *On the Heavens* he proposed two argumentations in support of his thesis. In the first one, he recognized that the moon eclipse would not have been always strictly a round shape unless the figure projecting its own shadow had not been a sphere, while in the second he made use of Greek travellers' knowledge, according to which going up to the North induce a change of the heavenly vault the observer uses to orient himself. These astuteness are among those that let leak out this man's greatness, but in proceeding with intuition alone, in absence of objective evidence, the error is around the corner. In fact, Aristotle thought that the Earth was stationary, and was all the rest that moved circularly around it. His same idea has then been elaborated by Ptolemy in his cosmological model, 2^{nd} century AD, in which the planets were moving in fixed spheres to account for their complicated path, and beyond them were situated the so-called fixed stars. Although not entirely accepted, the model has been adopted for many centuries also from the Catholic church until, in 1514, the Polish priest Nicholas Copernicus changed the point putting the Sun in place of the Earth. Round about

a century had to pass after that the idea of the latter has been supported simultaneously by the Galileo's Jupiter observations and the proposal of Kepler, due to which the orbits were ellipses instead of circles. But yet, even if the motion of the planets were consequently easier to predict, the reason of such an orbit were obscure, until in 1678 in an incredible work Sir Isaac Newton postulated the law of the universal gravitation [8]. Ptolemy's model had been definitely supplanted by the Copernican one, but the problem of fixed stars remained, especially because with this new force they would have been collapsed in a specific point, and it was not.

In the absence of data, the debate would have continued to stagnate between metaphysics and theology, unless in 1929 Edwin Hubble observed that galaxies are rapidly moving away from us. Therefore, if they are moving away from one another, there must have been a moment in which the space was infinitely dense. [7] In his *A Brief History of Time* Stephen Hawking wrote:

> "One may say that time had had a beginning at the big bang, in the sense that earlier times simply would not be defined. [..] In an unchanging universe a beginning in time is something that has to be imposed by some being outside the universe; there is no physical necessity for a beginning. One can imagine that God created the universe at literally any time in the past. On the other hand, if the universe is expanding, there may be physical reasons why there had to be a beginning. One could still imagine that God created the universe at the instant of the big bang, or even afterwards in just such a way as to make it look as though there had been a big bang, but it would be meaningless to suppose that it was created before the big bang. An expanding universe does not preclude a creator, but it does place a limit on when he might have carried out his job!"

Nowadays astronomers describe the universe in terms of two theories: the general theory and quantum mechanics. These are as basic as partial, opposed in terms of the treated sizes, subtending the possibility that there is, conceivably, something that summarizes them both, but as a matter of fact at the moment their alliance is valid only inside their domain. Thanks to this union and the data coming from the observations we have been able to fathom what there is out there, in a small extent giving us an idea of how works and how huge the universe is.

To realize of what the distance scale is, just think that the Earth is at an average distance of 150 million kilometres from the Sun [9]. This gap defines an AU, one astronomical unit. The nearest star is Alpha Centauri, part of a triple star system, and is located at 4,24 light years from us, or ~63241 AU [10]. In comparison, the farthest star ever seen, Icarus, is 9 billion light years far from our planet, i.e. $5,69 \cdot 10^{14}$ AU [11]. If we now consider that our own galaxy, namely the Milky Way in figure 1.1, is reputed as a typical galaxy and contains hundreds of billions of stars [12], and from the latest estimate the universe is evaluated to be inhabited by at least one thousand billion galaxies [13], how many are the planets spread all around?

The research of planets located beyond our solar system, namely orbiting a star different of the Sun, is quite new. The firsts observations date back to 1992, year in which Aleksander Wolszczan and Dale Frail, while working at the Arecibo Observatory in Puerto Rico and the National Radio Astronomy Observatory in New Mexico, detected two planets orbiting a pulsar, a dead star emitting beams of electromagnetic radiation [14]. After only three years, in 1995, Mayor -University of Geneva- and his then-student Queloz announced the first discovery of a planet orbiting a Sun-like star [15]. They used a technique that detects the exoplanet through the minute gravitational variation it causes on the star around which it rotates and that till now has

been used to study some of the more 4,000 exoplanets known to exist [16]. The difference that occurred in just three years is remarkable principally due to the fact that stars and planets come in different sizes, but to host life as we know it the planet itself has to be at a range of distance from the star that allows liquid water to pool on the surface of it. A giant hot-burning star's habitable zone would be more far compared to the one of a cooler dwarf. In addition, being us in the search of something that is similar to what we know, our survey inevitably falls on rocky planets, mainly focusing on Earth-sized body. But what is as much as crucial is the time of a star.

FIGURE 1.1: Milky Way [12].

If we consider that at the moment our first evidence of life, and we are talking about multi-celled, macroscopic creatures able to left us fossil record, dates back between 3,800 – 3,700 million years ago [17], and that at the same time we think that the brightest stars burn out in a few million years, imagine that life could be near such environments would be plausibly excludable. On the other hand, with regard to dwarfs, there would be no such contraindication, being their lifespan quite longer. Conversely, the planet would orbit nearer to them. This makes once scientists thought that such vicinity would have caused to expose always the same half, cooking one side and freezing the other one. After modelling they realized that maybe with planet-girdling winds the temperature would have been uniform [18], but another issue emerge in considering that even the coolest ones, namely the Red Dwarfs, produce flares in strength comparable to our sun that last from a few seconds to a few minutes and that the largest can strip away a planet's atmosphere [19]. Therefore, lying close to this stars would be quite dangerous, fact that makes our bet on Sun-like stars safer. At the same time the samples we have been collecting come mainly from our solar system and in the meanwhile, conducting studies of Sun-like stars' system formation in our Galaxy, we have knew how our solar system originated and with it how the sophistication of its molecular counterpart developed. In figure 1.2 can be seen an image of the Tarantula Nebula captured with the Hubble telescope. Just a look is sufficient to make you recognise about its complexity, enhanced by its mixing of stars, gas and dusts, fruits of its past activity and admonishers of what could then occur. But how the stars contained are formed? What

processes lead to what can be in this image seen?

FIGURE 1.2: The Tarantula Nebula, 49 $\pm$ 3 k pc (160,000 light-years) away from us, part of the H II region in the Large Magellanic Cloud (LMC) [20].

The first step to deal with is constituted by the so-called *Pre-stellar core*. Once the Jeans mass[1] of a dense cloud[2] is exceeded, the concentration of matter in the centre of the nebula raises up in concert with the density, while the temperature drops down as much as to cause the freeze-out of atoms and molecules onto sub-micron dust grains' surface. Here the hydrogenation of atoms and the most abundant molecule after H_2 in cold molecular gas, CO, occur and H_2O, H_2CO, CH_3OH and other species are formed.

In the second one, the *Protostellar envelope*, there is a proceeding in the collapse that cause the conversion of the gravitational energy into radiation that triggers the star's warm up which, however, remains limited in the so-called envelope. The frozen molecules sublimate back reacting to form more complex molecules. In the same time a fraction of matter is ejected outward releasing molecular outflows that once encounter the frozen part of the envelope create shocks in which the grain mantles and refractory grains are partially sputtered and vaporized.

As the envelope is being consumed only a disk around the star remain, which take the name of *Protoplanetary disk*. In this phase other complex molecules are formed in the central zone, the hotter region, starting from the ones produced in the previous phase while in the colder areas the molecules generated in the protostellar phase freeze-out again onto the grain mantles.

[1]The Jeans mass is the limit mass beyond which the collapse of the cloud starts. It is directly proportional to the mass of the cloud and indirectly to its dimentions and temperature.

[2]Because of turbulence and magnetic fields, dense molecular clouds can maintain their stability for millions of years but eventually the equilibrium is gravitationally rippled, giving rise to the process that brings to the star formation.

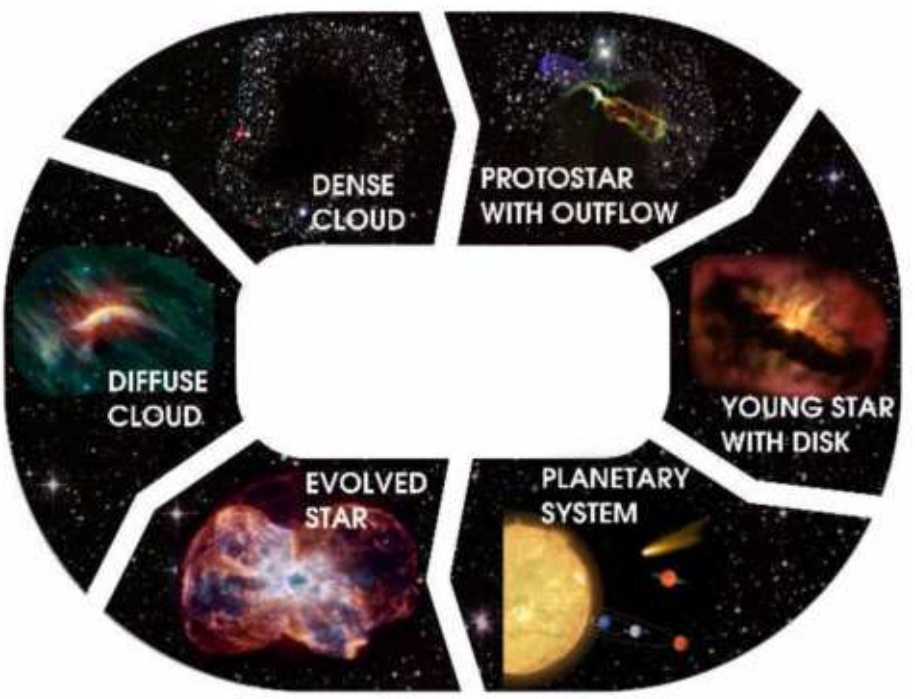

FIGURE 1.3: Stellar evolutionary phases [21].

What follows is said *Planetesimal formation* and is the moment in which the submicron dust grains coagulate into bigger rocks, called planetesimals, the seeds of the future planets, comets and asteroids. Some of the icy grain mantles are luckily preserved while the grains glue together. It's therefore quite probable that part of our chemical history stays there, stored. Kuiper Belt Object (KBOs), comets, meteorites, carbonaceous chondrites and interplanetary dust particles (IDPs) are at the moment thought to be the most ancient witness objects of our solar system.

The last phase is the *Planet formation*. Here rocky planets are formed and a huge amount of meteorites and comets fall on them. In the primitive Earth, that is accompanied by the new-born Moon, this cause the formation of the oceans as well as its second atmosphere. It must be thought that in theory the planetesimals that have built up our planet should not have contained water at all if they were come from the same place in which the Earth is located; on the contrary the quantity of H_2O present on our planet, as a whole, is estimated to be ~2 x 10^{-3} Earth masses [23], and this is nowadays explained by the most accredited theory which supports that these rich in water planetesimals come from outer regions [24] for two reasons: the rather similar HDO/H_2O ratio between Earth and carbonaceous chondrites [25] and the fact that due to numerical simulation up to 10% of the mass of our planet would have come from planetesimals, rather than from comets ([26];[24]). Contrariwise, regarding the atmosphere, both meteorites and comets are thought to have taken part in the atmosphere's formation process [27]. Meanwhile, simultaneously with the deposition of water onto the surface, the overall amount of what was embedded inside the sky's debris were brought, and with them the heritage embedded inside the planetesimals and rocks themselves [28]. But precisely, of what are we talking about?

Just think that since decades in comets has been found [29] [30]):

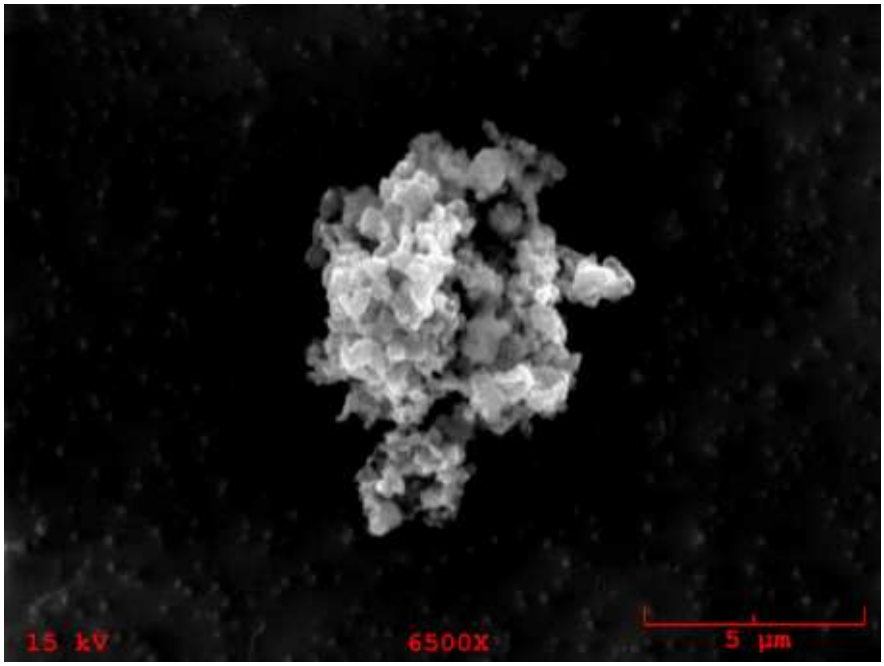

FIGURE 1.4: A semple of a cluster of dust grains, collected from the Earth's stratosphere [22].

- H_2O, CO, CO_2, CH_4, C_2H_2, C_2H_6, CH_3OH, H_2CO, NH_3, HCN, HNC, CH_3CN and H_2S in more than 10 comets;
- HCOOH, HNCO, HC_3N, OCS and S_2 in more than 1 comet;
- $HOCH_2CH_2OH$, $HCOOCH_3$, CH_3CHO, NH_2CHO, SO_2, H_2CS only in one comet, namely Hale-Bopp.

One must bear in mind that some species, i.e. HCN, has been produced once the primary species contained in the sublimated ice have been ejected; these are known as product species. At the same time there are others, i.e. H_2CO and CO, that have had contributions from both sides [28]. At last but not least, to use a euphemism that does not do it justice given its importance, we must add what has been discovered in the mission STARDUST in 81P/Wild2 comet [31]: glycine, the simplest amino acids.

For what concern KBOs, objects situated beyond Neptune and located between 30 and 50 AU, they are thought to still keep chemical information that dates back to the Solar Nebula. In the six biggest ones H_2O, CH_4, N_2 and CO [32] have been portrayed since a decade while C_2H_6 have been detected only in one of them [33]. Along the smaller ones, water, ammonia and methanol ices have been widely detected revealing how the most plentiful ingredients of KBOs and comets are shared.

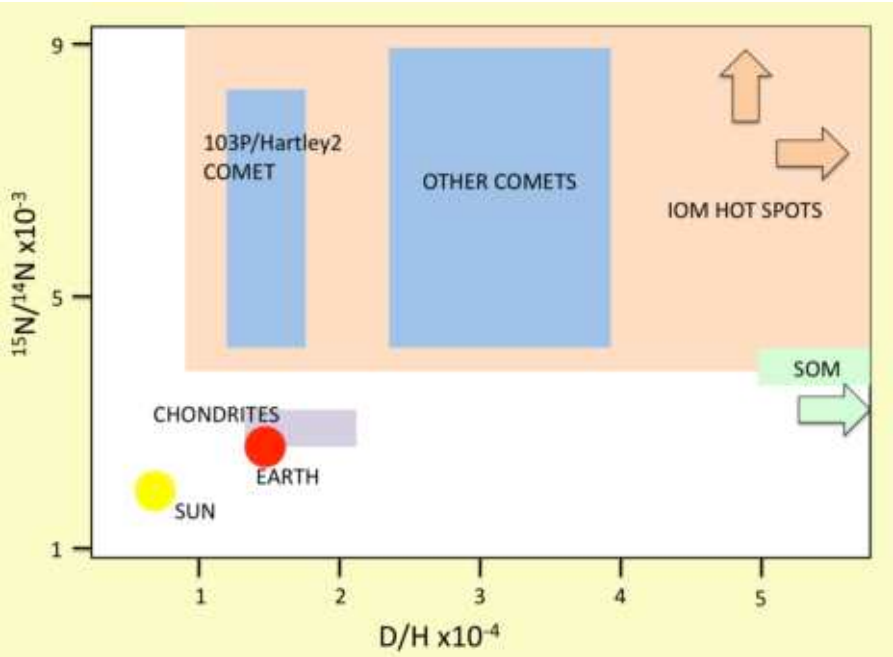

FIGURE 1.5: $^{15}N/^{14}N$ versus D/H in comets, chondrites, hot spots in the IOM of meteorites and IDPs, SOM in meteorites, Earth and Sun.[28].

Regarding meteorites, carbonaceous chondrites are instead composed of ~1-4% of carbon that based on their solubility is constituted by:

- IOM (insoluble organic matter): mainly formed by tiny aromatic units (up to six rings) linked by branched aliphatic linkages shorter than seven carbon atoms [28].
- SOM (soluble organic matter): chiefly made up of carboxylic acids, aliphatic and aromatic hydrocarbons and amino acids [34]. Interestingly amino acids with no terrestrial distribution have been found and in addition a subset of them has been observed in L-enantiomeric excess [35].

Another important element that allows us to understand what are the linkages that trace the time of our evolution back is given by the isotopic abnormalities. Specifically, it is thought that due to deuterium abnormalities in comets our ideas of their formation or is wrong [36] or alternatively the temperature of the Solar Nebula, due to local viscosities, was not monotonically increasing [37]. Additionally, they have also a wealth of ^{15}N, bulwark of a direct heritage of a pre-stellar core phase, a proto-planetary disk phase or a contamination of a near supernova explosion [28]. With regard to carbonaceous chondrites and IDPs what emerged is that they also have a D-enrichment as comets, but in some specific micrometre size regions (for the firsts) these are even higher where a ^{15}N enrichment is also present. Due to Remusat et al. [38] D abundance is associated with organic radicals and with SOM [39]. For comparison in figure 1.5 the relation between $^{15}N/^{14}N$ and D/H ratio are reported. Specifically, if an attempt is done in trying to correlate the origin of these isotopic species inequalities, one realizes that there are not [40] and if then we consider also the oxygen abnormalities combined with what are the short-lived nuclides, namely radionuclides with half-lives shorter than ~10^6 years, is deducible

that the Sun was likely born in a large cluster of stars where one or more massive stars exploded and that once born it irradiated the forming planetary system with a strong wind of energetic particles [28].

Hence, as our Solar system originated from a dense cloud core's collapse, others can follow the same destiny. The fact this happen or not is decreed by a limit value, ~10^5 H_2 molecules·cm^{-1}, that's the critical gas cooling density for gas-dust collision [41]. If the cloud that in this moment, being without a star is called "starless core", experiments a higher value the collapsing process can take place; otherwise two different processes can be delineated. In the first is possible they reach a state of hydrostatic equilibrium displaying an oscillating kinematic behaviour [42], whilst in the second one, being the object itself thermally subcritical, may disperse back into the interstellar medium.

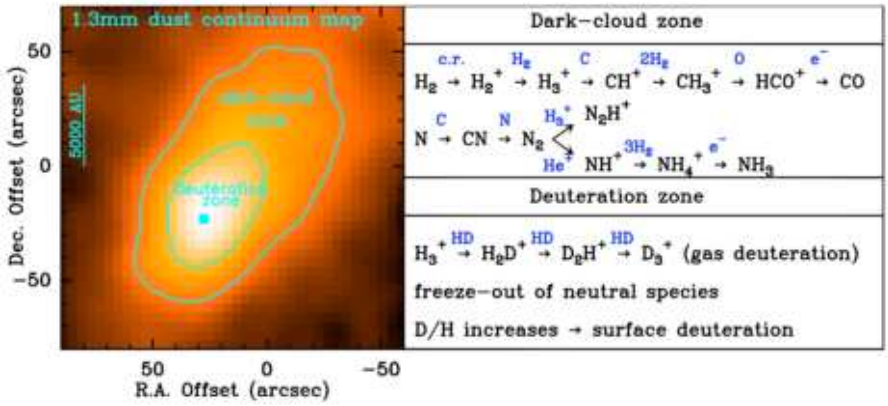

FIGURE 1.6: Pre-stellar core L1544 enclosed in the Taurus Molecular Cloud Complex ([28];[43]).

Focusing on the pre-stellar core, therefore on the one above the critical value, two regions of temperatures are identifiable. To see them the prototypical pre-stellar core captured by the IRAM-30 m antenna, L1544 in the Taurus Molecular Cloud Complex, is showed in figure 1.6 as example. Here two diverse zones are sketched out. In the outer one, that goes from 14000 to 7000 UA with gas density of ~10^{-3} melecules·cm^{-1} and temperature ~10 K, there are ion-molecule reactions [44] dominating the carbon chemistry and neutral-neutral reactions that begin the transformation of nitrogen into N_2 [28]. CO, NH_3 and N_2H^+ are also formed. In the inner one the density is above the critical value and the temperature is below 10 K due to the radiation shielding of the outer one. He, CO and N-bearing species as ammonia and N_2H^+ start to disappear from the gas-phase due to the accumulation process onto the surface of the grains. Measurements of the second showed a freeze-out of 80-90% while nitrogenated compounds experience a lower absorption due to an increment of their production rate in these circumstances [45]. It has to be thought that being these areas inaccessible to most of the radiation, except for cosmic-rays and FUV (far UV), the useful energy able to sufficiently excite a molecule in order to allow its desorption is minimum. As a matter of fact, consider the freeze-out and free-fall following formulas (n_H is the total density of hydrogen nuclei):

$$t_{freeze-out} \propto \frac{10^9}{n_H} \qquad t_{free-fall} \propto \frac{4 \cdot 10^4}{\sqrt{n_H}} \tag{1.1}$$

As is deducible there is a deficit in favour of the left formula that translates into a dust grain's accretion in terms of ice mantle. Meanwhile, the freeze-out of interfering species like CO and O, in conjunction with the larger fraction of the H_2 in the para form at ~20 K, contribute to get stalled the kinetic of the reaction reported in figure 1.6, de facto enhancing the ratio of H_2D^+/H_3 over the D/H elemental one. The deuteration zone of figure 1.6 is the one with the brightest ortho-H_2D^+ ever detected ([28];[46]). The result is a growth in the deuteration of $H_3{}^+$ that then give birth to singly and doubly deuterated formaldehyde and methanol, with the latter also in the triple form [47][48]. But why these molecules are observed? This is done because, with the aid of the non-deuterated counterpart, it allows us to measure the electron density, an elusive key actor in the process of the evolution of the cloud. What we obtain is therefore a precious tool that is able to trace the kinematic of the pre-stellar core. In fact, the electron density is with the ions responsible for the formation of a magnetic field. The latter can be peacefully passed across by neutral molecules which however, colliding with the ions themselves, influence the overall process and consequently the gravitational collapse of pre-stellar core itself.

Instead, concerning ^{15}N no abundance of it has been seen in NH_3 and N_2H^+ coming from the pre-stellar cores and protostellar envelopes and in the Pre-stellar core L1544, respectively. Conversely, an enrichment in HCN in pre-stellar cores [49] and in star regions across the Galaxy [50] have been detected. To note that the ^{15}N measured in comets has been obtained also using CN as target. Usage of these data in a chemical model of a dense cloud [40] in order to reproduce the beholden differentiation effectively brought out that the model itself was consistent if the poor correlation between D and ^{15}N-fractionation observed in some primitive material in our Solar System [28] were taken into account.

So far, interstellar dust grains have just been mentioned, but they are the main location on which actually reactions take place. They are subjected to photoprocesses that give birth to organic species that starting from methanol arrive up to amino acids [51] and free some material from the solid phase to the gas one. At the same time, they are subjected to cosmic rays that play a crucial role in the molecular desorption [52] and in mantle's composition alteration [53]. They have been studied through observation of absorption and laboratory work (e.g. [54]; [55]) and are even as crucial as indispensable mainly because they:

- constitute the surface on which atomic hydrogen can react to form its molecular counterpart, the first step of molecular complexity [56];
- protect the inner region absorbing the FUV photons that would otherwise give to the molecules onto the surface sufficient energy to broke them up;
- catalyse the fixation of oxygen into H_2O molecules ([57]:[58]);
- lower, wrapping it, the temperature of the inner zone enhancing as a consequence the growth of the ice mantel of the coldest area. Thickness reaches values of $2,5 \cdot 10^{-6}$ cm [59].

Anyway, not the same processes occur in the same region of the pre-stellar core's grains. Imagining to come from the interstellar space we would firstly see the heap of the pre-stellar core. Going into it we would be initially witness of how photoprocesses affects the mantle's grains, namely diminishing their thickness, and we would see the fixation of oxygen into water, of carbon into CH_4 and of nitrogen into NH_3. Proceeding further we would then enter in the zone in which the pre-stellar

core margins with the molecular cloud within which it is embedded [28]. Here the mantel starts to accumulate what after H_2 become the second most abundant compound, CO, while its corresponding double oxygenated analogous starts to form through cosmic-ray bombardment [60] and CO + OH reaction [61]. This is what someone would see until, ending up into the deepest level of the cloud, the observer would recognises that due to the domination of freeze-out process CO passes to be mainly in the solid form and that because of a D/H ratio higher than 0.1 a large amount of species as H_2CO and CH_3OH became singly or multiply deuterated.

As well as the aforementioned compounds, deuteration affects also water, and it constitutes the way through which we discerned its origin. In particular, having found it both in asteroids and comets, we can link the chemistry of the interstellar medium with the one of our Solar System. In fact, it is thought that water has mainly originated before the prestellar-core formation, thing also supported by chemical models ([62];[58]). Its formation can take place through an hydrogenation of atomic [63] as well as molecular oxygen [54] or even of ozone [64] and via OH + H_2 at 10 K [28]. All these processes, that thanks to the Herschel Space Observatory and chemical/dynamical/radiative transfer models have given us a prediction of 2.6 Jupiter masses of water ice and 0.5 Earth masses of water vapor [28], occur on the surface of dust grains of interstellar clouds located in zones in which the impinging radiation field is sufficiently high to overcome the UV side effects, i.e. photodesorption [65]. Nowadays two pathways are considered the responsible of water formation: in the first one it comes about at the surface of the grains at a temperature slightly above 15 K, while in the second one it mainly occurs in the gas phase at a temperature above 100 K [66].

The first way through which there is the formation of water is additionally considered the same through which the complex organic molecules (COMs) originate. Currently, bearing in mind that more and more experimental and theoretical efforts have to be made in order to better understand the overall surface chemistry of dust grains, Caselli and Ceccarelli in [28] sketched out from where COMs came from. Radicals, even if the debate is still open, are the main actors and the process is thought to proceed in two ways:

- A dissociation of the trapped compounds due to UV photons, or due to Taquet et al. an embedment in the freeze-out process of radicals already produced in the mantle of the grain [67], that impacted by heavy cosmic rays can temporarily enhance their mobility giving birth to reactions. See figure 1.7.
- The direct formation of methanol due to the increase level of CO that in the freeze-out process reacts with the contained frozen water. Then, due to the growth of the temperature, the alcohol come off and subjected to cosmic rays other COMs are formed, hypothesis supported by Garrod & Herbst [44].

Whether in one way or another, species as methyl cyanide (CH_3CN, [69]), methyl-cyanoacetylene (CH_3C_3N, [70]), acetaldehyde (CH_3CHO, [71]), ketene (CH_2CO, [72]), the aforementioned methanol ([73]), methyl-cyanodiacetylene (CH_3C_5N, [74]), methyl-triacetylene (CH_3C_6H, [75]), propylene (CH_2CHCH_3, [76]), methyl-diacetylene (CH_3C_4H), cyanopolyynes ($HC_{2n+1}N$, n=0,1,...,5) and $C_{2n+1}N$ radicals ([77]; [78]) and ions as C_6H^- ([79]) and C_8H^- ([80]) have been found in in the Taurus Molecular Cloud complex while in pre-stellar cores CH_3CHO ([71]), HCOOH ([81]), $HCOOCH_3$, CH_3OCHO and CH_2CO ([82]) have been found. To confirm the hypothesized processes, Öberg at al ([83]) carried out some laboratory experiments revealing that from methanol radicals such as CH_3 and O_3 a self-rearrangement leads to CH_3OCH_3 or, reacting with CHO, to CH_3CHO and $HCOOCHCH_3$.

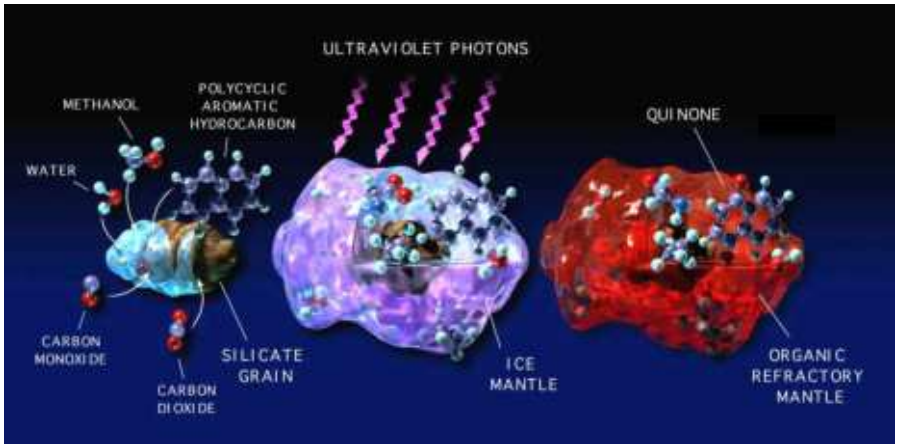

FIGURE 1.7: Representation of a dust grain with the embedded molecules in the freeze-out mantle subjected to UV photons. Quinone is one of the compound that has been identified, in addition to Amphiphiles, Hexamethylenetetramine - a precursor reactant to make amino acids, cyanides, etc.- and Nucleobases, at the NASA Ames Research Center [68].

The metastable equilibrium in which what were above described subsist until the collapse starts. The gravitational energy is at the center converted in radiation due to the density and temperature increase, and the velocity of the infalling gas increases with a $r^{-\frac{1}{2}}$ trend. Recent observations carried out with ALMA[3] and Herschel on IRAS 16293-2422 ([84]; [85]) brought out that in this specific case, as in some others, a cavity (called large Photon-Dominated-Regions, PDRs) illuminated and heated by the inner UV radiation is created by the outflowing gas, situated between the new-born star and the envelope. The latter cannot be always spherical, as in some cases have been found. This can be due to the presence of a circumstellar disk and/or multiple sources, as for example in IRAS 16293-2422 and NGC 1333-IRAS4 [86]. In any case, whether or not these differences are present, four main zones can be identified. From the outer to the inner one, they are:

1. The chemical composition is similar to a typical molecular cloud; no particular freeze-out species; its presence is delegated to the age and the density of the envelope.

2. Whether the age and the density of the envelope are sufficiently high, molecules freeze-out, making most of Class 0 and Class I[4] protostars CO-depleted in this

[3] The Atacama Large Millimeter/submillimeter Array.

[4] A YSO, Young Stellar Object, is generally classified on the base of its evolutionary stages, periods in which the star has different spectral energy distribution in the mid-infrared. Due to Lada (1987) there are 4 classes: from 0 to III. These are differentiated taking into account α, the *spectral index*. This value emerges from the relation $S_\nu \propto \nu^\alpha$, with S_ν radiative flux density and frequency ν.

Class	α
0	undetectable at $\lambda < 20\,\mu m$
I	$\alpha > 0.3$
FlatSpectrum	$0.3 > \alpha > -0.3$
II	$-0.3 > \alpha > -1.6$
III	$\alpha < -1.6$

same region [87]. Density is typically larger than ~10^5 molecules·cm^{-1}.

3. Exceeding ~25 K, namely the sublimation temperature of CH_4[5] if this latter is more abundant than 10^{-7} molecules·cm^{-1} it becomes the major destructor of C^+, with the consequent formation of C-chain molecules. This zone, called the Warm-Carbon-Chain-Chemistry (WCCC) source ([88]; [89]) because characterized by temperature around 30-60 K, have been detected also in L1527.

4. Beyond ~100 K all the dust compounds embedded in the mantle are released, giving birth to a complex chemistry, called hot core chemistry [90].

This complex chemistry is due to the sublimation of some species contained in the mantle, namely "mother" or "primary" species, that reacting between themselves give those called "secondary" or "daughter" species [28].

Two categories of hot cores can go forming. The first one to be discovered in the '90s, the Orion Molecular Cloud (OMC) [91], was found rich in COMs, and has been the prototype for this kind of typology, namely the *hot cores*. Over time others succeeded, smaller and bigger, making necessary to distinguish them on the basis of objective parameters. Specifically, if COMs are limited into a distance ≤ 0.01 pc from the star, with density $\geq 10^7$ molecules·cm^{-3} and temperature ≥ 100K we are in front of hot cores; otherwise, if temperature - that subtends to neutral-neutral reactions-, mass and densities are slower, we speak about *hot corinos* ([92]; [93]). The two tipes do not differ only for the aforementioned peculiarities, but also for their chemical base. Hot corinos are in fact much more abundant in COMs such as $HCOOCH_3$ and CH_3OCH_3 ([94]; [95]), and this is due to the different pre-stellar history along which the two entities evolved. Additionally, the fact that hot corinos can be formed by binary[6] or multiple systems further complicate their chemistry, as it emerged from the hot corino prototype IRAS 16293-2422 ([96]; [97]). Based on the chemistry of the envelope, four groups of species are identified [28]:

Group I: Millimeter line from single molecules like CN, HCO^+ and carbon-chains, associated with cold envelope.

Group II: Source A, rich in N- and S-bearing molecules.

Group III: Source B, rich in O-bearing COMs.

Group IV: Low-lying emitting lines from molecules like CH_3OH, H_2COH, CH_3CCH and OCS in cold envelope and high lying in the two sources A and B.

Another important site where a great amount of reactions occur is the outflow of material that shows up in the process of accretion toward the central object. Not just this process slows down the angular momentum of the overall gas and grains cluster but also, crashing against the quiescent material, acts as a crucial circumscribed [98] spot of chemical enrichment. The combination of temperature rise and violent shocks guarantee neutral-neutral reactions between compounds detached from the mantle on which they were before freeze-out. The forefather in the study of complex chemistry outflows has been L1157-B1 [99], in which hot cores and corinos tracers as methanol (CH_3OH) [100], ethanol (C_2H_5OH), formic acid (HCOOH) and methyl

[5] CH_4 is formed during the pre-stellar phase and is believed to have originated through an hydrogenation of neutral carbon, deposited into grains mantle previous CO formation.

[6] Called in literature A and B, have different composition probably due to different masses ([93]; [96]).

cyanide (CH_3CN) have been identified [101]. To note that the abundances normalized to methanol are at least one order of magnitude lower in molecular outflow than in hot corinos [28]. Equally interesting, species nowhere else detected containing different kind of atoms, such as PN (abundance: 10^{-10})[7] and HCl (that with an abundance of $3 - 6 \cdot 10^{-9}$, almost the same value found in high and low-mass protostellar envelope but 200 times slower than Cl elemental abundance rise the question of where the rest is), have been detected in L1157-B1 with the Herschel Space Observatory [102]).

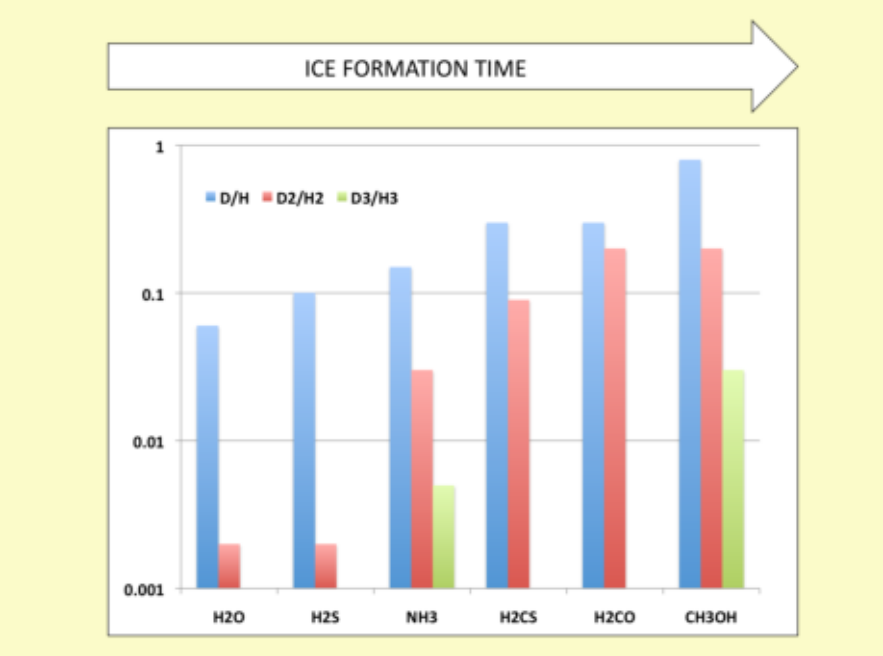

FIGURE 1.8: Relative abundances of singly, doubly and triply deuterated isotopologues [28].

In order to trace back the molecular age of those compounds in envelopes and outflows located, we must again entrust ourselves to deuteration comparisons. In "*Our astrochemical heritage*" Caselli and Ceccarelli [28] show an exhaustive graph in which the relative abundances between single, doubly and triply deuterated isotopologues are compared. In figure 1.8 the mentioned chart. The authors argued that the observed deuteration is an inherited product of the pre-stellar phase, fact supported by the 13 times excees in the D/H ratio of these compounds compared to the elemental one. Additionally, they reported that deuteration is not the same for every species, but that instead follows the typical D-species/D_2-species = 4 (ratio obtained taking in account the typical D/H deuteration ratio) only for H_2S and CH_3OH. Species as H_2O, NH_3, H_2CS and H_2CO are on the contrary acting differently, subtending that their formation onto the grains surface is allegedly attributable to a prolonged period in contrast with the ones of H_2S and CH_3OH, definitively shorter. Moreover, they also speculated that even no specific model has been yet presented, the formation of the molecules in figure 1.8 are likely arranged in chronological order that starting with H_2O ends up to methanol. Is finally worth to note that even if what above exposed follow a certain trend, is not always the rule, i.e. CH_2DOH/CH_3OD

[7] Compared to H_2.

ratio is indeed at least one order of magnitude larger in low-mass protostellar envelopes instead of the high-mass ones ([103]; [104]).

At the end, what we finally assist to is the formation of the planetary disk. This one is formed thanks to the angular momentum that has come to be originated at the moment in which the cloud started to collapse, decreeing its equilibrium loss and the start of its flattering process. The latter is likewise observed even if we are in presence of non-rotating collapsing cores, that is an initially non-rotating collapsing cloud [105], but this event instead of have been caused by the momentum itself is due to the interactions that come into being in the drag between ions and neutral molecules established along the collapse phase. What occur is that the gravitational flow drags the magnetic field deflecting the infalling gas along a 'pseudodisk' large till $\simeq$ 2000 AU. In response the magnetic field lines, being them twisted by the pseudodisk, de facto slow down the angular momentum of the inner region of the disk transferring it to the outer part. What pointed out is supported by carried out models ([106]; [107]) in which, in order to overpass the so-called breaking catastrophe, inclusion of non-ideal MHD[8] effects have been taken into account. Due to [108] and [109] models, shape disks of $\simeq$ 100-200 AU with masses as large as 10 % of the original core mass are possible, noteworthy because these are characteristics also owned by young self-gravitating protoplanetary disks whom, going to meet instability, gives rise to the formation of the planetary systems ([110]; [111]; [112]).

After pioneering works ([113]; [114]; [115]) in which the observation of these embedded disks has been made possible, other contributions have allowed to characterize their chemical content, e.g. [116] and [117]. With VLA, Very Large Array, NH_3 has been found in a 130 AU circumstellar disk around NGC 1333-IRAS4A2 [118], with the Plateau de Bure Interferometer (PdBI) at IRAM, $H_2{}^{18}O$ has been detected in the inner 25 AU of the NGC 1333-IRAS4B disk [119] and with ALMA a binary Class 0 source in *Ophiuchus*[9], namely IRAS 16293-2422, have revealed the infall toward source B and trace of rotation toward source A [120], elements that if confirmed would represent the first evidence of chemically and kinematically characterization of an embedded disk discovered thanks to a complex organic molecule, methyl formate [28]. On the base of what have been previously said and with the employment of different physical approaches, three chemical models have been devised:

Vissel at al. model: postulated the mixing lack of the materials involved, it takes into account the formation of a protoplanetary disk on the base of an initially spherical and slowly rotating cloud. Predictions about ice and gas-phase composition are detailed, while both outflow cavities and disk-envelope boundary are well shaped. In particular, in the disk constitution emerged the possibility of identifying its different regional chemical history [121].

Boyle's model: Assuming no accretion of the envelope material and no outflow, using the results obtained employing a previous hydrodynamic simulation [112], gas-phase and simple surface chemistry networks have been used [122] to trace the evolution of the disk. The result is a complex spiral that drawn a non-axisymmetric profile, figure 1.9. On the contrary of what have been seen in the previous model, a continuous mixing flows into an absence of identifiable chemical sectorization but, on the other hand, tracers such as H_2O, HNO, NH_3, H_2CO and HCO^+ have been identified.

[8] Namely *Magnetohydrodynamics*, the study of the magnetic properties and behaviour of electrically conducting fluids. Specifically, it assumes that the mass to magnetic-flux ratio is constant, implying that magnetic field lines follow the gas motion, i.e. is "frozen" into the neutral medium [28].

[9] A constellation located at the celestial equator, known as the *Serpens constellation*.

Furuya et al. model: sketching out the process that from a molecular cloud bring to a protostellar precursor, after an initial destruction of simple molecules, Furuya found that more complex ones such as CH_3OH and $HCOOCH_3$ are formed, thus becoming allies in the evolutionary tracking process [123].

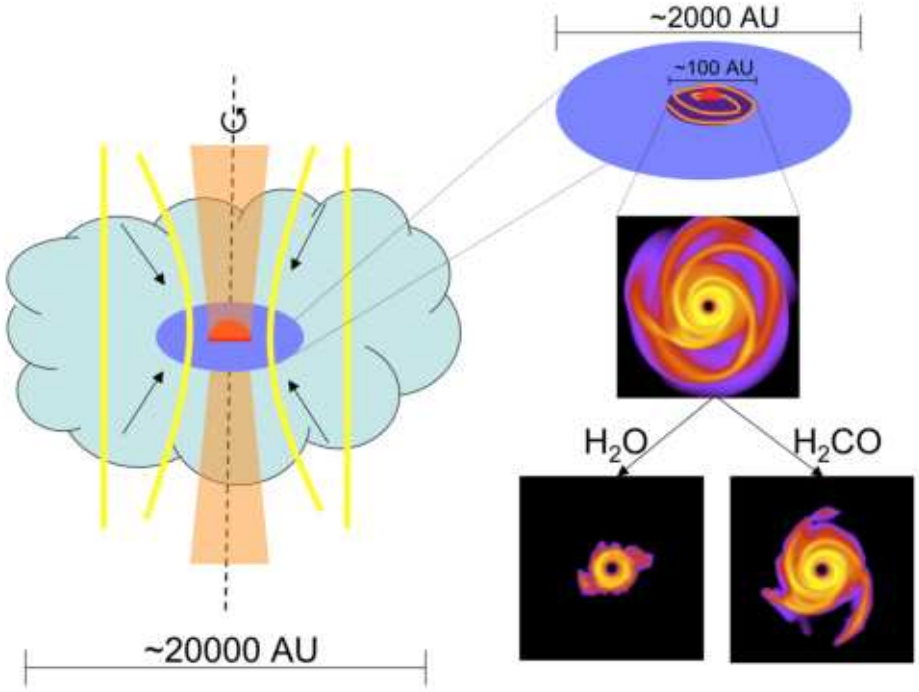

FIGURE 1.9: The earliest stages of a collapsing Class 0 source. In red the central protostar, in yellow the magnetic field lines, in blue the pseudodisk, in violet the central embedded disk and in orange the outflow. H_2O and H_2CO are good tracers of these young embedded disks [28].

Once these disks have come to form, their poor stability does not make them last for a long time; ~0.5 Myr after the formation of the protostar-disk-outflow system the ancestor envelope quickly disperses and the disk, assuming a form resembled the one in fig. 1.10 enters in a phase known as *Tauri T* or Class II phase. In this can last several Myr [28] for then leaving the place to the planetary system formation. But let us pause for a moment and have a look at how the remains of the protostellar disk appear to us.

The inner part, namely from the star up to 1 AU, is constituted by pure dust disks which contain H_2, CO, H_2O, OH and other simple organic molecules ([124]; [125]; [126]). At approximately 1 AU a "puffed-up" region [127] is visible in the near-infrared continuum, while in the central few AUs H_2O, CO and organic molecules such as HCN and C_2H_2 are visible in the mid-infrared range [128]. To note that what just reported doesn't strictly apply to all systems: in fact, for Herbig Ae/Be star[10] [129] none organic molecule have been found in this interval. Anyway, in both cases, in the midplane from ~1 AU onward is situated the disk on which, due to the low temperature, coagulation of dusts occurred. This cold and dense region hosts lots

[10] An extremely young star in the *Sagittarius* constellation.

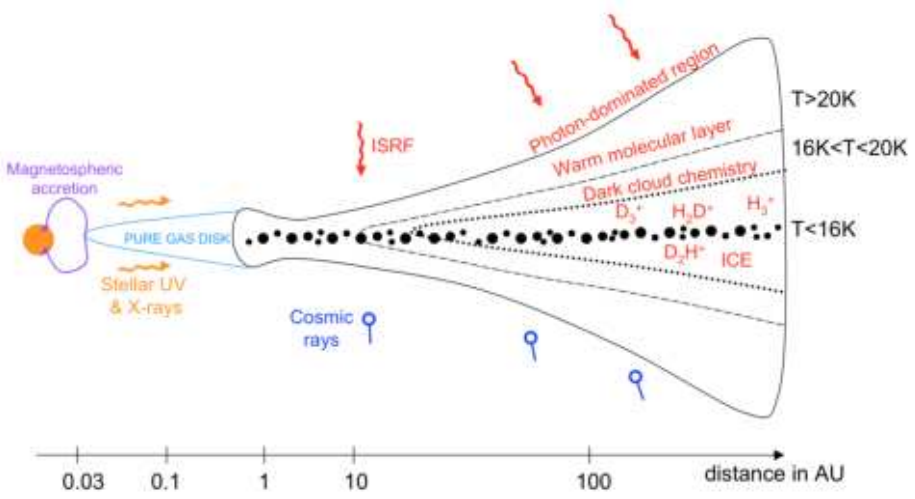

FIGURE 1.10: The various regions of a protoplanetary disk in which the envelope has been lost. The black dots onto the midplane represent the dust in their accretion process [28].

of frozen simple molecular species, the only ones that can there survive [130]. Thus, around this same dust midplane, these low-mass molecules throng and accumulate. There is, however, something to add: the presence of some degree of mixing coagulation maintains a population of small grains in the upper layer of the disk [28] and on this latter polycyclic aromatic hydrocarbons (PAHs) are present, there as in any active star-forming region [131]. Besides being ubiquitous, these compounds are extremely important due to both an organic and pre-biotic chemistry point of view as well as their essential role played in the release of energy, once photoionized, heating up the gas that consequently maintains flared the conformation of disks [132]. Additionally, they promote the molecularization of hydrogen [133] and more importantly, their mixing with icy mantle can preponderantly act in the formation process of more complex organic molecules[11] [134]. Just outside this layer, temperature rise enough to skim 20 K, an amount sufficient to allow to CO isotopologues ([135]; [136]), CN, HCN, HNC, CS, HCO^+, C_2H and H_2CO ([137]; [138]: [139]), N_2H^+ [140], SO [141], CS [142], DCO^+ [143], H_2D^+ [144], HDO [145] and HC_3N [146] to situate themselves there, constituting a dark-cloud chemistry zone [28]. But is sufficient to exit from this region for finding the warm molecular layer, dominated by radicals and ions photochemically excited. This same process, namely the excitation through stellar and interstellar UV fields at whom stellar X-rays are added is also found, enormously enhanced, in the PDR (the photon-dominated region), the last part of this conglomerate of dust and gas beyond which, in the interstellar space, abound the aforementioned radiations. Successive coagulation processes lead, even if the way to them is still unknown, to comets and finally the planets themselves.

Many are the chemical models that have been developed, but even if these prototypes play an important role, an equally strategic one is played by laboratory studies that acting in concert with the former, constitute a binomial without which, in thinking to solve the problem with the modelling alone, we would make a huge mistake. In traversing the modelled space, laboratory tests act as real lighthouses, able to guide, re-directing the shot when it seems to take unrealistic directions, the search

[11] Once grains start to coagulate.

for a predictive theoretical model that takes into account the experimental situations as well as the observational one, out of which the computerized resultant deviates completely from astrophysics. Taken together, these approaches are the basic tools of astrochemistry that, as was defined by Dalgarno [147] is nothing but "the study of the formation, destruction and excitation of molecules in astronomical environments and their influence on the structure, dynamics and evolution of astronomical objects". The molecules themselves therefore constitute an important tool thanks to which it is possible to probe the space and what in it is contained, its state, its past and therefore, understanding the trend, its possible future scenarios. Among the questions that fall within the branch of astrochemistry we can indeed count: how, when and where are these molecules produced and excited? How far does this chemical complexity go? How are they cycled through the various phases of stellar evolution, from birth to death? And, most far-reaching, can they become part of new planetary systems and form the building blocks for life elsewhere in the Universe? [21]. Therefore, with these premises the object on which this thesis has been written tries to interlock itself.

1.3 2-Propene-1-Imine

As we have until now seen, innumerable are the COMs that populate both the ISM and the objects that fit into it. The number of those that have been for the moment observed is over 200, with almost 70 having 6 or more atoms of which at least one is a carbon. This translates into the possibility of investigating compounds that actually take on, as they have been gradually doing in recent times, an increasingly considerable role in trying to understand how the distribution and evolution of extra-terrestrial molecules of biochemical interest occurred. To give an idea just think that in the effort of collecting important pre-biotic moleules in chondrites, up to 80 amino-acids in the Murchson meteorite alone have been collected [148]. Actually, their identification was made after hydrolysis of the sample [148], leaving them de facto unidentified if the latter had not been performed [149]. Danger et al. argued that amino-acids can be embedded into the matrix and are released through hydrolysis, or that the same hydrolysis, acting on precursors, produce the collected amino-acids or also that, finally, these amino-acids are broke down from precursor oligopeptides; other investigations will shed light on this. Simultaneously, from recent laboratory survey, Theule at al. have been succeeded in the hydrogenation into fully saturated methylamine CH_3NH_2 that then, thermally reacting with CO_2 in solid phase, can form carbamate, successively convertible through VUV radiation into glycine NH_2CH_2COOH. The latter can therefore pass from the salty form to the gas-phase-natural one once desorbed [150]. They also found that methanimine CH_2NH can be hydrogenated too, giving back CH_2NH_2. The network of hydrogenated HCN is reported in fig. 1.11.

Equally, glycine is also known to be produced from aminoacetonitrile, detected in Sgr B2(N) [151]. The latter can be formed by cyanogen hydrogenation [151] or photochemically in astrochemical environment, from ammonia and nitrile mixture (fig. 1.12A) but gives rise to very low yields [152]. On the other hand, the Strecker synthesis (1.12B) offers higher yields and likewise can occurs in astrophysical-like conditions ([51]; [153], [31]). It is considered the main pathway to the formation of amino-acids in the Urey-Miller experiment [154], in which an aldehyde reacts in liquid water with ammonia to form the corresponding imine after dehydration. The imine then reacts with hydrogen cyanide, leading to the corresponding aminonitrile

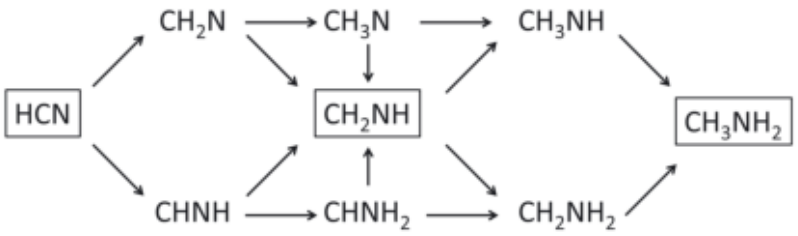

FIGURE 1.11: Hydrogenation network of HCN at low temperature. Stable molecules are framed [150].

that in turn, once hydrolysed, leads to amino-acids formation in a process that can be sustained up to 20 K [152]. Someone could cleverly argue that in the astrophysical condition till now presented there is very little liquid water, but from theoretical investigations emerged that the condensation of ammonia with formaldehyde can leads to the corresponding amino alcohol [155] that in presence of acid can produces the respective imine [156]. What just said has also been validated from an experimental point of view, in which have been stated that ammonia can condensate onto either formaldehyde or acetaldehyde at 50-100 K [157] to form the relative amino alcohol. Additionally, further theoretical survey brought to light that the condensation of hydrogen cyanide onto imine can also occur in solid aqueous phase [155].

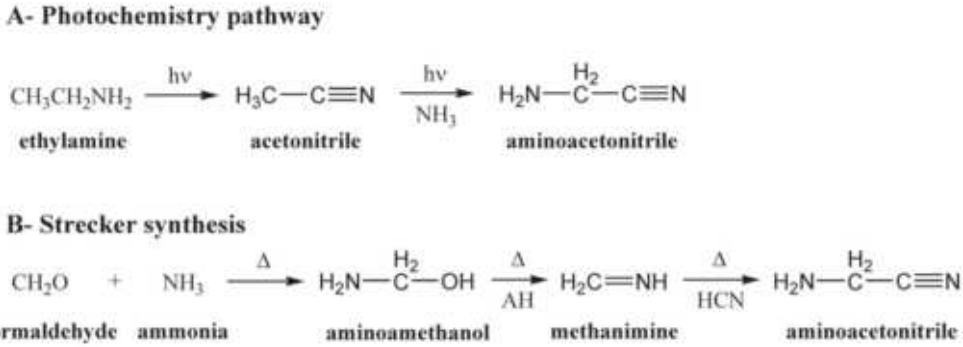

FIGURE 1.12: Experimental pathway leading to aminoacetonitrile in astrophysical like conditions.

Is therefore clear that detecting some of the aforementioned compounds would it possible to trace occurring reactions and get clues about more complex products that for the moment have not yet been observed but there staying. To date, four are the imine that have been detected in space: methanimine, firstly identified towards Sgr B2 [158] but then also outside the galactic centre in giant molecular clouds [159], towards dark and translucent clouds [160] and outer galaxies like Arp220 [161] and NGC 253 [162]; 3-imino-1,2-propadienylidene (CCCNH) detected in TMC 1 [163]; the *E* and *Z* ethanimine isomers (CH_3CHNH) in the molecular cloud complex Sgr B2 [164]; ketemine (CH_2CNH), completing a triad of C_2H_3CN isomers, again in the giant molecular cloud complex Sgr B2 [163].

Therefore, in a parallel way, if three carbons and one nitrogen skeletons have been already identified, why cannot others be equally probable? About that, also compounds such as propionitrile [165], acrylonitrile [166] and cyanoacetylene have already been identified [167], and others could follow if the relative spectra were

available. What in fact astrophysicists need for their research in the chemical evolution of interstellar dust clouds, protostellar systems and similar in the effort to unearth their targets, namely a molecule of specific interest, is its relative fingerprint, i.e. its spectroscopic spectrum. Is in this prospective that the object of this thesis makes its appearance.

2-Propen-1-Imine (propenaldimine, acraldehyde imine) is an analogous of acrylonitrile and cyanoacetylene, of whom spectral data obtained in this microwave study would be essential for such a search. 2-Propen-1-Imine, CH_2CHCNH, has a conformational equilibrium associated with rotation about the central C-C bond that is similar to the propenal one [168], but here this equilibrium is complicated both by the possibility of *syn* and *anti* configurations of the imino hydrogen and by the *syn-anti* interconversion rate. Ketimines (RR'C=NH) are known to rapidly interconvert in condensed phase, but the microwave study of the relative concentrations of the *syn* and *anti* rotamers of ethanimine (CH_3HC=NH) occurring at the low pressure pyrolysis of ethylamine, an isomer, indicates that the *syn*/*anti* ratio is determined by the kinetics of the pyrolysis, implying slow interconversion for that aldimine [169]. Four are the rotamers of 2-Propen-1-Imine, reported in fig. 1.13, of which we will try to trace the microwave rotational spectrum.

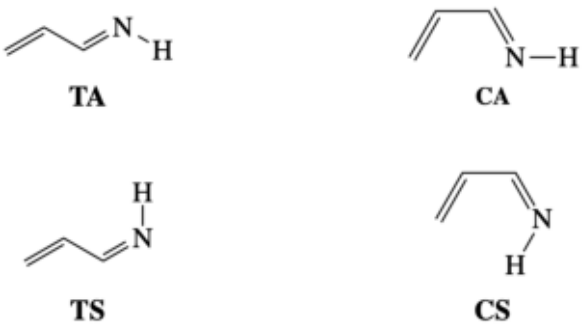

FIGURE 1.13: The four 2-Propen-1-Imine isomers [152].

The letters *T* and *C* define the rotamer relative the C-C bond, respectively for the *syn* and *cys* forms, while letters *A* and *S* refer to the *anti* and *syn* position of the imino hydrogen position [169]. From literature ([169], [170]) spectral lines assessment of the *cis* rotamer is reported to be unsuccessful, therefore, even if the chances of identifying them are rare, an effort will be attempted in this regard. It has to be taken into account that in rare cases such, as that of glyoxal, it has been possible. In that circumstance the most abundant species were exhibiting no microwave spectrum, but in the case of this specific study spectral interferences imputable to others pyrolysis sub-products are expected to make more difficult the microwave spectroscopy analysis. Starting from computational calculations, experimental analyses will then be carried out allowing us to trace, in addition to the spectrum of the molecule, the rotational and distortion constants of the molecule itself. This step will be carried out with the use of a software[12] that going to convergence, through consecutive refinements conducted while new data are added to the catalogue used, will return the constants value that best summarize what is seen in the spectrum. In this regard, therefore, a parenthesis must be opened to briefly illustrate the theoretical bases on which the software will operate.

[12]CALPGM program suite: https://spec.jpl.nasa.gov/ftp/pub/calpgm/calpgm.pdf

Chapter 2

Theoretical bases

2.1 Classical angular momenta and rotational energy

In order to give a comprehensive quantum mechanical explanation of how a molecular rotor behave is necessary to start from its classical point of view. Assume to start from a rigid rotor; let's turn the attention to the classical moment of inertia

$$\mathbf{P} = \mathbf{I}\boldsymbol{\omega} \tag{2.1}$$

in which $\boldsymbol{\omega}$ is the angular velocity and $\mathbf{I}$ is the moment of inertia tensor written as

$$\begin{bmatrix} I_{xx} & I_{xy} & I_{xz} \\ I_{yx} & I_{yy} & I_{yz} \\ I_{zx} & I_{zy} & I_{zz} \end{bmatrix} \tag{2.2}$$

with

$$\begin{aligned} I_{xx} &= \sum_{n}^{N} m_n (y_n^2 + z_n^2) \\ I_{yy} &= \sum_{n}^{N} m_n (x_n^2 + z_n^2) \\ I_{zz} &= \sum_{n}^{N} m_n (x_n^2 + y_n^2) \\ I_{xy} = I_{yx} &= -\sum_{n}^{N} m_n x_n y_n \\ I_{zx} = I_{xz} &= -\sum_{n}^{N} m_n x_n z_n \\ I_{yz} = I_{zy} &= -\sum_{n}^{N} m_n y_n z_n \end{aligned} \tag{2.3}$$

where n refers to the n^{th} element of the object. Setting the origin at the center of mass authorize us to split the total kinetic energy into two sums: the one relative to the center of mass and the other that makes reference to the contributions coming from the elements relative to the center of the mass itself. These two components, namely the translational and rotational motions, can therefore be separately treated. If then the coordinate system is properly chosen is possible to render vanish the products of inertia. This leave only the diagonal elements, respectively known as the principal

moments of inertia, whom once solved give back three roots for the cubic equation.

$$\begin{vmatrix} I_{xx} - I & I_{xy} & I_{xz} \\ I_{yx} & I_{yy} - I & I_{yz} \\ I_{zx} & I_{zy} & I_{zz} - I \end{vmatrix} = 0 \tag{2.4}$$

If the principle axes system are then designatd as x, y, z, the components of angular momentum become:

$$\begin{aligned} P_x &= I_x \omega_x \\ P_y &= I_y \omega_y \\ P_z &= I_z \omega_z \end{aligned} \tag{2.5}$$

The rotational kynetic energy is defined as

$$E_r = \frac{1}{2} \mathbf{I} \cdot \boldsymbol{\omega}^2 \tag{2.6}$$

which can, relative to the principal axes, be written as

$$E_r = \frac{1}{2} \left(\frac{P_x^2}{I_x} \right) + \frac{1}{2} \left(\frac{P_y^2}{I_y} \right) + \frac{1}{2} \left(\frac{P_z^2}{I_z} \right) \tag{2.7}$$

If then a torque is applied, its dependence from P_i is

$$\begin{aligned} \frac{dP_x}{dt} + \omega_y P_z - \omega_z P_y &= \tau_x \\ \frac{dP_y}{dt} + \omega_z P_x - \omega_x P_z &= \tau_y \\ \frac{dP_z}{dt} + \omega_x P_y - \omega_y P_x &= \tau_z \end{aligned} \tag{2.8}$$

while, when no torque is applied in a free rotating system, the Euler's equations of motion are obtained

$$\begin{aligned} \frac{dP_x}{dt} + \left(\frac{1}{I_y} - \frac{1}{I_z} \right) P_y P_z &= 0 \\ \frac{dP_y}{dt} + \left(\frac{1}{I_z} - \frac{1}{I_x} \right) P_z P_x &= 0 \\ \frac{dP_z}{dt} + \left(\frac{1}{I_x} - \frac{1}{I_y} \right) P_x P_y &= 0 \end{aligned} \tag{2.9}$$

With a bit of manipulation results

$$P_x \left(\frac{dP_x}{dt} \right) + P_y \left(\frac{dP_y}{dt} \right) + P_z \left(\frac{dP_z}{dt} \right) = 0 \tag{2.10}$$

that integrated and multiplied returns

$$P_x^2 + P_y^2 + P_z^2 = const = P^2 \tag{2.11}$$

Is evident therefore that when no torque is applied the square of the total angular momentum in a body-fixed axes system is constant. In the same way, also the rotational kinetic energy remains constant

$$E_r = \left(\frac{P_x^2}{I_x} + \frac{P_y^2}{I_y} + \frac{P_z^2}{I_z} \right) = const \tag{2.12}$$

Due to the convention, instead of x, y and z, the axes are called a, b and c, with $I_a \leq I_b \leq I_c$. Based on the relations shown below it is possible to identify different kinds of rotors

Rotor	I_i relations
Linear	$I_a = 0$, $I_b = I_c$
Spherical	$I_a = I_b = I_c$
Symmetric prolate	$I_a < I_b = I_c$
Symmetric oblate	$I_a = I_b < I_c$
Asymmetric	$I_a < I_b < I_c$

2.2 Associated operators

By solving the tensor containing the moments of inertia it is possible to find the eigenvalues corresponding to the eigenfunctions describing the system under consideration. In this case, the system is a molecular one consisting of a set of particles which to be described need the resolution of the Schrödinger equation. Is for this reason that we therefore need to associate to the angular moment an Hamiltonian operator that can describes its behaviour. It will be due to this Hamiltonian that, taking into account the molecular conformation and consequently the relative inertia moments, the energy associated to the corresponding auto states will be stated.

The classical angular momentum is defined as

$$\mathbf{P} = \sum_n^N \mathbf{r}_n \times \mathbf{p}_n \tag{2.13}$$

Through the correspondence principle is possible to define the associated quantum mechanical operator as, in a space fixed system

$$\hat{\mathbf{P}}_{k=X,Y,Z} = \frac{\hbar}{i} \frac{\partial}{\partial k} \tag{2.14}$$

that give back the angular momentum component operators

$$\begin{aligned} \hat{P}_X &= \sum_n^N \frac{\hbar}{i} \left[Y \frac{\partial}{\partial Z} - Z \frac{\partial}{\partial Y} \right]_n \\ \hat{P}_Y &= \sum_n^N \frac{\hbar}{i} \left[Z \frac{\partial}{\partial X} - X \frac{\partial}{\partial Z} \right]_n \\ \hat{P}_Z &= \sum_n^N \frac{\hbar}{i} \left[X \frac{\partial}{\partial Y} - Y \frac{\partial}{\partial X} \right]_n \end{aligned} \tag{2.15}$$

These in spherical coordinates can be written as

$$\begin{aligned}\hat{P}_X &= \frac{\hbar}{i}\left[-\sin\phi\left(\frac{\partial}{\partial\theta}\right)-\cot\theta\cos\phi\left(\frac{\partial}{\partial\phi}\right)\right]\\ \hat{P}_Y &= \frac{\hbar}{i}\left[\cos\phi\left(\frac{\partial}{\partial\theta}\right)-\cot\theta\sin\phi\left(\frac{\partial}{\partial\phi}\right)\right]\\ \hat{P}_Z &= \frac{\hbar}{i}\left(\frac{\partial}{\partial\phi}\right)\end{aligned} \tag{2.16}$$

and the operator of the squared total angular momentum as

$$\hat{P}^2 = -\hbar^2\left\{\left(\frac{1}{\sin\theta}\right)\left(\frac{\partial}{\partial\theta}\right)\left[\sin\theta\left(\frac{\partial}{\partial\theta}\right)\right]+\frac{1}{\sin^2\theta}\left(\frac{\partial^2}{\partial\phi^2}\right)\right\} \tag{2.17}$$

If, with the employment of Levi-Civita symbol

$$\epsilon_{lmk} = \begin{cases}+1 & (l,m,k) = (1,2,3),(2,3,1),(3,1,2)\\ -1 & (l,m,k) = (3,2,1),(1,3,2),(2,1,3)\\ 0 & l=m, m=k, k=m\end{cases} \tag{2.18}$$

we then concentrate on the commutation of this operators

$$\begin{aligned}\left[\hat{P}^2,\hat{P}_l\right] &= 0\\ \left[\hat{P}_l,\hat{P}_m\right] &= i\hbar\epsilon_{lmk}\hat{P}_k\end{aligned} \tag{2.19}$$

emerges that $\hat{P}^2$ have a common set of eigenfunctions with all the component operators, while these latter do not among themselves. Taking into account the z coordinate we can therefore use the first relation to create the base on which these same operators are defined. The relative common eigenfunctions are designate as

$$\begin{aligned}\hat{P}^2\psi_{J,M} &= K_J\psi_{J,M}\\ \hat{P}_Z\psi_{J,M} &= K_M\psi_{J,M}\end{aligned} \tag{2.20}$$

with K_J and K_M eigenvalues of $\hat{P}^2$ and $\hat{P}_Z$ relative to the eigenstate $\psi_{J,M}$. After the application of the ladder operators

$$\begin{aligned}\hat{P}_+ &= \hat{P}_X + i\hat{P}_Y\\ \hat{P}_- &= \hat{P}_X - i\hat{P}_Y\end{aligned} \tag{2.21}$$

and other manipulation [171], it results that the relation is:

$$\begin{aligned}\hat{P}^2\psi_{J,M} &= \hbar^2 J(J+1)\psi_{J,M}\\ \hat{P}_Z\psi_{J,M} &= \hbar M\psi_{J,M}\end{aligned} \tag{2.22}$$

with $J = 0, 1, 2, 3, \ldots$ and $M = J, J-1, J-2, \ldots$, -J. Now, taking into account how the ladder operators act on $\hat{P}_Z$, it can be seen that

$$\begin{aligned}\left[\hat{P}_Z,\hat{P}_\pm\right] &= \pm\hbar\hat{P}_\pm\\ \left[\hat{P}_+,\hat{P}_-\right] &= 2\hbar\hat{P}_Z\end{aligned} \tag{2.23}$$

Specifically, observing how the ladder operators modify the action of $\hat{P}_Z$ on a given state

$$\begin{aligned}\hat{P}_Z\hat{P}_\pm |J,M\rangle &= \left(\hat{P}_\pm\hat{P}_Z + \left[\hat{P}_Z,\hat{P}_\pm\right]\right)|J,M\rangle \\ &= \left(\hat{P}_\pm P_Z \pm \hbar\hat{P}_\pm\right)|J,M\rangle \\ &= \hbar\left(M\pm 1\right)\hat{P}\pm|J,M\rangle\end{aligned} \tag{2.24}$$

and comparing this results with the action of the $\hat{P}_Z$ operator alone

$$\hat{P}_Z|J,M\pm 1\rangle = \hbar\left(M\pm 1\right)|J,M\pm 1\rangle \tag{2.25}$$

one can notices that $\hat{P}_\pm|J,M\rangle$ is $|J,M\pm 1\rangle$ multiplied by a scalar

$$\begin{aligned}\hat{P}_+|J,M\rangle &= c_+|J,M+1\rangle \\ \hat{P}_-|J,M\rangle &= c_-|J,M-1\rangle\end{aligned} \tag{2.26}$$

If then we express 2.23 in term of the commuting pair $\hat{P}^2$ and $\hat{P}_Z$ we can write

$$\begin{aligned}\hat{P}_-\hat{P}_+ &= \left(\hat{P}_X - i\hat{P}_Y\right)\left(\hat{P}_X + i\hat{P}_Y\right) = \hat{P}^2{}_X + \hat{P}^2{}_Y + i\left[\hat{P}_x,\hat{P}_y\right] = \hat{P}^2 - \hat{P}^2{}_Z - \hbar\hat{P}_Z \\ \hat{P}_+\hat{P}_- &= \left(\hat{P}_X + i\hat{P}_Y\right)\left(\hat{P}_X - i\hat{P}_Y\right) = \hat{P}^2{}_X + \hat{P}^2{}_Y - i\left[\hat{P}_x,\hat{P}_y\right] = \hat{P}^2 - \hat{P}^2{}_Z + \hbar\hat{P}_Z\end{aligned} \tag{2.27}$$

Using then the normalizations

$$\int_{-\infty}^{+\infty}\psi^*{}_{J,M+1}\psi_{J,M+1}\mathrm{d}\tau = 1 \qquad \int_{-\infty}^{+\infty}\psi^*{}_{J,M-1}\psi_{J,M-1}\mathrm{d}\tau = 1 \tag{2.28}$$

and remembering that $\hat{P}_-$ and $\hat{P}_+$ are Hermitian conjugate, the values of c_+ and c_- are then given by

$$\begin{aligned}c_+ &= i\hbar\left[J(J+1) - M(M+1)\right]^{\frac{1}{2}} \\ c_- &= -i\hbar\left[J(J+1) - M(M-1)\right]^{\frac{1}{2}}\end{aligned} \tag{2.29}$$

that substituted into equations 2.26 return

$$\begin{aligned}\hat{P}_+|J,M\rangle &= i\hbar\left[J(J+1) - M(M+1)\right]^{\frac{1}{2}}|J,M+1\rangle \\ \hat{P}_-|J,M\rangle &= -i\hbar\left[J(J+1) - M(M-1)\right]^{\frac{1}{2}}|J,M-1\rangle\end{aligned} \tag{2.30}$$

Multiplied for its complex conjugate it gives back the non-vanishing matrix element

$$\begin{aligned}\langle J,M|\hat{P}_+|J,M\rangle &= i\hbar\left[J(J+1) - M(M+1)\right]^{\frac{1}{2}} \\ \langle J,M|\hat{P}_-|J,M\rangle &= -i\hbar\left[J(J+1) - M(M-1)\right]^{\frac{1}{2}}\end{aligned} \tag{2.31}$$

Any other moltiplication for an alternative member of the orthogonal set of functions, say $\psi_{J,M\pm x}$ with $x \geq 2$, due to

$$\delta_{ij} = \begin{cases}1 & i = j \\ 0 & i \neq j\end{cases} \tag{2.32}$$

must therefore return zero. Looking again at the 2.22 is now evident that the non-vanishing matrix elements of $\hat{P}^2$ and $\hat{P}_Z$ are

$$\langle J, M| \hat{P}^2 |J, M\rangle = \hbar^2 J(J+1) \tag{2.33}$$
$$\langle J, M| \hat{P}_Z |J, M\rangle = \hbar M \tag{2.34}$$

Obviously, being the matrix representation of an operator on the base composed of its own eigenvectors always diagonal, if the operator is Hermitian then the eigenvalues are always real. Conversely, it's not in reference to $\hat{P}_X$ and $\hat{P}_Y$, that can be expressed as

$$\langle J, M| \hat{P}_Y |J, M \pm 1\rangle = \frac{\hbar}{2}\left[J(J+1) - M(M \pm 1)\right]^{\frac{1}{2}} \tag{2.35}$$
$$\langle J, M| \hat{P}_X |J, M \pm 1\rangle = \mp\frac{i\hbar}{2}\left[J(J+1) - M(M \pm 1)\right]^{\frac{1}{2}} \tag{2.36}$$

In the same manner what has been presented until now is equally true for the nuclear spin vector, at which is associated its nuclear spin operator $\hat{I}$. If the body-fixed system is employed (in order to distinguish the axis let's use their relative lower-case letters), $\hat{P}_z$ will still commute with $\hat{P}^2$, leading to another common set of eigenfunctions, $\psi_{J,K,M}$, that when see projected on them the operators return

$$\hat{P}^2 |J, K, M\rangle = K_J |J, K, M\rangle \tag{2.37}$$
$$\hat{P}_z |J, K, M\rangle = K_K |J, K, M\rangle \tag{2.38}$$
$$\hat{P}_Z |J, K, M\rangle = K_M |J, K, M\rangle \tag{2.39}$$

K_J and K_M must be the same eigenvalues prevuously obtained, while the value of K_K can be similarly found from commutation of the angular momentum operator expressed in the internal coordinate system. Summing it up, the overall values we have are

$$\langle J, M| \hat{P}^2 |J, M\rangle = \hbar^2 J(J+1) \tag{2.40}$$
$$\langle J, M| \hat{P}_z |J, M\rangle = \hbar M \tag{2.41}$$
$$\langle J, M| \hat{P}_Z |J, M\rangle = \hbar K \tag{2.42}$$

The squared angular momentum operator will be given by

$$\langle J, K, M| \hat{P}_g^2 |J', K', M'\rangle = \sum_{J'', K'', M''} \langle J, K, M| \hat{P}_g |J'', K'', M''\rangle \times \langle J'', K'', M''| \hat{P}_g |J', K', M'\rangle \tag{2.43}$$

and regarding $\hat{P}^4$ and $\hat{P}_i^2$ by

$$\langle J, K, M| \hat{P}^4 |J', K', M'\rangle = \left(\langle J, K, M| \hat{P}^2 |J, K, M\rangle\right)^2 = \hbar^4 J^2 (J+1)^2 \tag{2.44}$$
$$\langle J, K, M| \hat{P}^2{}_z |J, K, M\rangle = K^2 \hbar^2 \tag{2.45}$$
$$\langle J, K, M| \hat{P}^2{}_y |J, K, M\rangle = \frac{\hbar^2}{2}\left[J(J+1) - K^2\right] \tag{2.46}$$
$$\langle J, K, M| \hat{P}^2{}_x |J, K, M\rangle = \frac{\hbar^2}{2}\left[J(J+1) - K^2\right] \tag{2.47}$$

Staying in the body-fixed principal axes x, y, z, we can now associate an operator to the rotational Hamiltonian

$$\hat{\mathscr{H}}_r = \frac{1}{2}\left(\frac{\hat{P}_x}{I_x} + \frac{\hat{P}_y}{I_y} + \frac{\hat{P}_z}{I_z}\right) \tag{2.48}$$

with

$$\hat{P}_x = \frac{\hbar}{i}\left(y\frac{\partial}{\partial z} - z\frac{\partial}{\partial y}\right) \quad \hat{P}_y = \frac{\hbar}{i}\left(z\frac{\partial}{\partial x} - x\frac{\partial}{\partial z}\right) \quad \hat{P}_z = \frac{\hbar}{i}\left(x\frac{\partial}{\partial y} - y\frac{\partial}{\partial x}\right) \tag{2.49}$$

If the above Hamiltonian commutes, as it does, with its angular momentum operators, its matrix elements will be given from the diagonal elements of the angular momentum operator themselves.

2.3 Asymmetric rotor

When all the three principal moments of inertia I are $\neq 0$ and none are among of them equal, the rotational spectrum, compared to the symmetric-top one, increase its complexity. Generally speaking, the strategy consists in assuming that the wave functions can be expanded in terms of an orthogonal set of functions and by setting up the secular equations for the unknow coefficients and energies. The resulting secular determinant can be broken down into a number of sub-determinants, whose orders increase with J. The solutions of these sub-determinants lead to the required energy levels and expansion coefficients [172]. In an asymmetric rotor, those who were first reliable tools for interpreting the system cease to be such that. This is due to the absence of a constant component of the angular momentum of the motion or, specifically, due to the fact that $\hat{P}_z$ no longer commutes with $\hat{\mathscr{H}}_r$, while only J and M remain "good" quantum numbers. For this reason, it has been employed the double subscript system proposed by King et al. [173] for which the rotor tends to the prolate or alternatively to the oblate symmetric-top one.
The asymmetric rotor nature can be summarized by the parameters

$$\kappa = \frac{2B - A - C}{A - C} \tag{2.50}$$

where A, B and C are the rotational constants relative to a, b, c axes. While the most asymmetric-top rotors approach $\kappa = 0$, the prolate symmetric-top rotor ($I_b = I_c$) has $\kappa = -1$ and the oblate one has $\kappa = +1$. Therefore, the energy can be defined by the level $-K$ and $+K$, always degenerate in the symmetric case. This means that for every J level there are $(2J+1)$ rotational sublevels. The bigger the asymmetry of the molecule, the higher the discrepancy between the two K levels in comparison with the symmetric degenerate one. Figure 2.1 shows the relationship this pseudo-quantum numbers are subjected to; it appears clear the meaning of the writing $J_{K_{-1}K_1}$. To note that the same K energy sublevel is higher for a prolate than an oblate rotor one and again, now visible from the figure, the splitting between Ks levels increases while J rises.

It has to be reported that in literature is still in use τ, another pseudo-quantum number, that reassumes the two so far mentioned. For the highest sublevel of a given J, the value assumed by τ is J, for the next higher $J-1$ and so on, until arrive to $-J$. Therefore, existing $(2J+1)$ discrete rotational sublevels for a specific J, there are $(2J+1)$ corresponding sublevels of τ, ranging from $-J$ to J [172]. Looking at the

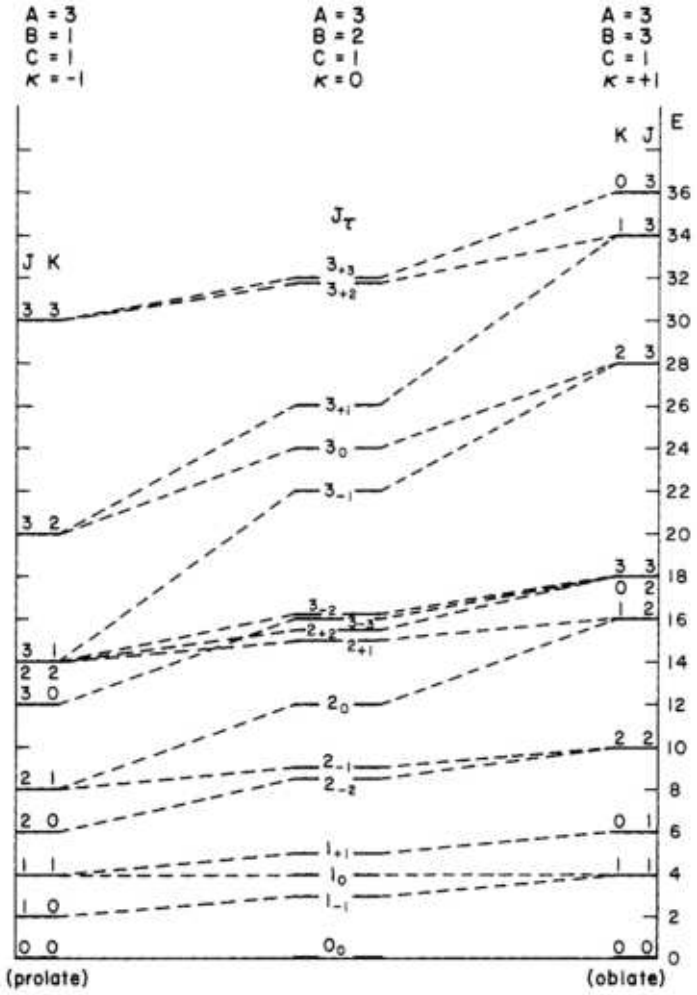

FIGURE 2.1: Relations among the energy levels in the oblate and prolate limits for the symmetric top rotor [172].

figure 2.1 is possible to notice that

$$\tau = K_{-1} - K_1 \tag{2.51}$$

with, which the combination of the rotational constants A, B, C, will allow to clarify the quantum mechanical Hamiltonian. The latter one, in a molecule-fixed axes system that originates in the center of mass and rotates with the molecule under investigation that has the axes coinciding with the principal axes of inertia a, b and c, for a rigid asymmetric rotor can be written as

$$\hat{\mathscr{H}}_r = A\hat{P}_a^2 + B\hat{P}_b^2 + C\hat{P}_c^2 \qquad with = \begin{cases} A & = \frac{\hbar^2}{8\pi^2 I_a} \\ B & = \frac{\hbar^2}{8\pi^2 I_b} \\ C & = \frac{\hbar^2}{8\pi^2 I_c} \end{cases} \tag{2.52}$$

With the rearrangement proposed by Ray [174] the Hamiltonian become

$$\hat{\mathscr{H}}_r = \frac{1}{2}(A+C)\hat{P}^2 + \frac{1}{2}(A-C)\hat{\mathscr{H}}_{(\kappa)} \tag{2.53}$$

$$\hat{\mathscr{H}}_{(\kappa)} = \hat{P}_a^2 + \tau\hat{P}_b^2 - \hat{P}_c \tag{2.54}$$

where $\hat{\mathscr{H}}_{(\kappa)}$ is the Reduced Hamiltonian. The advantage of this formulation is that the eigenvalues of $\hat{\mathscr{H}}_{(\kappa)}$, namely the energies, depend only on the inertial asymmetry parameter τ, leaving unaltered the dependence from the individual rotational constants.

Even though the use of this contrivance, the Hamiltonian is such that the resolution of the Schrödinger equation is not possible. Is for this reason that the asymmetric rotor expression is represented by a linear combination of symmetric rotor functions

$$\Psi_{J,\tau,M} = \sum_{J,K,M} a_{J,K,M}\psi_{J,K,M} \tag{2.55}$$

with

$$\psi_{J,K,M} = \Theta_{J,K,M}e^{iK\phi}e^{iM\chi} \tag{2.56}$$

where

$$\Theta_{J,K,M} = N_{J,K,M}\left(\sin\frac{\theta}{2}\right)^{|K-M|}\left(\cos\frac{\theta}{2}\right)^{|K+M|}F\left(\sin^2\frac{\theta}{2}\right) \tag{2.57}$$

Being the symmetric rotor wave functions orthonormal, as stated by

$$\delta_{J,K,M} = \begin{cases} 1 & J',K',M' = J,K,M \\ 0 & J',K',M' \neq J,K,M \end{cases} \tag{2.58}$$

$\hat{P}^2$, $\hat{P}_z$ and $\hat{P}_Z$ result simultaneously diagonal, but remembering that $\hat{\mathscr{H}}_r$ is a function of P_a^2, P_b^2 and P_c^2, is in term of these latter that the matrix elements have to be defined. The Schrödinger equation of our system can be defined as

$$\hat{\mathscr{H}}_r\Psi = E\Psi \tag{2.59}$$

that can be written as

$$\hat{\mathscr{H}}_r\Psi_{J,\tau,M} = E\Psi_{J,\tau,M} \tag{2.60}$$

where, not being $\Psi_{J,\tau,M}$ a complete base for the asymmetric rotor, can be written as in 2.55; this gives

$$\sum_{J,K,M} a_{J,K,M}\hat{\mathscr{H}}_r\psi_{J,K,M} = E\sum_{J,K,M} a_{J,K,M}\psi_{J,K,M} \tag{2.61}$$

In a different form, it can be expressed as

$$\sum_{J,K,M} a_{J,K,M}\int_{-\infty}^{+\infty}\psi^*{}_{J',K',M'}\hat{\mathscr{H}}_r\psi_{J,K,M}\mathrm{d}\tau = E\sum_{J,K,M} a_{J,K,M}\int_{-\infty}^{+\infty}\psi^*{}_{J',K',M'}\psi_{J,K,M}\mathrm{d}\tau \tag{2.62}$$

Now, since we previously note that the total angular momentum is a constant of the motion, there are no off-diagonal matrix elements in J; the matrices for each J value can therefore be independently treated. Additionally, being the matrix elements also independent from the spacial orientation of $\hat{\mathbf{P}}$, we can also not consider M. We then

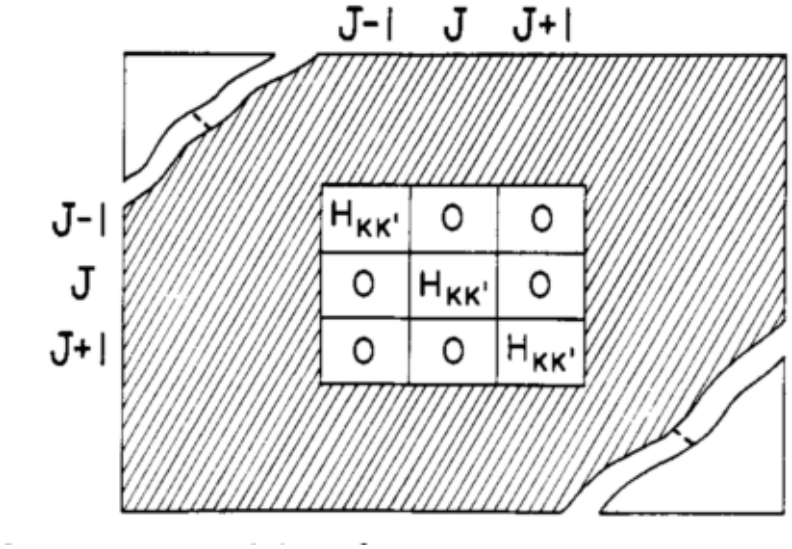

FIGURE 2.2: A graphical rappresentation of K blocks into J ones [172].

obtain the following homogeneous linear equations in K,

$$\sum_{K,K'=-J}^{+J} \left(\hat{\mathscr{H}}_{K',K} - \delta_{K,K'}\lambda\right) a_{J,K,M} = 0 \tag{2.63}$$

The values of λ are given by the resolution of the secular equation, for each of which there are $(2J+1)$ values. A clue of how it graphically appears is given in figure 2.2.

$$\left|\hat{\mathscr{H}} - \mathbf{I}\lambda\right| = 0 \tag{2.64}$$

Since in the equation 2.53 $\frac{1}{2}(A+C)\hat{P}^2$ contributes only diagonally and not K dependently, and $\frac{1}{2}(A-C)$ can be consider as a multiplicative factor of $\hat{\mathscr{H}}_{(\kappa)}$, a reduced energy matrix $\mathbf{E}_{(\kappa)}$ can only to this latter be associated. Consequently the secular determinant can be written as

$$|E_\kappa - \mathbf{I}\lambda| = 0 \tag{2.65}$$

for which the values of energy are

$$E_{K,K} = \langle J,K,M|\,\hat{\mathscr{H}}_{(\kappa)}\,|J,K,M\rangle = F\left[J(J+1) - K^2\right] + GK^2 \tag{2.66}$$

$$E_{K,K\pm2} = \langle J,K,M|\,\hat{\mathscr{H}}_{(\kappa)}\,|J,K,M\rangle = H\left[f(J,K\pm1)\right]^{\frac{1}{2}} \tag{2.67}$$

where

$$f(J,K\pm1) = \frac{1}{4}\left[J(J+1) - K(K\pm1)\right]\left[J(J+1) - (K\pm1)(K\pm2)\right] \tag{2.68}$$

The total rotational energy can therefore be written as

$$E = \frac{1}{2}(A+C)\,J(J+1) + \frac{1}{2}(A-C)\,E_{J\tau(\kappa)} \tag{2.69}$$

with F, G and H as constants depending on how the main axes are assigned. In this

case, dealing with a prolate molecule, among the six cases the type I^r is employed, for which the symmetry axis z is associated with a axis and the energy matrix become diagonal ($H = 0$) [172]. Being the diagonal matrix element

$$-J(J+1)+2K^2_{-1} \tag{2.70}$$

the energy is

$$E = CJ(J+1)+(A-C)K^2_{-1} \tag{2.71}$$

To this point the Hamiltonian would be therefore already solvable, but for completeness it has to be said that due to its symmetry[13] a group of symmetry operations take place. These latter are known as the *Four-group Symmetry group* and can be summarized in table 2.1. Taking into account that the matrix elements are just numerical

TABLE 2.1: The Four-group characters

Symmetry Species	E	C_2^a	C_2^b	C_2^c
A	1	1	1	1
B_a	1	1	-1	-1
B_b	1	-1	1	-1
B_c	1	-1	-1	1

B refers to twofold rotation about the two not considered axes and *A* refers to a function that is invariant with respect to all symmetry operations. In subscript and apexes reference is made to the axis in question.

quantities, they have to remain invariant under a coordinates transformation. This means that $\hat{\mathscr{H}}$ belongs to the species A, fact also supported by the symmetry of the wave function, that has to remain the same. As a consequence, a secular determinant for any J, hence the one referring to Ks, can be splitted up among all the components of the Four-group, facilitating the final calculation. From the knowledge of the eigenvalues, namely the energies measured in the experimental sessions, the resolution of the energy matrix 2.63 makes it therefore possible, for every submatrix, traces the energies back to their relative states. The successive normalized eigenvectors will consequently be able to give, after diagonalization, the reduced energies of the energy matrix itself, process for which iterative matrix diagonalizations procedures must be used [172].

2.4 Slightly asymmetric rotor

What has been presented in the last chapter concerned a top-asymmetric rotor. However, even if what has been said is true for many molecules, it does not include them all. Some of these are affected by great asymmetries, but there are also others that can be classified as slight asymmetric rotors. For these latter, their energies can be imagined as an expansion in series of powers of an asymmetric parameter. In this regard, the Wang parameter [175] will be introduced below.

[13] In addition to the identity operation E about each one of the principal axes of inertia, a rotation of 180° is possible.

Let's take into consideration the near-prolate rotor type I^r; introducing this new parameter it is possible to express the Hamiltonian as

$$\hat{\mathscr{H}}_r = A\hat{P}_a^2 + B\hat{P}_b^2 + C\hat{P}_c^2 = \frac{1}{2}(B+C)\hat{P}^2 + \left[A - \frac{1}{2}(B+C)\right]\hat{\mathscr{H}}(b_p) \tag{2.72}$$

with

$$\hat{\mathscr{H}}(b_p) = \hat{P}_a^2 + b_p(\hat{P}_c^2 - \hat{P}_b^2) \tag{2.73}$$

where the a axis is the unique axis of quantisation [172]. The Wang asymmetric parameter is defined as

$$b_p = \frac{C-B}{2A-B-C} = \frac{\kappa+1}{\kappa-3} \quad \begin{cases} -1 & \leq b_p \leq 0 \\ b_p & = -\frac{1}{3} \text{ (maximum asymmetry level)} \end{cases} \tag{2.74}$$

The nonvanishing matrix elements are

$$\langle J,K,M|\,\hat{P}^2\,|J,K,M\rangle = \hbar J(J+1) \tag{2.75}$$

$$\langle J,K,M|\,\hat{\mathscr{H}}(b_p)\,|J,K,M\rangle = K^2 \tag{2.76}$$

$$\langle J,K,M|\,\hat{\mathscr{H}}(b_p)\,|J,K\pm,M\rangle = b_p\left[f(J,K\pm1)\right]^{\frac{1}{2}} \tag{2.77}$$

As previously mentioned, through symmetric operations is possible to simplify the Wang operator in order to obtain four submatrices, with the only difference that now the matrix elements of these are given by equations 2.76 and 2.77. As a result we have

$$E = \frac{1}{2}(B+C)\,J\,(J+1) + \left[A - \frac{1}{2}(B+C)\right]W_{J\tau}\,(b_p) \tag{2.78}$$

Hence, until now, the asymmetric rotor can be decomposed into:

Prolate symmetric limit

$$\begin{cases} B = C \\ b_p = 0 \\ W_{J\tau}\,(b_p) = K_{-1}^2 \end{cases} \tag{2.79}$$

Asymmetric rotor

Near asymmetric limit

$$\begin{cases} B = C \\ b_p \approx 0 \\ W_{J\tau}\,(b_p) = K_{-1}^2 + C_1 b_p \\ +C_2 {b_p}^2 + C_3 {b_p}^3 + \ldots \end{cases} \tag{2.80}$$

where C_i terms, in reference to b_p, are evaluated by perturbation techniques considering $\hat{\mathscr{H}}(b_p)$ as the perturbation operator. The same is valid for the oblate rotor type III^r, with the difference that for the subscript of b instead of $_p$ is used $_0$, giving the parameter b_0. It's value is then

$$b_0 = \frac{A-B}{2C-B-A} = \frac{\kappa-1}{\kappa+3} \quad \begin{cases} -1 & \leq b_0 \leq 0 \\ b_p & = -\frac{1}{3} \text{ (maximum asymmetry level)} \end{cases} \tag{2.81}$$

with the associated energy

$$E = \frac{1}{2}(A-B)\,J\,(J+1) + \left[C - \frac{1}{2}(A+B)\right]W_{J\tau}\,(b_0) \tag{2.82}$$

Oblate symmetric limit

$$\begin{cases} A = B \\ b_0 = 0 \\ W_{J\tau}(b_0) = K_1^2 \end{cases} \tag{2.83}$$

Asymmetric rotor

Near asymmetric limit

$$\begin{cases} A = B \\ b_0 \approx 0 \\ W_{J\tau}(b_0) = K_1^2 + C_1 b_0 \\ + C_2 {b_0}^2 + C_3 {b_0}^3 + \dots \end{cases} \tag{2.84}$$

2.5 The non-rigid rotor

Until now we have treated the object under investigation as a rigid body, thing that could not be far from the truth. What we actually have is that between each nucleus there is a restoring force such that, when subjected to rotation, the molecule is led to deform the binding distances and the angles between the nuclei that form it. Our molecule then passes from being in an equilibrium configuration to a distorted one, with the consequence that the moment of inertia can no longer be considered constant and independent of the rotational state. Although the effect of this phenomenon is decidedly lower than the contribution that comes from the principle term of the rotational Hamiltonian, it is not possible to do without considering it. Indeed, being the former proportional to the rotational energy, it becomes more and more evident as the rotational energy increases, albeit giving a smaller contribution, even at low J.

Since we can consider the distortion as a departure from what is the equilibrium configuration, we can express the displacement term[14] as a power series expansion in terms of the $3N-6$ R_i independent internal displacement coordinates, with

$$R_i = \delta r_i = r_i - r_i^e \tag{2.85}$$

If we assume that harmonic forces are retained, the potential energy can be expressed as

$$V = \frac{1}{2}\sum_{i,j} f_{ij} R_i R_j \tag{2.86}$$

where R_i are the internal coordinates and $f_{ij} = f_{ji}$ with f as the force harmonic constant[15]. The classical Hamiltonian can hence be expressed as

$$\hat{\mathscr{H}} = \frac{1}{2}\sum_{\alpha,\beta} \mu_{\alpha\beta}\hat{P}_\alpha \hat{P}_\beta + \frac{1}{2}\sum_{i,j} G_{ij}\hat{p}_i\hat{p}_j + V \qquad \begin{cases} \alpha, \beta\text{: take on values x,y,z} \\ \text{i, j: enumerate the various} \\ \text{internal coordinates} \end{cases} \tag{2.87}$$

where the first term represents the rotational energy with $\mu_{\alpha\beta}$ as an element of the inverse moment of inertia tensor and $\hat{P}_{\alpha,\beta}$ as the α,β component of $\hat{P}^2$. The second and third coefficients are related respectively to the kinetic and potential energy of the vibrational part, in which $\hat{p}_\mathrm{i}$ is the momentum conjugate to the coordinate R_i

[14] For small displacement.

[15] f respect to R_i rappresents a bond-streatching, an angle-bending or an interaction (i.e stretch-bend) force constant.

and G_{ij} the elements that arises when internal coordinates are used in molecular vibration problems [176]; but being us in this circumstance interested only in the rotation of the molecule, the second coefficient will not be herein considered. Hence, differentiating the Hamiltonian in respect to R_i in the no-vibration assumption we get

$$\frac{1}{2}\sum_{\alpha,\beta}\frac{\partial\mu_{\alpha\beta}}{\partial R_i}\hat{P}_\alpha\hat{P}_\beta+\frac{\partial V}{\partial R_i}=0 \qquad\qquad i=1,2,...,3N-6 \tag{2.88}$$

Approximating $\mu_{\alpha\beta}$ by a series expansion about the equilibrium $\mu^e_{\alpha\beta}$ we can write

$$\mu_{\alpha\beta}=\mu^e_{\alpha\beta}+\sum_i\mu^i_{\alpha\beta}R_i+... \qquad\qquad \mu^i_{\alpha\beta}=\left(\frac{\partial\mu_{\alpha,\beta}}{\partial R_i}\right)_e \tag{2.89}$$

Being at the equilibrium the first term is equal to zero and, having assumed a small displacement, only linear terms are considered. Likewise, differentiating the equation 2.86 with respect to R_i and considering the equation 2.89

$$\begin{aligned}\frac{1}{2}\sum_{\alpha,\beta}\mu^i_{\alpha\beta}\hat{P}_\alpha\hat{P}_\beta+\sum_j f_{ij}R_j&=0\\ R_j&=-\frac{1}{2}\sum_{i,\alpha,\beta}\left(f^{-1}\right)_{ji}\mu^i_{\alpha\beta}\hat{P}_\alpha\hat{P}_\beta\end{aligned} \tag{2.90}$$

that inserted in equation 2.89 gives

$$\mu_{\alpha\beta}=\mu^e_{\alpha\beta}-\frac{1}{2}\sum_{i,j,\gamma,\delta}\mu^{(i)}_{\alpha\beta}\left(f^{-1}\right)_{ij}\mu^{(j)}_{\gamma\delta}\hat{P}_\gamma\hat{P}_\delta \tag{2.91}$$

Now, replacing the equation 2.90 into 2.86, the potential energy looks like[16]

$$V=\frac{1}{8}\sum_{i,j,\alpha,\beta,\gamma,\delta}\mu^{(i)}_{\alpha\beta}\left(f^{-1}\right)_{ij}\mu^{(j)}_{\gamma\delta}\hat{P}_\alpha\hat{P}_\beta\hat{P}_\gamma\hat{P}_\delta \tag{2.92}$$

causing the classical rotational Hamiltonian to become equal to

$$\mathscr{H}=\frac{1}{2}\sum_{\alpha,\beta}\mu^e_{\alpha\beta}\hat{P}_\alpha\hat{P}_\beta+\frac{1}{4}\sum_{\alpha,\beta,\gamma,\delta}\tau_{\alpha,\beta,\gamma,\delta}\hat{P}_\alpha\hat{P}_\beta\hat{P}_\gamma\hat{P}_\delta \tag{2.93}$$

where

$$\tau_{\alpha,\beta,\gamma,\delta}=-\frac{1}{2}\sum_{ij}\mu^{(i)}_{\alpha\beta}\left(f^{-1}\right)_{ij}\mu^{(j)}_{\gamma\delta} \tag{2.94}$$

Now, while the first component of the classical rotational Hamiltonian for a semi-rigid rotor still represents the usual rigid rotor energy, the second one gives us the correction relative to its distortion, namely the centrifugal distortion. To note, regards the distortion constants there is no dependence on the rotational as well as the vibrational coordinates[17]. In any case, in a real situation certain constants depend on the vibrational coordinates and therefore of these must be considered functions. What in practice happens is that the principal moment of inertia, obtained from the

[16] $\sum_l f_{il}\left(f^{-1}\right)_{lj}=\delta_{ij}$

[17] Since, given the initial assumptions, at least for the latter it could not be otherwise.

spectrum of the ground state, is in fact the mediation on all the rotational levels of the ground level in question, returning what the true inertia moments are. About that, Wilson and Howard [177] and Darling and Dennison [178] have proposed a general vibro-rotational quantum mechanical Hamiltonian operator that, thanks to various perturbative treatments, managed to express the vibro-rotational energies of the relative levels.

We can see this same Hamiltonian as

$$\hat{\mathscr{H}} = \hat{\mathscr{H}}_r + \hat{\mathscr{H}}_d \tag{2.95}$$

$$\hat{\mathscr{H}}_r = \sum_\alpha B' \hat{P}_\alpha^2 \tag{2.96}$$

$$\begin{aligned}\hat{\mathscr{H}}_d &= \hat{\mathscr{H}}_d^{(4)} + \hat{\mathscr{H}}_d^{(6)} \\ &= \frac{\hbar^4}{4} \sum_{\alpha,\beta,\gamma,\delta} \tau_{\alpha,\beta,\gamma,\delta} \hat{P}_\alpha \hat{P}_\beta \hat{P}_\gamma \hat{P}_\delta + \hbar^6 \sum_{\alpha,\beta,\gamma,\delta,\epsilon,\eta} \tau_{\alpha,\beta,\gamma,\delta,\epsilon,\eta} \hat{P}_\alpha \hat{P}_\beta \hat{P}_\gamma \hat{P}_\delta \hat{P}_\epsilon \hat{P}_\eta\end{aligned} \tag{2.97}$$

with $\alpha, \beta, \gamma, \delta, \epsilon, \eta$ =x, y or z and the rotational constants as $B' = \frac{\hbar^2}{2I_\alpha}$[18], in which has been included the correction to the sextic term[19]. As a whole there are 729 coefficients, a fact that would create very long times to go back to the parameters of the Hamiltonian from experimental energies; a time that moreover can be vain to wait if we consider that few are the parameters that take part. For this reason, Watson ([179];[180];[181]) introduces a reduced Hamiltonian able to fit experimental data in terms of fundamental molecular parameters and does so by exploiting the fact that the eigenvalues must remain the same even after certain transformations. In this case, let U be a unitary operator[20]

$$U = e^{iS} \tag{2.98}$$

with S Hermitian, for which we can write

$$\tilde{\mathscr{H}} = U^{-1} \hat{\mathscr{H}} U \tag{2.99}$$

The transformation, through symmetry operations designated by S of equation 2.98 that are the same as the total symmetry species of the molecular point group, will enormously reduce the coefficients to be considered and with these the time requested, remaining however able to parameterize the energies from experimental source. The same Wilson devised a more elegant notation to define the general power series of equation 2.96, the so-called *standard form* [179]

$$\hat{\mathscr{H}}_{st} = \sum_{p,q,r=0}^{\infty} h_{pqr} \left(\hat{P}_x^p \hat{P}_y^q \hat{P}_z^r + \hat{P}_z^r \hat{P}_y^q \hat{P}_x^p \right) \tag{2.100}$$

to which derives the form of S of equation 2.98

$$S = \sum_{p,q,r=0} s_{pqr} \left(\hat{P}_x^p \hat{P}_y^q \hat{P}_z^r + \hat{P}_z^r \hat{P}_y^q \hat{P}_x^p \right) \tag{2.101}$$

With the action of the unitary transformation elements corrisponding to the relative

[18] With the $'$ it is indicated that B is an actual constant, which takes into account the vibrations too.
[19] Obtained from the same procedure used in order to obtain the quartic one [172].
[20] $U^{-1} = U\dagger$

molecular point group is then possible to "streamlined" the Hamiltonian terms obtaining for example an orthorhombic system for which only even n[21] are present, thus returning to a totally even group like A in table 2.1. Now that we have seen how these parameters come from, it is possible to understand what are the terms that make up the reduction that was specifically used, namely the *Symmetry top reduction S*. To get to this one must first see what the coefficients of the reduced form are. We can write $\hat{\mathscr{H}}$ as

$$\begin{aligned}\hat{\mathscr{H}} = &\left(B_x - 4R_6\right)\hat{P}_x^2 + \left(B_x - 4R_6\right)\hat{P}_y^2 + \left(B_z - 4R_6\right)\hat{P}_z^2 - D_J\hat{P}^4 - D_{JK}\hat{P}^2\hat{P}_z^2 \\ &-D_K\hat{P}_z^4 - \delta_J\hat{P}^2\left(\hat{P}_+^2 + \hat{P}_-^2\right) + R_5\{\hat{P}_z^2\left(\hat{P}_+^2 + \hat{P}_-^2\right) + \left(\hat{P}_+^2 + \hat{P}_-^2\right)\hat{P}_z^2 \\ &+R_6(\hat{P}_+^4 + \hat{P}_-^4)\end{aligned} \tag{2.102}$$

with the coefficients given by the first-order energy expression in table 2.2.

TABLE 2.2: Distortion Coefficients for the First-Order Energy

$\delta_J = D_J - \frac{2\delta\left(B+C\right)}{B-C} - 2R_6$
$\delta_J K = D_J K - 2\sigma\delta_J + 4\left(R_5 + 2\sigma R_6\right)\frac{B+C}{B-C}$
$\delta_K = D_K - 4\sigma\left(R_5 + 2\sigma R_6\right) - 10R_6$
$\sigma = \frac{2A-B-C}{B-C}$
$D_J = -\frac{1}{32}\{3\tau_{xxxx} + 3\tau_{yyyy} + 2\left(\tau_{xxyy} + 2\tau_{xyxy}\right)\}\hbar^4$
$D_K = D_J - \frac{1}{4}\{\tau_{zzzz} - \left(\tau_{xxzz} + 2\tau_{xzxz}\right) - \left(\tau_{yyzz} + 2\tau_{yzyz}\right)\}\hbar^4)$
$D_J K = -D_J - D_K - \frac{1}{4}\tau_{zzzz}\hbar^4$
$R_5 = -\frac{1}{32}\{\tau_{xxxx} - \tau_{yyyy} - 2\left(\tau_{xxzz} + 2\tau_{xzxz}\right) + 2\left(\tau_{yyzz} + 2\tau_{yzyz}\right)\}\hbar^4$
$R_6 = \frac{1}{64}\{\tau_{xxxx} + \tau_{yyyy} - 2\left(\tau_{xxyy} + 2\tau_{xyxy}\right)\}\hbar^4$
$\delta_J = -\frac{1}{16}\{\tau_{xxxx} + \tau_{yyyy}\}\hbar^4$

[172]

With the transformation operation $\tilde{\mathscr{H}}$ remains of the same shape as $\hat{\mathscr{H}}$, with the only difference that now the coefficients are given in the table 2.3, remembering that

TABLE 2.3: Distortion Coefficients for $\tilde{\mathscr{H}}$

$\tilde{D}_J = D_J + \frac{R_5}{\sigma}$
$\tilde{D}_J K = D_J K - \frac{6R_5}{\sigma}$
$\tilde{D}_K = D_K + \frac{5R_5}{\sigma}$
$\tilde{\delta}_J = \delta_J$
$\tilde{R}_6 = R_6 + \frac{R_5}{2\sigma}$

[172].

$$\sigma = \frac{2B_z - B_x - B_y}{B_x - B_y} \tag{2.103}$$

[21] $n = p + q + r$

we use, being us in the I^r representation, $\sigma = -\frac{1}{b_p}$ [22]. Consequently, the relative Hamiltonian, reduced by the utilization of the Hermitian S, can now be express as

$$\hat{\mathscr{H}}^{(S)} = \hat{\mathscr{H}}_r + \hat{\mathscr{H}}_d^{(4)} + \hat{\mathscr{H}}_d^{(6)} \tag{2.104}$$

in which, including also sextic terms,

$$\begin{aligned}
\hat{\mathscr{H}}_r &= B_x^{(S)}\hat{P}_x^2 + B_y^{(S)}\hat{P}_y^2 + B_z^{(S)}\hat{P}_z^2 \\
&= \frac{1}{2}\left(B_x^{(S)} + B_y^{(S)}\right) + \left[B_z^{(S)} - \frac{1}{2}\left(B_x^{(S)} + B_y^{(S)}\right)\right]\hat{P}_z^2 \\
&\quad + \frac{1}{4}\left(B_x^{(S)} - B_y^{(S)}\right)\left(\hat{P}_+^2 + \hat{P}_-^2\right) \qquad (2.105)\\
\hat{\mathscr{H}}_d^{(4)} &= -D_J\hat{P}^4 - D_{JK}\hat{P}^2\hat{P}_z^2 - D_K\hat{P}_z^4 + d_1\hat{P}^2\left(\hat{P}_+^2 + \hat{P}_-^2\right) + d_2\left(\hat{P}_+^4 + \hat{P}_-^4\right) \qquad (2.106)\\
\hat{\mathscr{H}}_d^{(6)} &= H_J\hat{P}^6 + H_{JK}\hat{P}^4\hat{P}_z^2 + H_{KJ}\hat{P}^2\hat{P}_z^4 + H_K\hat{P}_z^6 + h_1\hat{P}^4\left(\hat{P}_+^2 + \hat{P}_-^2\right) \\
&\quad + h_2\left(\hat{P}_+^4 + \hat{P}_-^4\right) + h_3\left(\hat{P}_+^6 + \hat{P}_-^6\right) \qquad (2.107)
\end{aligned}$$

Actual rotational constants are given by

$$\begin{aligned}
\tilde{B}_x &= B_x + 4\left(B_z - B_y\right)s_{111} \\
\tilde{B}_y &= B_y + 4\left(B_z - B_x\right)s_{111} \\
\tilde{B}_z &= B_z + 4\left(B_x - B_y\right)s_{111}
\end{aligned} \tag{2.108}$$

in which the Hermitian s is defined as

$$s_{111} = \frac{2R_5}{2B_z - B_x - B_y} \tag{2.109}$$

2.6 The hyperfine structure

So far in our analysis we have practically never considered the nucleus, but even this can play an important role, which specifically leads to what is known as nuclear hyperfine structure. In practice, looking at a set of molecules, we can say that mostly all the stable ones, and in particular the organic ones, possess the ground electrons paired with each other[23]. In the first order approximation of a stationary molecule the contributions of the electric and magnetic fields are absent because they cancel each others out; but when it begins to rotate, weak magnetic fields are generated and interacting with the nuclear magnetic moment produces in response a slight magnetic field that causes a displacement of the observed lines. In figure 2.3 there is a representation of the phenomenon.

In other words, the dipolar nuclear moment interaction originates from the interaction of a non-spherical distribution of the nuclear charge. This is the reason why atoms with nuclear spin of 0 and $\frac{1}{2}$, having spherical symmetry, are exempted from this phenomenon. Hence, is the interaction of the moment of nuclear quadrupole with the equally non-spherical electronic distribution around such nucleus that generates an electric field gradient in proximity of the nucleus itself. In responce a consequent torque is formed and this, in the attempt of realigning the nuclear spin in the direction of the field gradient, originates the nuclear precession frequency and the

[22] To bring us back to the symmetric Hamiltonian we use the equivalences $D_J = \tilde{D}_J, D_{JK} = \tilde{D}_{JK}, D_K = \tilde{D}_K, d_1 = -\delta_J, d_2 = \tilde{R}_6$.

[23] Therefore allocated in the singlet Σ state.

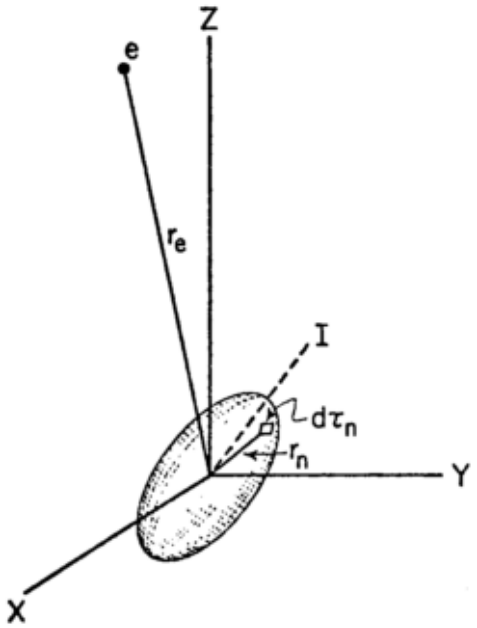

FIGURE 2.3: Nuclear interaction with extra-nuclear charges in an external fixed axes system [172].

annexed quadrupole nuclear spectrum. Since the dimensions of the core are finite we can express E like

$$E = \int \rho_n V \mathrm{d}\tau_n \tag{2.110}$$

where $\rho_n = \rho(X, Y, Z)$ is the density in the elemental nuclear volume $\mathrm{d}\tau_n = \mathrm{d}X\mathrm{d}Y\mathrm{d}Z$ with the potential V. Conveniently, V can be expanded with a Taylor's expansion

$$\begin{aligned} V = V_0 &+ \left(\frac{\partial V}{\partial X}\right)_0 X_n + \left(\frac{\partial V}{\partial Y}\right)_0 Y_n + \left(\frac{\partial V}{\partial Z}\right)_0 Z_n + \frac{1}{2}\left(\frac{\partial^2 V}{\partial X^2}\right)_0 X_n^2 \\ &+ \frac{1}{2}\left(\frac{\partial^2 V}{\partial Y^2}\right)_0 Y_n^2 + \frac{1}{2}\left(\frac{\partial^2 V}{\partial Z^2}\right)_0 Z_n^2 + \left(\frac{\partial^2 V}{\partial X \partial Y}\right)_0 X_n Y_n \\ &+ \left(\frac{\partial^2 V}{\partial X \partial Z}\right)_0 X_n Z_n + \left(\frac{\partial^2 V}{\partial Z \partial Y}\right)_0 Z_n Y_n + \ldots \end{aligned} \tag{2.111}$$

which inserted in equation 2.110 returns the first (E_0), the second (or dipole E_d) and the higher (E_Q) term

$$E_0 = V_0 \int \rho_n \mathrm{d}\tau_n \tag{2.112}$$

$$\begin{aligned} E_d = &\left(\frac{\partial V}{\partial X}\right)_0 \int X_n \rho_n \mathrm{d}\tau_n + \left(\frac{\partial V}{\partial Y}\right)_0 \int Y_n \rho_n \mathrm{d}\tau_n \\ &+ \left(\frac{\partial V}{\partial Z}\right)_0 \int Z_n \rho_n \mathrm{d}\tau_n \end{aligned} \tag{2.113}$$

$$
\begin{aligned}
E_Q = &\frac{1}{2}\left(\frac{\partial^2 V}{\partial X^2}\right)_0 \int X_n^2 \rho_n \mathrm{d}\tau_n + \frac{1}{2}\left(\frac{\partial^2 V}{\partial Y^2}\right)_0 \int Y_n^2 \rho_n \mathrm{d}\tau_n \\
&+\frac{1}{2}\left(\frac{\partial^2 V}{\partial Z^2}\right)_0 \int Z_n^2 \rho_n \mathrm{d}\tau_n + \left(\frac{\partial^2 V}{\partial X \partial Y}\right)_0 \int \rho_n X_n Y_n \mathrm{d}\tau_n \\
&+\left(\frac{\partial^2 V}{\partial X \partial Z}\right)_0 \int X_n Z_n \rho_n \mathrm{d}\tau_n + \left(\frac{\partial^2 V}{\partial Z \partial Y}\right)_0 \int \rho_n Z_n Y_n \mathrm{d}\tau_n \\
&+... \qquad (2.114)
\end{aligned}
$$

Now, being equation 2.112 independent in respect to the nuclear orientation, it does not interest us. Furthermore, equation 2.113 cancels because of the simmetry of $\rho_n = \rho(X, Y, Z)$ that integrated will always garantee that positive values cancel the corrisponding negtive ones. What remains is the second derivative given by equation 2.114. Once again consider a body fixed system and place the molecule on it with z parallel to I; the terms given by the integrals of the crossed components vanish, and it results

$$
\int \rho_n x_n^2 \mathrm{d}\tau_n = \int \rho_n y_n^2 \mathrm{d}\tau_n = \frac{1}{2}\int \rho_n (x_n^2 + y_n^2)\mathrm{d}\tau_n = \frac{1}{2}\int \rho_n (r_n^2 - z_n^2)\mathrm{d}\tau_n \qquad (2.115)
$$

Consequently, it is possible to express equation 2.114 as

$$
E_Q = \frac{1}{4}\left[\left(\frac{\partial^2 V}{\partial x^2}\right)_0 + \left(\frac{\partial^2 V}{\partial y^2}\right)_0\right]\int \rho_n (r_n^2 - z_n^2)\mathrm{d}\tau_n + \frac{1}{2}\left(\frac{\partial^2 V}{\partial z^2}\right)_0 \int \rho_n z_n^2 \mathrm{d}\tau_n \qquad (2.116)
$$

Remembering that the charge causing the field gradient can be considered zero over the volume due to the Laplace's equation $\nabla^2 V = 0$

$$
\left(\frac{\partial^2 V}{\partial x^2}\right)_0 + \left(\frac{\partial^2 V}{\partial y^2}\right)_0 = -\left(\frac{\partial^2 V}{\partial z^2}\right)_0 \qquad (2.117)
$$

This latter equation, 2.117, makes possible to write the equation 2.116 as

$$
E_Q = \frac{1}{4}\left(\frac{\partial^2 V}{\partial z^2}\right)_0 \int \rho_n (3z_n^2 - r_n^2)\mathrm{d}\tau_n \qquad (2.118)
$$

Defining Q^* as the intrinsic nuclear quadrupole moment with the value

$$
Q^* = \frac{1}{e}\int \rho_n (3z_n^2 - r_n^2)\mathrm{d}\tau_n \qquad (2.119)
$$

equation 2.118 becomes

$$
E_Q = \frac{1}{4}\left(\frac{\partial^2 V}{\partial z^2}\right)_0 eQ^* \qquad (2.120)
$$

In the quantum mechanical case $\mathbf{I}$ and Q^* are not observable quantities [24] but can be expressed as a function of Q as

$$
Q^* = \frac{2(I+1)}{(2I-1)}Q \qquad (2.121)
$$

Essentially Q^*, whose information is shown in table 2.4, becomes a parameter that accounts for the nuclear deviation from sphericity.

[24] Only $\mathbf{I}^2$ has eigenvalues.

TABLE 2.4: Possible values of Q^*

Q^*'s value	geometry
positive	prolate
0	spherical
negative	oblate

At positive and negative Q^* corresponds respectively prolate and oblate rotors [172].

From a quantum point of view, the nuclear spin **I** moment is coupled with the molecular rotational angular momentum **J** to give the total angular momentum **F**. We can think of **I** and **J** in precession around **F** as in figure 2.4. The associated quantum numbers are F, M_F and J [25] and have values

$$F = J + I, J + I - 1, J + I - 2, ..., |J - I| \tag{2.122}$$
$$M_F = F, F - 1, F - 2, ..., -F \tag{2.123}$$

In $\hbar$ units the eigenvalues are given by

$$\langle F, M_F | \hat{\mathbf{F}}^2 | F, M_F \rangle = F(F+1) \tag{2.124}$$
$$\langle F, M_F | \hat{F}_Z | F, M_F \rangle = M_F \tag{2.125}$$

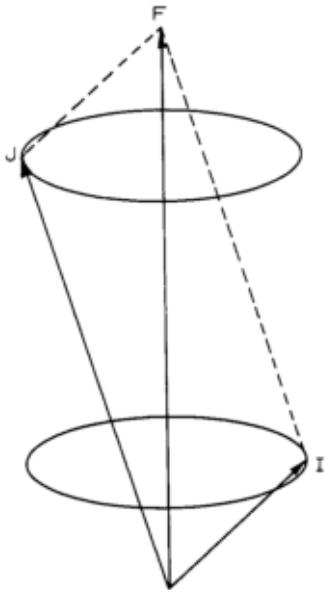

FIGURE 2.4: Coupling vector diagram of **I** and **J** forming **F** [172].

[25] J^2 remains a constant of the motion even after a treatment of the first order.

To obtain the relative Hamiltonian, to the equation 2.114 has to be added and subtracted $\frac{1}{6}\nabla^2 V \int \rho_n R_n^2 \mathrm{d}\tau_n$; the result one obtains is

$$\begin{aligned} E_Q = \frac{1}{6}\Bigg[& \left(\frac{\partial^2 V}{\partial X^2}\right)_0 \int (3X_n^2 - R_n^2)\rho_n \mathrm{d}\tau_n + \Big[\left(\frac{\partial^2 V}{\partial Y^2}\right)_0 \int (3Y_n^2 - R_n^2)\rho_n \mathrm{d}\tau_n \\ & + \Big[\left(\frac{\partial^2 V}{\partial Z^2}\right)_0 \int (3Y_n^2 - R_n^2)\rho_n \mathrm{d}\tau_n + 6\left(\frac{\partial^2 V}{\partial X \partial Y}\right)_0 \int X_n Y_n \rho_n \mathrm{d}\tau_n \\ & + 6\left(\frac{\partial^2 V}{\partial X \partial Z}\right)_0 \int X_n Z_n \rho_n \mathrm{d}\tau_n + 6\left(\frac{\partial^2 V}{\partial Y \partial Z}\right)_0 \int Y_n Z_n \rho_n \mathrm{d}\tau_n \Bigg] \\ & + \frac{1}{6}\left[\left(\frac{\partial^2 V}{\partial X^2}\right)_0 + \left(\frac{\partial^2 V}{\partial Y^2}\right)_0 + \left(\frac{\partial^2 V}{\partial Z^2}\right)_0\right] \int R_n^2 \rho_n \mathrm{d}\tau_n \end{aligned} \tag{2.126}$$

Remembering the Laplace's equation $\nabla^2 V = 0$, 2.126 can be expressed as

$$E_Q = -\frac{1}{6}\mathbf{Q} \otimes \nabla \mathbf{E} = \frac{1}{6} \sum_{i,j=X,Y,Z} Q_{ij} V_{ij} \tag{2.127}$$

where

$$\nabla \mathbf{E} = \mathbf{e}_X \frac{\partial \mathbf{E}}{\partial X} + \mathbf{e}_Y \frac{\partial \mathbf{E}}{\partial Y} + \mathbf{e}_Z \frac{\partial \mathbf{E}}{\partial Z} \tag{2.128}$$

$$\mathbf{Q} = \int \rho_n \left[3\mathbf{R}_n \mathbf{R}_n - \left(\mathbf{e}_X \mathbf{e}_X + \mathbf{e}_Y \mathbf{e}_Y + \mathbf{e}_Z \mathbf{e}_Z\right) R_n^2\right] \mathrm{d}\tau_n \tag{2.129}$$

in which Q represents the quadruple dyadic moment[26], while $\nabla \mathbf{E}$ is the electric field gradient of an extra nuclear charge, with R_n that stands for the vector locating points of the nuclear volume in the space-fixed X, Y, Z. From here it is possible to develop the quantum mechanical operator for the quadrupole interaction energy [172] as

$$\hat{\mathscr{H}}_Q = \frac{eQq_J}{2J(2J-1)I(2I-1)} \left[3(\mathbf{I}\cdot\mathbf{J})^2 + \frac{3}{2}\mathbf{I}\cdot\mathbf{J} - \mathbf{I}^2\cdot\mathbf{J}^2\right] \tag{2.130}$$

Derived for the first time by Casimir [182], it is applicable to a coupling nucleus of any type of molecule, with Q_J related to the type of molecule considered. Thinking that

$$\mathbf{F}^2 = (\mathbf{J}+\mathbf{I})^2 = \mathbf{J}^2 + 2\mathbf{J}\cdot\mathbf{I} + \mathbf{I}^2 \tag{2.131}$$

$$\mathbf{I}\cdot\mathbf{J} = \frac{1}{2}\left(\mathbf{F}^2 - \mathbf{J}^2 - \mathbf{I}^2\right) \tag{2.132}$$

$\mathbf{I}\cdot\mathbf{J}$ eigenvalues in $\hbar$ units are

$$\langle F, J, I| \left(\mathbf{J}\cdot\mathbf{I}\right) |F, J, I\rangle = \frac{1}{2}\left[F(F+1) - J(J+1) - I(I+1)\right] = \frac{1}{2}C \tag{2.133}$$

$$\langle F, J, I| \left(\mathbf{J}\cdot\mathbf{I}\right)^2 |F, J, I\rangle = \frac{1}{4}C^2 \tag{2.134}$$

[26] If we consider a particular orthogonal Cartesian reference system the dyad can also be expressed as the sum of elementary dyads, therefore as $a_i\bar{k}_i b_j\bar{k}_j = \left(\sum_{i=1}^3 a_i\bar{k}_i\right)\left(\sum_{j=1}^3 b_j\bar{k}_j\right) = \sum_{i=1}^3 \sum_{j=1}^3 a_i b_j \bar{k}_i\bar{k}_j$.

Consequently, the energy of the Hamiltonian 2.130 can be expressed as

$$E_Q = \frac{eQq_J}{2J(2J-1)I(2I-1)}\left[\frac{3}{4}C(C+1) - J(J+1)I(I+1)\right] \tag{2.135}$$

where

$$C = F(F+1) - J(J+1) - I(I+1) \tag{2.136}$$

and q_J expressible as

$$\begin{aligned} q_J = q_{aa}\langle J,i,M_J = J|\,\Phi^2_{Za}\,|J,i,M_J = J\rangle + q_{bb}\langle J,i,M_J = J|\,\Phi^2_{Zb}\,|J,i,M_J = J\rangle \\ +q_{cc}\langle J,i,M_J = J|\,\Phi^2_{Zc}\,|J,i,M_J = J\rangle \end{aligned} \tag{2.137}$$

q_{ij} in the equation 2.137 is the molecular field gradient at the coupling nucleus with reference to the inertial axes, and is utterable as

$$\frac{\partial^2 V}{\partial a^2} = q_{aa}, \qquad \frac{\partial^2 V}{\partial a \partial b} = q_{ab}, \qquad \ldots \tag{2.138}$$

while Φ^2 (always with a, b, c referred to the internal axes) is given by[27]

$$\frac{\partial a}{\partial Z} = cos\theta_{Z,a} = \Phi_{Z,a} \tag{2.139}$$

Combining the equations 2.137 and 2.135, we get

$$E_Q = \sum_{g=a,b,c} \chi_{gg}\langle J,i,M_J = J|\,\Phi^2_{Z,g}\,|J,i,M_J = J\rangle\left[\frac{\frac{3}{4}C(C+1) - J(J+1)I(I+1)}{2J(2J-1)I(2I-1)}\right] \tag{2.140}$$

where

$$\chi_{aa} = eQq_{aa,}, \qquad \chi_{bb} = eQq_{bb}, \qquad \chi_{cc} = eQq_{cc} \tag{2.141}$$

Now, thanks to the relation

$$\langle J,i,M_J = J|\,\Phi^2_{Z,g}\,|J,i,M_J = J\rangle = \frac{2}{(J+1)(2J+3)}\langle J,i|\,J^2_g\,|J,i\rangle + \frac{1}{2J+3} \tag{2.142}$$

that subsists between the diagonal elements of the matrix of Φ^2 when $M_J = J$ and the diagonal elements of the matrix J^2_g in the representation of the unperturbed rotor in the base J, I, M_J, the same 2.140 can be written in the slenderer alternative configuration

$$E_Q = \frac{2}{(J+1)(2J+3)}\sum_{g=a,b,c}\chi_{gg}\langle J,i|\,J^2_g\,|J,i\rangle\left[\frac{\frac{3}{4}C(C+1) - J(J+1)I(I+1)}{2J(2J-1)I(2I-1)}\right] \tag{2.143}$$

[27] Z, keep in mind, fixed in space.

2.7 Microwave transitions and selection rules

So far it has been seen from where the Hamiltonians originated, what they are made of and how it is possible to trace the quantized energy associated with the system, but it has not yet been seen what behaviour these transitions have and what measurable parameters they are associated to. In the attempt to give a comprehensive, even profoundly limited, picture of this theoretical introduction we will therefore in this section try to discuss about these two latter topics. In a molecular system having a dipole moment, electromagnetic radiation will associate with the former to give a transition when $h\nu = \Delta E$. In this case the electric dipole, being coupled with the electric component of the radiation, will generally be responsible for rotational transitions. We can therefore say that the frequency associated with this transition from a lower state m to an upper state n, namely the resonance frequency, is given by

$$\nu_{mn} = \frac{E_n - E_m}{h} \tag{2.144}$$

Therefore, being $\rho(\nu_{mn/nm})$ the density of the radiation $\nu_{mn/mn}$, $B_{mn/nm}$ the absorption and emission coefficients of a particular particle and A_{mn} the spontaneous emission coefficient[28], the probability of such an event is

$$p_{m\to n} = \rho(\nu_{mn})B_{m\to n} \tag{2.145}$$
$$p_{m\leftarrow n} = \rho(\nu_{mn})B_{m\leftarrow n} + A_{m\leftarrow n} \tag{2.146}$$

It can be demonstrated [183] that for an isotropic radiation the probability is

$$p_{m\to n} = \frac{8\pi^3}{3h^2}\left[|\langle m|\,\mu_X\,|n\rangle|^2 + |\langle m|\,\mu_Y\,|n\rangle|^2 + |\langle m|\,\mu_Z\,|n\rangle|^2\right]\rho(\nu_{mn}) \tag{2.147}$$

where, as we know,

$$|\langle m|\,\mu_F\,|n\rangle| = \int \psi_m^* \mu_F \psi_n \mathrm{d}\tau \tag{2.148}$$

with $F = X, Y, Z$. Being the dipole moment matrix Hermitian, it follows that

$$B_{mn} = B_{m\to n} = B_{m\leftarrow n} = \frac{8\pi^3}{3h^2}\left[|\langle m|\,\mu_X\,|n\rangle|^2 + |\langle m|\,\mu_Y\,|n\rangle|^2 + |\langle m|\,\mu_Z\,|n\rangle|^2\right] \tag{2.149}$$

where the quantities $\langle m|\,\mu_{i=X,Y,Z}\,|n\rangle$ are the matrix elements of the dipole in the representation of the space fixed axes system which diagonalize the energy matrix [29]. By indicating the cosine of this angle as $\Phi_{(Fg)}$ and assuming to have a transition from a state $|J, K, M,\rangle$ to a $|J', K', M'\rangle$ one for an asymmetric molecule, therefore referring to τ instead of K, the induced absorption coefficient or stimulated emission is

$$B_{J,\tau,M\to J',\tau',M'} = \frac{8\pi^3}{3h^2}\sum_{F=X,Y,Z}\left|\langle J,\tau,M|\,\mu_F\,|J',\tau',M'\rangle\right|^2 \tag{2.151}$$

[28] Called "the Einstein coefficients" because by him formulated. Among other things, Einstein had assumed the equivalence of the two B_s, which was then confirmed by quantum mechanical calculations and experimental evidence.

[29] More generally, being able to express μ_F in relation to the body fixed system as

$$\mu_F = \sum_g cos(Fg)\mu_g \tag{2.150}$$

with μ_g component of the permanent dipolar moment along the main axis of inertia and $cos(Fg)$ the cosine of the angle between the internal and external reference system.

Just the fact of observing transitions in certain levels rather than others, that translated means the components for which the matrix elements do not vanish, gives rise to what are known as the *selection rules* which for an asymmetrical rotor are

$$\Delta J = 0, \pm 1 \qquad \Delta M = 0, \pm 1 \tag{2.152}$$

while for ΔK values can assume the ones in table 2.5 The induced emission coeffi-

TABLE 2.5: Assumable ΔK values

Dipole Content	ΔK_{-1}	ΔK_{+1}
$\mu_a \neq 0$	$0, \pm 2, ...$	$\pm 1, \pm 3, ...$
$\mu_b \neq 0$	$\pm 1, \pm 3, ...$	$\pm 1, \pm 3, ...$
$\mu_c \neq 0$	$\pm 1, \pm 3, ...$	$0, \pm 2, ...$

Values assumed by K in an asymmetric rotor [172].

cient turns out to be

$$A_{m \to n} = \frac{64\pi^4 \nu_{mn}^3}{3hc^3} \left[|\langle m| \mu_X |n\rangle|^2 + |\langle m| \mu_Y |n\rangle|^2 + |\langle m| \mu_Z |n\rangle|^2 \right] \tag{2.153}$$

but being A dependent on the cube of ν its contribution is irrelevant in the microwave region. If we now ask ourselves what is the power associated with a transition we notice that, given V the volume of the sample, the number of molecules undergoing a transition from m to n is given by

$$P_{m \to n} = V N_m p_{m \to n} h\nu_{mn} = V N_m B_{mn} \rho(\nu_{mu}) h\nu_{mn} \tag{2.154}$$

while that for a stimulated emission is

$$P_{m \leftarrow n} = V N_n B_{mn} \rho(\nu_{mn}) h\nu_{mn} \tag{2.155}$$

Not being in the case of a maser, the population of m is generally greater than that of n, which produces a negative ΔP. Assuming a condition of thermal equilibrium[30] we can use the Boltzmann distribution[31] and express the absorbed power as

$$P_{abs} = -\Delta P = V N_m \left(1 - e^{\frac{-h\nu_{mn}}{k_B T}} \right) B_{mn} \rho(\nu_{mn}) h\nu_{mn} \tag{2.157}$$

By defining the absorption coefficient α

$$\alpha = -\frac{1}{\Delta P} \frac{\Delta P}{\Delta x} \tag{2.158}$$

and the volume element as $\Delta V = S\Delta x$, the energy density as and the number of particles as $\rho(\nu) = P/cS$, the number of molecules in the state m $N_m = NF_m$ with

[30] Thermal relaxation is rapid if compared with the rate of exchange of the molecular energy related the applied field.

[31] At the equilibrium the Boltzmann distribution requires

$$\frac{N_n}{N_m} = e^{\frac{-h\nu_{mn}}{k_B T}} \tag{2.156}$$

F_m the fraction of molecules in the state m, we define

$$\alpha = \frac{NF_m\left(h\nu_{mn}\right)^2}{ck_BT}\left(1 - \frac{1}{2}\frac{h\nu_{mn}}{k_BT} + ...\right)B_{mn} \tag{2.159}$$

that in the case of rotational spectroscopy, expanding in series and truncating it to the first member since $h\nu < k_BT$

$$\alpha \approx \frac{NF_m\left(h\nu_{mn}\right)^2}{ckT}B_{mn} \tag{2.160}$$

Assuming an isotropic radiation [32], replacing the value of B_{mn} and multiplying by a normalized function S(ν, ν_0) we obtain

$$\alpha_\nu = \frac{8\pi^3 NF_m\nu^2}{3ck_BT}\left(1 - \frac{1}{2}\frac{h\nu}{k_BT}\right)S\left(\nu,\nu_0\right)\left[\left|\langle m|\,\mu_X\,|n\rangle\right|^2 + \left|\langle m|\,\mu_Y\,|n\rangle\right|^2 + \left|\langle m|\,\mu_Z\,|n\rangle\right|^2\right] \tag{2.161}$$

with ν any frequency in the absorption range and ν_0 the frequency of the absorption peak. When ν_0 equals ν then what is known as peak absorption coefficient α_{max} is obtained, which is

$$\alpha_{max} = \frac{8\pi^2 NF_m\nu_0^2}{3ck_BT(\Delta\nu)}\left(1 - \frac{1}{2}\frac{h\nu_0}{k_BT}\right)\left|\langle m|\,\mu\,|n\rangle\right|^2 \tag{2.162}$$

However, there are two factors that mainly affect the measurement of the absorption frequency. The first is the Doppler effect, a phenomenon resulting from the non-homogeneity of the molecular beam. Let v denote the speed with which the nth molecule moves with respect to the incident radiation. The frequency variation that is recorded is given by the Doppler formula

$$\nu = \nu_0\left(1 + \frac{v}{c}\right) \tag{2.163}$$

in which v, having a positive or negative value, will respectively increase or decrease the detected frequency. The molecules of a gas in thermal equilibrium, having a Maxwell-Boltzmann velocity distribution, will give rise to a Doppler shift according to

$$S_d(\nu,\nu_0) = S_0 e^{\left[-\frac{mc^2}{2k_BT}\left(\frac{\nu-\nu_0}{\nu_0}\right)^2\right]} \tag{2.164}$$

The line broadening from the Doppler effect $2\left(\Delta\nu\right)_d$, referred to half of the recorded line, will have a value given by [33]

$$2(\Delta\nu)_d = \frac{2\nu_0}{c}\left(\frac{2Nk_BT\ln 2}{M}\right)^{\frac{1}{2}} \tag{2.165}$$

which replaced in equation 2.164 expresses the line-shape function caused by the Doppler effect as

$$S_d(\nu,\nu_0) = S_0 e^{\left[-(\ln 2)\left(\frac{\nu-\nu_0}{(\Delta\nu)_d}\right)^2\right]} \tag{2.166}$$

[32] Ideal case.

[33] M = molecular weight in atomic mass.

If then the equation 2.165 is inserted in the equation 2.161[34], for $h\nu \ll k_B T$ therefore in this case of study, what is obtained when the pressure is much lower than the critical pressure[35] is

$$\alpha_\nu(p \leqslant p_c) = C\nu^2 p e^{\left[-(\ln 2)\left(\frac{\nu-\nu_0}{(\Delta\nu)_d}\right)^2\right]} \tag{2.167}$$

with C a constant independent of the pressure and the frequency. Substituting in equation 2.167 the resonance frequency ν_0 as ν and the critical pressure p_c as p let the maximum absorption coefficient becomes

$$(\alpha_{max})_d = C\nu_0^2 p_c \tag{2.168}$$

Obtaining C_ν, from the ratio between the absorption coefficient of a frequency ν and the maximum absorption coefficient, we obtain the normalized Doppler-broadened line shape function whose in figure 2.5 is visible the trend.

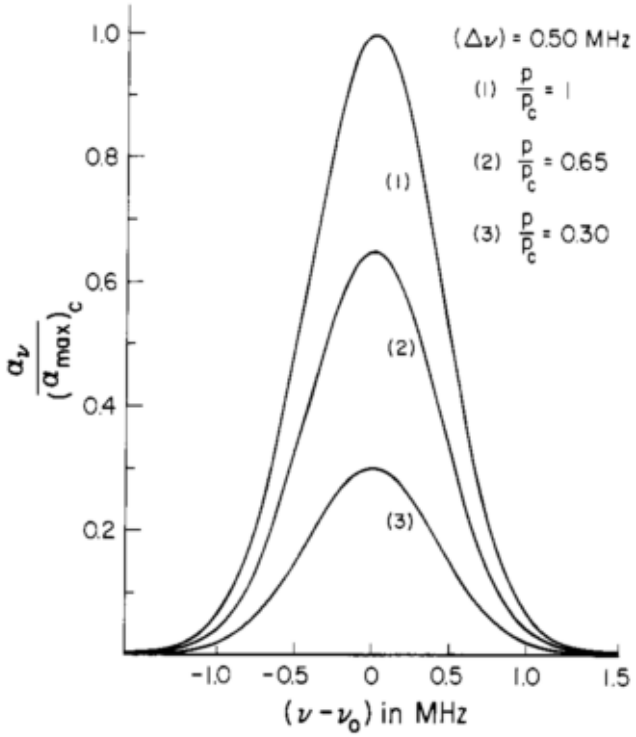

FIGURE 2.5: Doppler-brodened line shape [172].

[34]With $N = 9.68 \times 10^{18} \frac{p_{mm}}{T}$ where p_{mm} is the pressure in mm of Hg and T the absolute temperature.

[35]The value beyond which the lines begin to expand due to the collisions between the molecules belonging to the sample.

The second factor that most affects the broadening of the line is the pressure enlargement due to collisions between the investigated molecules. The lifetime of a line, that is the time in which a state of excitement persists before decaying, is dictated by the uncertainty principle. We can roughly write

$$\Delta t \Delta E \approx \hbar \tag{2.169}$$

which corresponds to the frequency spread

$$\Delta\nu = \frac{\Delta E}{h} \approx \frac{1}{2\pi(\Delta t)} \tag{2.170}$$

Now, assuming that there are only spontaneous emissions as the cause of lifetime,

$$\Delta t = \frac{1}{A_{mn}} = \frac{3hc^3}{64\pi^4\nu_{mn}^3 |\langle m|\, \mu\, |n\rangle|^2} \tag{2.171}$$

which with equation 2.153 becomes

$$\Delta\nu \approx \frac{32\pi^3\nu_{mn}^3}{3hc^3} |\langle m|\, \mu\, |n\rangle|^2 \tag{2.172}$$

Due to collisions, however, this time decreases. By calling τ the average time a state lives, the same difference in frequency can be referred to as $\Delta\nu = \frac{1}{2\pi\tau}$ At low pressure when at the half-width $\Delta_\nu \ll \nu_0$ the function can be described by a Lorentzian one

$$S(\nu, \nu_0) = \frac{1}{\pi}\left[\frac{\Delta\nu}{(\nu_0 - \nu)^2 + (\Delta_\nu^2)}\right] \tag{2.173}$$

where $\Delta\nu = \frac{1}{2\pi\tau}$, τ is the mean time between collisions and ν_0 is the resonant frequency peak. Bearing in mind that at very low pressure τ is inversely proportional to the pressure, therefore that the difference of the one is proportional to the difference of the other, and that the number of absorbent particles also increases linearly with pressure, knowing that

$$\Delta_\nu \approx 300 p_{mn} \frac{\Delta\nu_t}{T} \tag{2.174}$$

and taking into account that $N = 9.68 \times 10^{18} \frac{p_{mn}}{T}$ it is possible to write the absorption coefficient as a function of pressure and temperature. It is

$$\alpha_\nu = C\nu^2\left[\frac{(\Delta\nu)_1 p^2}{(\nu - \nu_0)^2 + (\Delta_\nu)_1^2 p^2}\right] \tag{2.175}$$

with p the pressure, $\Delta\nu_1$ the widening of the frequency to $p = 1$ mm and T=300 K. Obtaining C, once again independent from pressure and frequency, and imposing $\nu = \nu_0$ we obtain the maximum absorption coefficient

$$\alpha_{max} = \frac{C\nu_0^2}{(\Delta\nu)_1} \tag{2.176}$$

and expressing the relationship of the two results

$$\frac{\alpha_\nu}{\alpha_{max}} = \frac{\left(\frac{\nu}{\nu_0}\right)^2}{\left[\frac{\nu-\nu_0}{p(\Delta\nu)_1}\right]^2+1} \tag{2.177}$$

whose progress is shown in the figure 2.6.

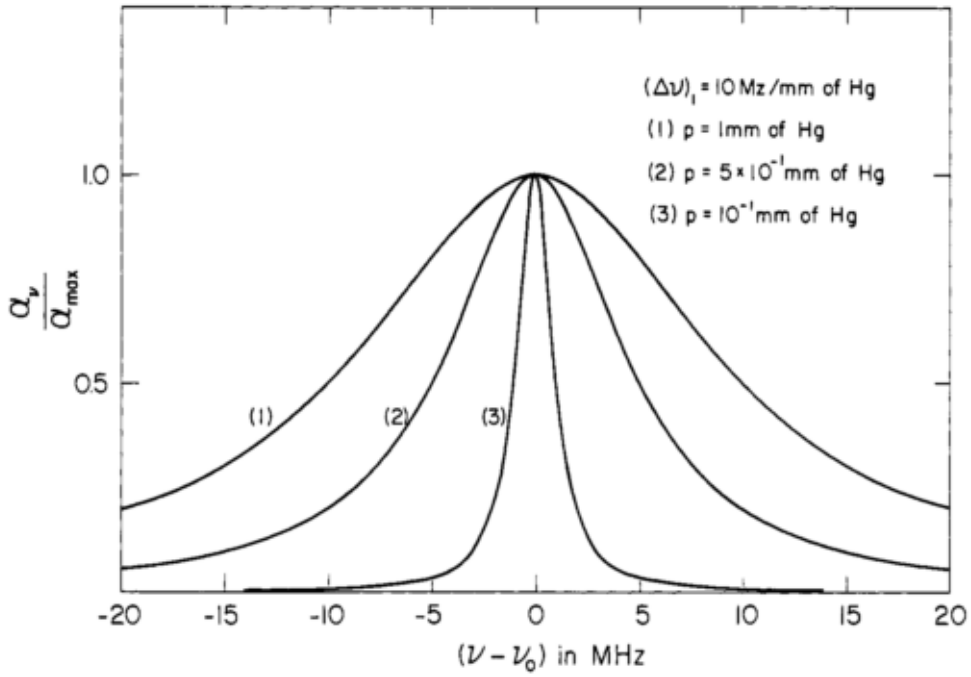

FIGURE 2.6: Pressure broadening where the line width is directly proportional to the pressure [172].

Even more general is the function of Van Vleck-Weisskopf [184], for which

$$S(\nu,\nu_0) = \frac{\nu}{\pi\nu_0}\left[\frac{\Delta\nu}{(\nu_0-\nu)^2+(\Delta_\nu)^2} + \frac{\Delta\nu}{(\nu_0+\nu)^2+(\Delta_\nu)^2}\right] \tag{2.178}$$

which is applicable to both low and relatively higher pressure regimes. As an example in the figure 2.6 we see how at low pressures when the Δ_ν decreases the second term of equation 2.178 drops its contribution until resemble a pure Lorentzian function.

Chapter 3

Software

Over the years, spectroscopists have gradually enriched the collection of molecular species spectra. Initially started from more identifiable atmospheric and astronomical molecules, over time they broaden the research target increasing the volumes of the registered catalogs[36]. At the same time, with the progress of the instrumentation itself, the need to keep certain archives always up to date emerged and the necessity of a shared catalog with a common formalism became as clear as essencial. The first to move in this direction, building the AFGL database [185](later HITRAN, an acronym for High Resolution Transmission), have been those who were working in the infrared region, while those that were working in longer wavelengths, having them effective Hamiltonians capable of well fitting the spectra, began to develop the first softwares that starting from dipolar moments were able to predict intensities. Successively, with the arrival of increasingly performing microprocessors and algorithms, sotfware have become more and more complicated allowing to approximate complex molecular Hamiltonians with perturbation theory, pushing further the proliferation of these analyzes; but with a problem, namely the same encountered in developing catalogs: a common formalism.

Initially written in FORTRAN at Caltech University under the name of CALPAM,[37] H.M Pickett created in his suite the first angular moments operators formulation. The software, downloadable at the Jet Propulsion Laboratory website [186], was developed using the idea that most angular moments could have been well modeled with second-rank tensor in a spherical harmonics base. With the use of an expression to which commutation and anti-commutation operations are applicable and with the use of scalars, isotropic and anisotropic operators the organization of the input in generalizable matrix blocks returns an almost complete set of quantum mechanical parameterizations [187]. In addition to others, the most used compilations that have been used also in this work are Spfit and Spcat, acronyms standing respectively for Spin Fitting and Spin Cataloging.

The Spfit input data are those contained in the *.par and in the *.lin[38] files, which stand respectively for spectroscopic parameters and observed frequencies with corresponding spectroscopic assignments. At runtime the operators contained in the *.par are parsed and the codes that associate the symmetry, Hamiltonian block and angular momentum type are set [187]. Once the run is over the initial *.par is overwritten with the new results given in the fit that takes into account the contributions coming from the lines of the *.lin file. Spfit's output files include the *.fit (bearing the least-squares of the fitted parameters and the difference between the observed and calculated transition), the *.bak (copy of the input *.par), the *.par (in which a new set of parameters, their numbers and the number of input transitions are provided)

[36] An archive in which spectra are stored.

[37] Which stands for California Programs, but also in the other accepted form, Calculation Programs.

[38] "*" refers to the name * of the file to be recalled in the prompt when the program is launched.

[188] and most importantly the *.var (in which there are the new parameters and the correlation matrix among the fitted parameters). In both cases, inputs and outputs are in text files format.

Spcat input files are the *.var and the *.int. The first, produced by Spfit, contains the spectroscopic variables of the molecule under examination while the second provides information about intensities, such as temperature, component of the dipole moment, partition function, frequencies of transitions and the required limit of quantum numbers. Once processed, the data provided in the output are the *.cat, *.str, *.egy and *.out files, corresponding respectively to the catalog (the most important of the four) of the predicted tansitions frequencies, the strenght, the energies and the eigenvalues.

The manner in which Pickett identified the operators of the effective Hamiltonian is shown below. Given this simple rotational Hamilonian (i.e. asymmetric rigid rotor, no distortion terms)

$$H_{rot} = AN_a^2 + BN_b^2 + CN_c^2 \tag{3.1}$$

the numerical code that identifies N is 10000, which multiplied by the code of the specific rotational constant will form the corrisponding term. If **N** is an end over end rotational operator of the angular momentum and **S** is the total electronic spin angular momentum, $\mathbf{J} = \mathbf{N} + \mathbf{S}$ which for the singlet state is reduced to $\mathbf{J} = \mathbf{N}$[39]. The general operator code (in the nine digits representation) used by Pickett is

$$S_2 S_1 n|Op|kjv'v'' \tag{3.2}$$

where Op stands for the operator and it is indicated by two digits, v' and v" are the "pure" energy terms defined by the state identifiers v' and v" (can be on diagonal, v'=v", or off diagonal v'$\neq$v"), j can be used to define the rotational constant (J=1) or the distortional constants (j$\leq$9), k applies to N_z^2 (i.e. the projection of the angular momentum onto a fixed axis within the molecule), S_1 to spin-spin coupling and S_2 to symmetries of the periodic functions utilized. The 3.2 operator code refers to the matrix element

$$\left[N(N+1)\right]^j K^{2k} \left(\mathbf{N}\cdot\mathbf{S}\right)^n \langle NK| \, |Op| \, |N'K'\rangle \tag{3.3}$$

with N quantum number for molecular rotation, K quantum number for the projection of **N** along the *a* inertial axis, **S** the total spin electron angular momentum. As an example of this notation, considering a prolate rotor in the representation I^r, $Op = 0$ stands for a scalar, $1 = N_aN_a$, $2 = N_bN_b$, $3 = N_cN_c$, $4 = N_+^2 + N_-^2$, $5 = N_+^4 + N_-^4$, $6 = N_+^6 + N_-^6$, $20 = N_a$, $21 = N_bN_c + N_cN_b$, etc., from which it is apparent that also the ladder operators are included in this operator code. To clarify, the operator for the centrifugal distortion d_2 ($N_+^4 + N_-^4$) in the Watson's S-reduction Hamiltonian for a vibrational state $v = 1$ is indicated with the abbreviation |5|0011. In the case where $v = 0$, the abbreviation is reformulated as |5|0000 [188]. The headers of the files are shown below, indicating the abbreviations and their meanings.

Having the *.var and *.par files the same header[40], table 3.1 shows how they are organized while as example in figure 3.1 the header of the *.par file of the TA conformer is presented. The black background is due to the text editor, in this case Sublime text, but the arrangement of the information remains unchanged between

[39] Here the electronic orbital angular momentum $\mathbf{L} = 0$, otherwise $\mathbf{N} = \mathbf{R} + \mathbf{L}$ with **R** rotational angular momentum of the molecule.

[40] The only difference among these two files is that once the part dedicated to the parameters is finished, in the *.var file the diagonalization matrix is reported.

different editors. Table 3.3 reports the meanings of the different acronyms listed in Table 3.1. Keep in mind that if, as specified in table 3.3, the VSYM in the *.var

TABLE 3.1: *.var and *.par organization

* file name											
NPAR	*NLINE*	*NITR*	*NXPAR*	*THRESH*	*ERRTST*	*FRAC*	*CAL*				
CHR	*SPIND*	*NVIB*	*KNMIN*	*KNMAX*	*IXX*	*IAX*	*WTPL*	*WTMN*	*VSYM*	*EWT*	*DIAG*
(Additional lines)											
(Parameters lines)											
⋮											

A summary of the abbreviations of *.var and *.par. Second and third lines are freeform[189].

```
Allyl-imine -- (trans,anti)
  20  278    5    0     0.0000E+00     1.0000E+06     1.0000E+00 1.0000000000
s   1   2   0  50   0   1   1   1  -1   99  0  8
s   3   1   0  50   0   1   1   1   0   99  0  8
        10099   4.577363421565976E+04 1.35305146E-03 /A
        20099   4.560931356295580E+03 8.46004772E-05 /B
        30099   4.148248498978513E+03 8.20531493E-05 /C
```

FIGURE 3.1: How the header of the TA.par and TA.lin look like.

TABLE 3.2: Parameter lines in *.var and *.par files

IDPAR	**PAR**	**ERPAR**	**LABEL**
Parameter identifier	Parameter value	Parameter uncertainty	Parameter label

Acronyms and relative meanings for the parameters and relative values and errors for *.par and *.var files [189].

and *.par is negative, in table 3.1 there will be a third row with the same acronyms of the second, fact that also happens in the figure 3.1. Namely, in the case of study that in this thesis will shortly be presented this was done to take into account the quadrupole moment that otherwise would not have been considered. Specifically, we set two "fictitious" vibrational states: both refer to the ground state but one is defined without hyperfine structure (SPIND = 1) while the other takes it into account (SPND = 3). Then there is, both in *.par and *.var files, the section dedicated to the parameters which is summarized in table 3.2. Above was said that Spfit need the *.par and the *.lin files to run. In the figure 3.2 some lines of the TA.lin file are therefore presented. Starting from the left side, the quantum numbers are grouped starting from the higher to the lower ones, as J', K_a', K_c', n', F ', J, K_a, K_c, n, F. F, the quantum number of the total angular momentum, for the state that has no quadrupole coupling (n, n'= 0) will assume the value of J, while in the case in which n, n' = 1 (that is when SPND = 3, quadrupole considered) it will take J and J$\pm$ 1 values. Continuing in the same order one then finds the experimental frequencies [MHz], the associated error [MHz] and the WGT (the relative weight to be considered in the weighted average).
Spfit's product was said to be the *.fit file. The latter is divided into three parts. The

TABLE 3.3: *.var and *.par's acronyms

First line's nomenclature	
NPAR	Maximum number of parameters
NLINE	Maximum number of state
NITR	Maximum number of iterations
NXPAR	Number of parameters to exclude from the list when fitting special lines
THRESH	Initial Marquardt-Levenberg parameter
ERRTST	Maximum [(obs-calc)/error]
FRAC	Fractional importance of variance
CAL	Scaling for infrared line frequencies
Second line's nomenclature	
CHR	Character to modify parameter names file sping.nam. In this case we use "s", which stands for Watson S set
SPIND	If positive means an asymmetric rotor quanta. Indicates the degeneracy of spins
NVIB	Positive, prolate rotor (z = a, y = b, x = c). Number of vibronic states on the first option line, identity of the vibronic state on all but the first option line
KNMIN,KNMAX	Minimum and maximum K values
IXX	Binary flags for inclusion of interactions: bit 0 set means no $\Delta N \neq 0$ interactions
IAX	Axis for statistical weight ($1 = a$)
WTPL,WTMN	Statistical weights for even and odd state
VSYM	If VSYM is negative, signal that the next line is also an option line. If VSYM is positive or zero, signal that this is the last option line. In the multiple option line mode, the magnitude of VSYM is ignored
EWT	It concerns symmetric rotators; in this case 99 is an out of scale value arbitrarily assigned by the operator
DIAG	It is related to different kinds of energy ordering (in our case, DIAG = 0 means energy ordering within the Wang sub-blocks)
XOPT	It is related to the phase choice (in our case, XOPT = 8 means the standard)

Acronyms and relative meanings for the first and second nomenclature line of *.par and *.var files [189].

FIGURE 3.2: A fistful of TA.lin lines.

upper part summarizes the parameters used and a series of other additional parameters [41]; in the central part there is a list of all the recorded lines disposed in the

[41] For further information, look at the website https://spec.jpl.nasa.gov/ftp/pub/calpgm/spinv.pdf

same arrangement of the *.lin file with the estimated frequency on the right of the corrispective experimental one and, continuing further to the right, the differences between the two. Finally, at the bottom of the document the normalized matrix, the new parameters with the relative estimated errors, the average of the differences between the observed and estimated frequencies and two errors are shown. The latter ones are the Microwave RMS and the RMS Error, whose forms are reported in the equation 3.4.

$$\begin{aligned} MicrowaveRMS &= \sqrt{\left(\frac{\sum (obs - calc)}{N_{lines}}\right]^2} \\ RMSerror &= \sqrt{\left[\frac{\sum (obs - calc) \cdot error}{N_{lines}}\right]^2} \end{aligned} \tag{3.4}$$

We mentioned above that information about the molecule is contained in the *.int file. An example of how its header appeares is reported in figure 3.3, while in table 3.4 one can recognise what the index names refer to and in table 3.5 and 3.6 the meanings of these latters.

```
Allyl imine -- trans,anti
111   55001   119120.8571   0   100    -9.0   -9.0   500.   300.
111   1.31
112   1.66
***
```

FIGURE 3.3: The header of the TA.int.

TABLE 3.4: *.int organization

* file name								
FLAGS	*TAG*	*QROT*	*FBGN*	*FEND*	*SRT0*	*STR1*	*FQLIM*	TEMP
Value line	Dipole constant							
⋮								

A summary of the abbreviations of *.int. Second and third lines are freeform [189].

TABLE 3.5: FLAGS index in the *.int file

FLAGS $TYP \cdot 10000 + I1 \cdot 1000 + V2 \cdot 100 + V1 \cdot 10 + SYM$	
IRFLG	If 0 constants are in MHz
OUTFLG	0 for short form *.out
STRFLG	1, 2 to enable *.str output
EGYFLG	0 to enable *.egy energy listing; 2 to enable *.egy derivative listing

Acronyms and their meanings for the FLAGS index in the *.int file [189].

TABLE 3.6: *.int acronyms

First line's nomenclature	
TAG	Catalog species tag (integer)
QROT	Partition function for TEMP
FBGN	Beginning integer F quantum (round up)
FEND	Ending integer F quantum (round up)
SRT0	Log strength cutoffs
STR1	Log strength cutoffs
FQLIM	Frequency limit in GHz
TEMP	Temperature for intensity calculation in degrees K (default is 300K)
Dipole constants	
IDIP	Dipole identifier. The value is given by $TYP \cdot 10000 + I1 \cdot 1000 + V2 \cdot 100 + V1 \cdot 10 + SYM$. In our case the TYP (dipole typology) and I1 (isotopic species) indices will be zero, while the vibrational indices V2 and V1 will both be 1. SYM identifies the axis along which the identified dipole moment lies and is equal to 1 for the dipole along the axis a and 2 along the axis b. Basically the indexes are respectively 111 and 112
DIPOLE	Dipole value

Acronyms and relative meanings for the second and third line of *.int files [189].

Having now *.var and *.int files, Spcat can return the corresponding *.cat file to the user: an example is given with the figure 3.4 while the corresponding information contained is arranged as shown in table 3.7.

```
2456.6570  0.0055 -8.6063 3  157.3250 61  55001140530 427 130  31 328 131
2457.1646  0.0057 -8.5921 3  157.3250 63  55001140530 427 131  31 328 132
2457.1811  0.0057 -8.6201 3  157.3250 59  55001140530 427 129  31 328 130
3330.2280  0.0065 -8.3837 3  185.4514 69  55001140534 332 134  33 429 133
```

FIGURE 3.4: The appearance ot the TA.cat file.

TABLE 3.7: Order (and format) of the information contained in the *.cat file

$1^{st}col.$	$2^{nd}col.$	$3^{rd}col.$	$4^{th}col.$	$5^{th}col.$	$6^{th}col.$	$7^{th}col.$
frequency of the transaction	estimated error	intensity log_{10} of the expected transition	degrees of freedom	energy of the lower state of the transaction	upper state degeneracy	tags and quantum numbers of the level considered

Meanings of the values for the first line of the TA.cat files [189] of figure 3.4. *Col.* stays for column and columns beyond the 7^{th} are included in the $7^{th}col.$

Chapter 4

Instrumentation

The experimental data used for the drafting of this work have been collected in the year 2019, during a period abroad made possible by the *Erasmus+ for internship* program. Specifically, the experiments have been carried out at the Center for Astrochemical Studies (CAS) of the Max Planck für extraterrestrische Physik of Garching (Germany), employing the CASAC frequency modulation spectrometer. The instrument is equipped with a pair of Pyrex tubes with a length of 3 m and a diameter of 5 cm each in which it is possible to study the target molecules that can be produced through two different ways: one tube is devoted to the study of molecules produced by pyrolysis while the second one is dedicated to the study of molecules produced by DC-discharge. Anyway, in this specific case the data collected derive from the use of the first cell only. The configuration of the overall instrument is for completeness presented in figure 4.1.

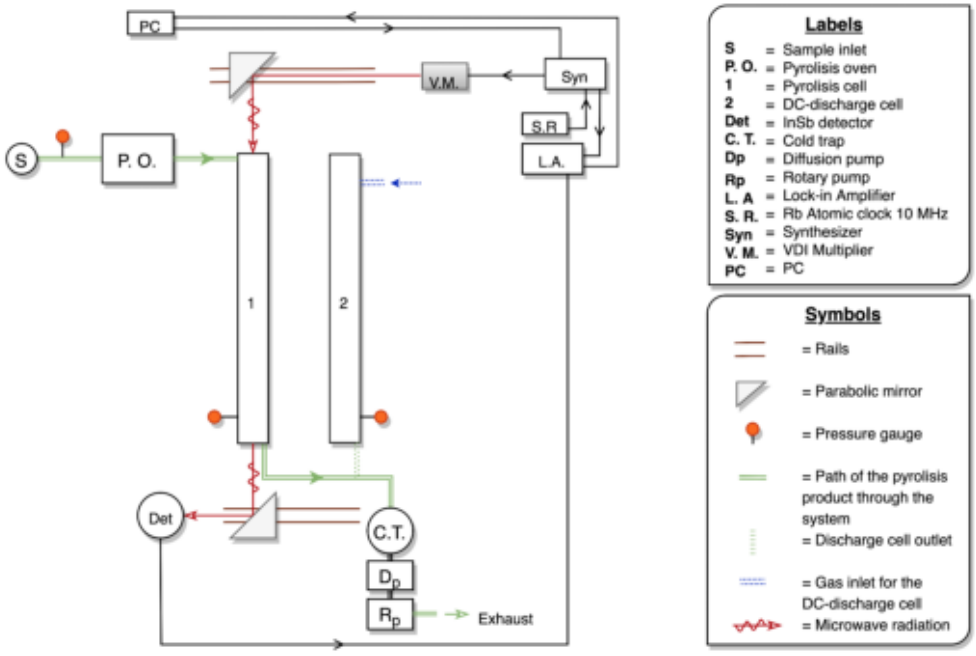

FIGURE 4.1: The header of the TA.int.

Both cells are kept under vacuum with the aid of two pumps arranged in series: once the rotary pump (R_p in figure 4.1) reaches a pressure of approximately 10 mTorr the diffusive pump (D_p in figure 4.1) starts to operate by further lowering the pressure to values close to a few 10^{-4} Torr units. A series of valves makes it possible to reduce

the flow or isolate the cells from the pumping system. Additionally, if circumstances require it, a cold trap (*C. T.*, figure 4.1) can be filled by liquid nitrogen.

The analysis begins when at point *S* of figure 4.1 the vapors of the precursor contained in a sample holder enter, sucked by the pressure difference generated by the pumps, through a T-shape Pyrex pype. The flow that brings them from one to the other is regulated by a metering valve and at one of the two T-shape Pyrex pype extremity. Here the first capacitance pressure gauge (*Baratron*) monitors its pressure (that usually ranges from 100 mTorr to 1 T). The last end connects with a quartz tube which, passing through the electric oven (*Carbolite*) [42], transports the pyrolysed gas into the absorption cell. At the entrance of the latter an additional valve allows to further regulate the flow of the pyrolised gas which is now let to expand in the cell (*1*, figure 4.1). An additional check of the pressure is done by the second *Baratron* pressure gauge, located at the end of the cell itself; its value at this point generally ranges from 0.5 mTorr to 10 mTorr.

Regarding the microwave signal, this is generated by the synthesizer (*Syn*, figure 4.1, model *Keysight E8257D*) operating in the centimeter wavelengths (1 to 60 GHz). In order to have achieve an absolute frequency calibration the synthesizer is connected to an atomic Rubidium standard (*Stanford Research Systems*) which provides a frequency of 10 MHz. The frequencies then arrive at the *VDI multiplier chain* (*Virginia Diodes*) which brings them up between 82 and 1100 GHz. The electromagnetic waves leaving the *VDI* hit a parabolic mirror allocated on a rail[43] and passing through a high density polyethylene window enter the cell. The electromagnetic waves leaving the VDI hit a parabolic mirror allocated on a rail, pass through a high density polyethylene window, enter the cell and emerge from another high density polyethylene window; then, hitting a second parabolic mirror get focused t a liquid-He cooled InSb hot electron bolometer (QMC Instr. Ltd.) used as a detector. Frequency modulation is achieved by modulating the carrier signal with a sine wave at a rate of 15 kHz, and then demodulating the detector output at 2f using a digital lock-in amplifier (SRS SR830). In this way, the second derivative of the actual absorption profile is recorded by the computer controlled acquisition system [190].

[42] 1600°C can be reached.

[43] The rail allows the mirror adjustment parallelly to the beam in order to optimize the signal and change the configuration of the instrument whether the DC-discharge cell is requested.

Chapter 5

Analysis of the Spectra and Results

The first to experimentally determine the rotational constants of 2-Propen-1-Imine, CH_2CHCNH, was Robert E. Penn in 1978. Once obtained it through the pyrolysis of diallylamine, he determined the rotational constants and some other parameters of this unstable molecule [169]. 2-Propen-1-Imine consists of four rotamers characterized as *trans* or *cis* with respect to rotation about the central C-C bond by the letters *T* and *C* respectively, and *syn* or *anti* with respect to the imino hydrogen position by the letters *S* and *A*, respectively. In view of the fact that *trans* rotamers of similar molecules such as butadiene, propenal and glyoxal are much more stable than *cis* rotamers, it is expected to find a dominance of TS and TA rotamers in the microwave spectra ([191];[192];[193]). In this regard, taking advantage from a more advanced instrumentation, the collection of a more precise set of lines of these two aforementioned conformers will allow to reach an enhanced level of accuracy which translates into the possibility of obtaining more accurate rotational constants values and centrifugal distortion parameters. This precision increasement will consequently lead to the generation of a more accurate prediction lines catalog that will then provide astrophysicists with a reliable tool in the search and detection of the pure rotational spectra of 2-Propen-1-Imine in the microwave survey of the interstellar medium.

After empirical tests prior to the conducted analysis, it has been seen that moving from 400°C (Penn) to 900°C in temperature and keeping a pressure of about 150 mTorr (0.2 mbar) in input of the oven and 2-3 mTorr (2.5-4 µbar) in the cell (adjusting the flow) were the best conditions with which conduct the analyzes. In order to obtain an accurate central transition frequency, the absorption line has been modeled using proFFit line profile analysis code[194] with the employment of a Voigt profile analysis. Specifically, the search of more precise lines of the 2-Propen-1-Imine's conformers has been conducted starting from previous reported lines (Penn, 1978) and from ab-initio calculation data; their assignment has been then accomplished in a straightforward way. Starting from low frequencies the .lin file of the conformer under investigation has been gradually updated with the corresponding registered lines; at the same time, adopting the Watson S-reduced Hamiltonian for asymmetric-top molecules ([179], Spfit has been made to run in order to return, through an iterative non-linear least squares fitting procedure, a new set of constants. Costituing them the model of the whole molecule itself, it has been possible to predict from scratch the transitions that in the successive experimental analysis would have been searched and registered into the .lin file. In this regard, successively rising in J, K_a and K_c values, every new line contribution has made possible to refine the constants: realizing how the successive observed transitions were differing from the *.cat file expected ones it has been possible to tackle them with the addition in the *.par file of distortional parameters that, taking into account the contribution given by the centrifugal distortions, have allowed the calculation to converge reasonably. To see the errors associated with the individual lines, refer to Appendix A and Appendix B for

TA and TS, respectively.
Approximately, about 300 lines for TA and 350 for TS have been recorded in the range that goes from ~85 GHz up to ~350 GHz, reaching a maximum value for the quantum number J of 71 and 69 for the conformer TA and TS respectively. The line measured by Penn have also been included in the fit, but with lower statistical weight to take into account their lower measurement. Specifically, for the data taken from the literature we assumed an uncertainty of 500 kHz while different statistical weights ($w_i = 1/\sigma_i^2$) have been adopted for each ith datum to account for the different measurement precisions. Generally, in our measurements an estimated uncertainty (σ_i) of 15 kHz is assigned to *a-type* and *b-type* lines for both TA and TS.

5.1 TA rotamer

The TA conformer of the planar molecule 2-Propen-1-Imine, figure 5.1, is a near-prolate ($\kappa = -0.980$) asymmetric rotor aligned mainly along the a principal axis.

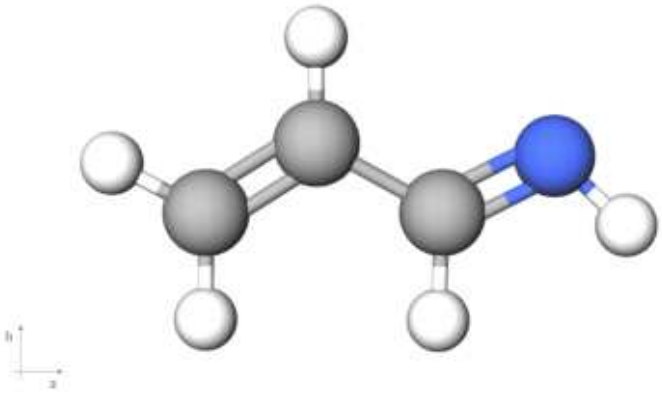

FIGURE 5.1: *Trans Anti* 2-Propen-1-Imine.

The angle between CNH has a value of circa 111.7°and the NH bond has a lenght of about 1.014 Å[169]. The rotamer has dipole moments $\mu_a = 1.31$ D (Debye) and $\mu_b = 1.66$D which consequently lead to transitions along the a and b axes; *a-type* and *b-type* transitions are therefore in the spectrum obtained. Entirely, 256 new rotational transitions have been collected including R ($\Delta J = +1$) *a-type* lines and P ($\Delta J = -1$), Q ($\Delta J = 0$) and R *b-type* lines, with J values ranging from 7 to 71 (lower belonging to Penn), K_a values from 0 to 19 and energies from 3 to 11.5 cm^{-1}. Quadrupole splitting due to electric quadrupole coupling of the ^{14}N nucleus ($I = 1$) has been observed in quite a large number of transitions (in this case the F number is considered instead of J). Owing to the hyperfine structure, a total number of 198 line frequencies have been measured. Not infrequently, due to the merging of a pair of hyperfine components during the analysis, rather than the three components that should in principle have been seen in this case only two lines have been observed. In these cases the frequency of the transition has been averaged between the two components taking into account the relative intensities.
The final fits have a weighted root mean square (RMS) deviations of 0.905 MHz and lead to the determination of the complete set of quartic centrifugal distortion constants, six sextic constants, i.e. $H_J, H_{JK}, H_{KJ}, H_K, h_1$ and h_3 and a quadrupole constant

(i.e. $(\chi_{bb-cc})/4$). The resulting parameters are listed in Table 5.1[44].

5.2 TS rotamer

Likewise TA, the TS conformer of 2-Propen-1-Imine is a near-prolate ($\kappa = -0.978$) asymmetric rotor principally aligned along the a principal axis. A rappresentation of the conformer is reported in figure 5.2.

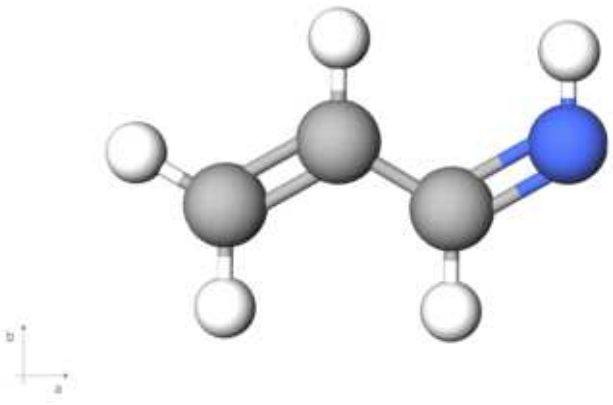

FIGURE 5.2: *Trans Syn* 2-Propen-1-Imine.

The CNH angle of the rotamer has a value of circa 115.1°and a lenght of the NH bond of about 1.003 Å[169]; the dipole moments are $\mu_a = 2.39$ D (Debye) and $\mu_b = 0.77$ D and as the previous compound led to transitions along the a and b axes giving rise to *a-type* and *b-type* transitions. 364 new rotational transitions have been collected, including R ($\Delta J = +1$) *a-type* lines and P ($\Delta J = -1$), Q ($\Delta J = 0$) and R *b-type* lines, with J values ranging from 7 to 69 (lower belonging to Penn), K_a values from 0 to 20 and energies from 3 to 11.5 cm^{-1}. Also for this rotamer the splitting due to electric quadrupole coupling of the ^{14}N nucleus ($I = 1$) has been observed in numerous transitions (F number is considered instead of J), leading to the collection of 201 frequency lines related to the hiperfine splitting. Also in this case the unresolved TS HFS (Hyper Fine Structure) transition frequencies have been averaged taking into account the relative intensities. The final fit returned an RMS deviations of 0.949 MHz and led to the determination of the complete set of quartic centrifugal distortion constants, six sextic constants, i.e. $H_J, H_{JK}, H_{KJ}, H_K, h_1$ and h_3, one octic constant, i.e. L_{KKJ}, and two quadrupole constants, i.e. $(\chi_{aa})3/2$ and $(\chi_{bb-cc})/4$. The resulting parameters are listed in Table 5.1.

[44]For a comparison of the quadrupole moments among different molecules, refer to the website http://nqcc.wcbailey.net/TOC.html

TABLE 5.1: Spectroscopic parameters of the two 2-Propen-1-Imine conformers.

Constants	TA CH_2CHCNH^a	TA CH_2CHCNH^b	TS CH_2CHCNH^a	TS CH_2CHCNH^b
Rotational constants[MHz]				
A_0	45773.63422(135)[c]	45774.02(10)	43755.67054(123)	43759.74(38)
B_0	4560.931356(85)	4560.96(1)	4564.540114(72)	4564.70(3)
C_0	4148.248499(82)	4148.29(1)	4134.462807(67)	4134.44(4)
Quartic centrifugal distortion constants [kHz]				
D_J	0.909800(71)		0.950364(54)	
D_{JK}	-7.54150(122)		-7.58688(97)	
D_K	296.5592(288)		259.0191(311)	
d1	-107.1845(78)		-114.8365(96)	
d2	–0.00584542(211)		-0.00622036(183)	
Sextic centrifugal distortion constants [Hz]				
H_J	0.0002832(195)		0.0002076(154)	
H_{JK}	-0.00617(47)		-0.00616(33)	
H_{KJ}	-0.4991(119)		-0.20255(191)	
H_K	2.181(219)		34.738(247)	
$h_1 \times 10^{-3}$	0.08064(157)		0.07626(266)	
$h_3 \times 10^{-3}$	0.00568(109)		0.00317(38)	
Octic centrifugal distortion constants[mHz]				
L_{KKJ}	0.8813(298)			
N quadrupole coupling constants [MHz]				
$(\chi_{aa})3/2$			-0.650(96)	
$(\chi_{bb-cc})/4$	-1.7430(55)		-0.8147(47)	
RMS deviation [MHz]				
	0.905			0.949

The results of this study compared with those of Penn [169]. [a]This work, [b] Penn's one. [c] Standard error in parentheses are in units of the last digit.

Taking into account the uncertenties associated with some of the presented constants further analysis at higher frequencies is in progress to better refine the results so far obtained. As an example of how this uncertanties can affect the prediction

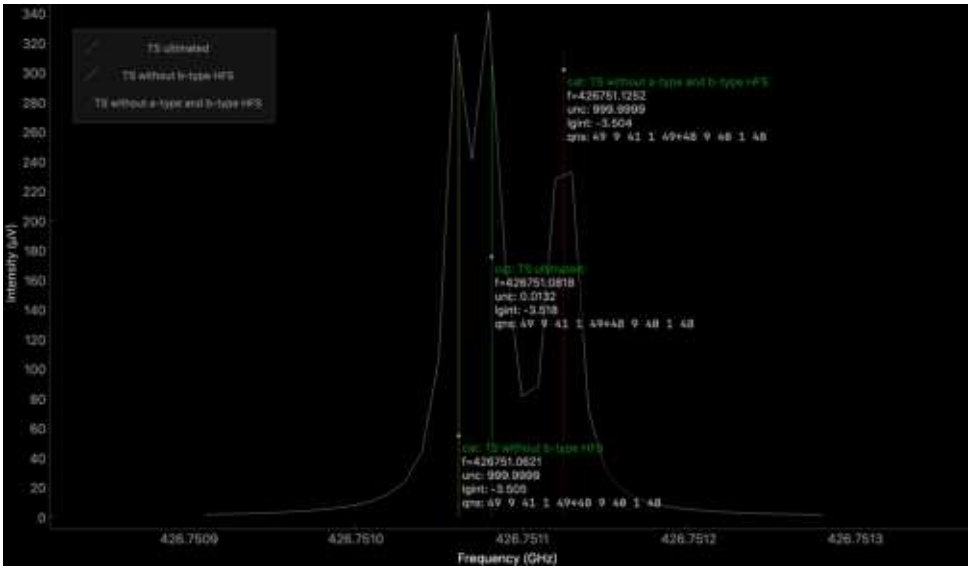

FIGURE 5.3: *Trans Syn* 2-Propen-1-Imine rotamer.

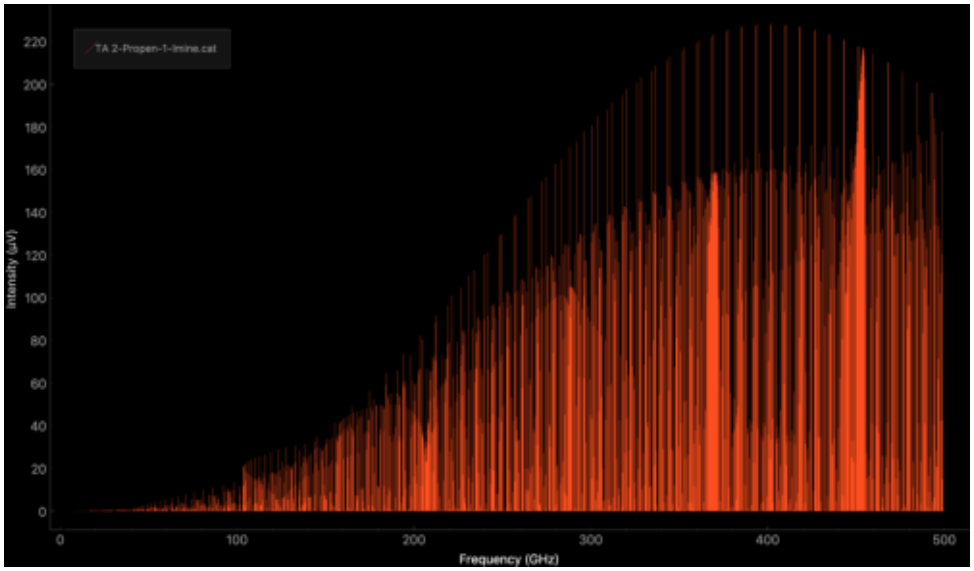

FIGURE 5.4: *Trans Anti* 2-Propen-1-Imine transition catalog, 300K.

of a line transition of the cat file, in figure 5.3 the same TS rotamer line, namely the one of "49 9 41 1 49-48 9 40 1 48" transition, is presented over the lines acquisition process. It is evident that the red line, that refers to the fit made without HFS lines, is clearly more distant than the other two. With the addition of the *b-type* lines the .cat return a forecast (yellow line) clearly shifted towards the region in which, with the addition of the *a-type* lines too, the green one gets itself into position. The profile width has been obtained by setting a frequency of 15 kHz, analogous to the uncertainty adopted in the experimental measurements. The profile of the red line is clearly distinguishable, while the two deriving from the lines obtained from a larger data pool, having a distance lower than the maximum experimental resolution, tend

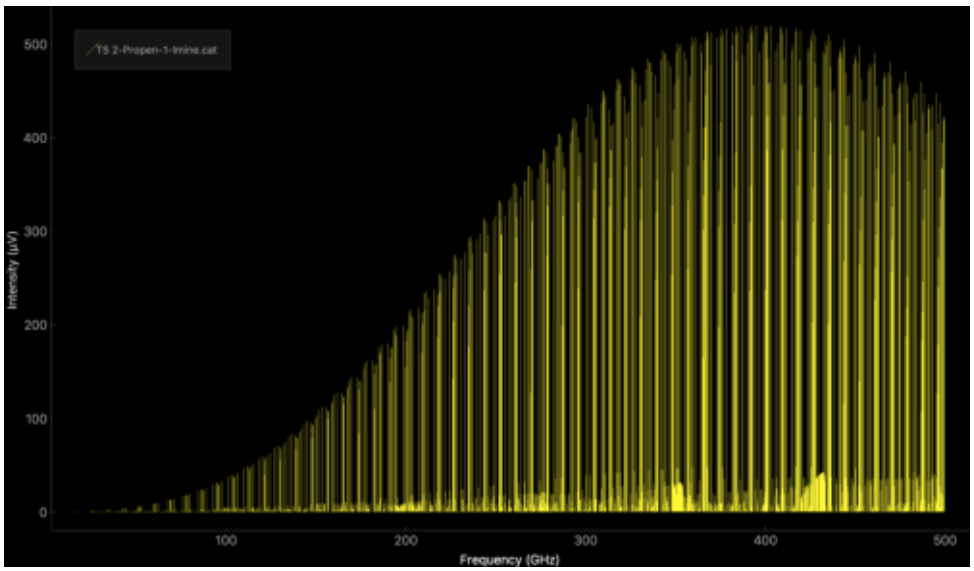

FIGURE 5.5: *Trans Syn* 2-Propen-1-Imine transition catalog, 300K.

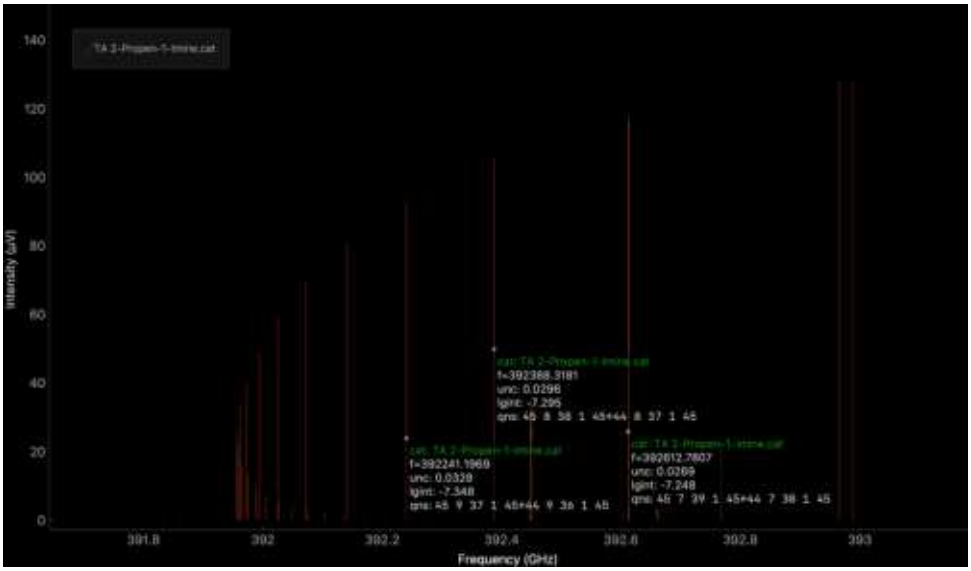

FIGURE 5.6: *Trans Anti* 2-Propen-1-Imine R branch detail.

to merge. It should be remembered that the recording of the lines have been carried out up to a maximum value of 350 GHz and that the final prediction therefore does not take into account higher quantum numbers and the related centrifugal distortions. For this reason, the analysis conducted for both TA and TS 2-Propen-1-Imine rotamers are not still considered satisfactory for the creation of an exhaustive catalog that takes into account the totality of their rotational transitions. In this regard, it is therefore necessary to go to higher frequency regions so as to be able to further refine the rotational constants and the distortion parameters, perhaps with the addition of some other octics and with the insertion of some decadics coefficients. In any case,

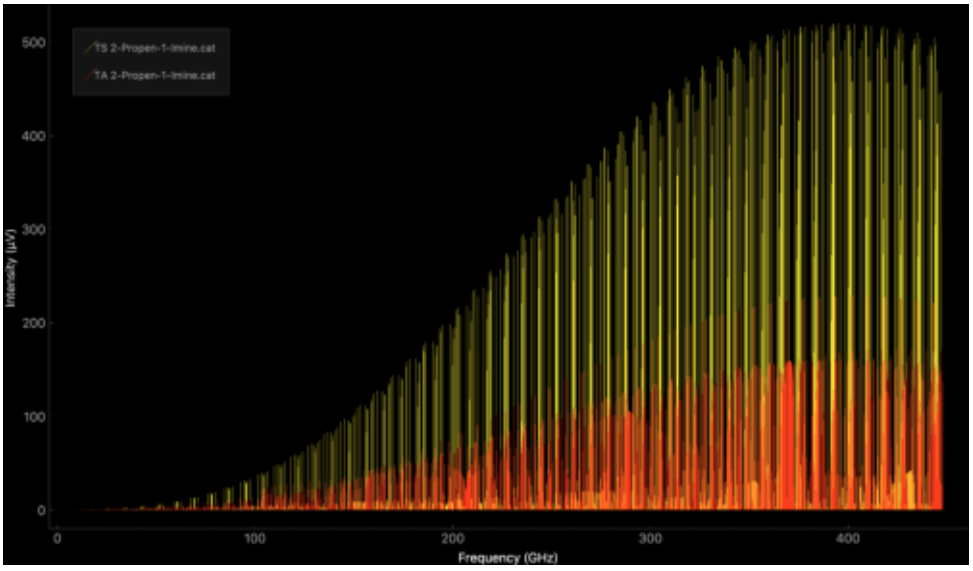

FIGURE 5.7: A comparison between *Trans Syn* 2-Propen-1-Imine transition catalog and *Trans Anti* 2-Propen-1-Imine transition catalog at 300 K.

the transitions obtained from the product catalog with the lines registered for the TA and TS rotamers are respectively shown in figure 5.4 and 5.5. For all the catalogs the forecast has been made up to 450 GHz; for what has been aforementioned, a prediction that takes into account higher frequencies would have been at least misleading. Note how for both, but especially for TA, various branches are visible. In this regard, in figure 5.6 an R branch taken from a blow-up of the graph in figure 5.4 is reported. Attempts in the direction of identifying the CS and CA rotamers have also been made but without success. To conclude, the transitions obtained at 300 K of the CT and TS catalog are combined on the same graph and reported the figure 5.7; it is possible to see how the TA rotamer is much more abundant.
Apart from depending on the numerical value of the square of the transition moment, intensities depend on the population of the lower state of a transition; the population N_J of the J^{th} level relative to N_0 can be obtained from the Boltzmann's distribution law.

The use of extremely precise instrumentation such as that of the CAS has therefore led to the collection of extremely refined lines which, if properly extended to both higher frequencies and the other two missing rotamers (as previously said) will allow to obtain the flawlessness required to be able to provide solid and exhaustive catalogs. In this way, a valuable base will be provided to be able to identify the two conformers TA and TS of 2-Propene-1-Imine in the interstellar medium, thus adding another contribution to what is the search for life as we know it outside of our planet.

Chapter 6

Conclusion

As we have seen in the introduction the steps that come to succeed one another before to reach the formation of a solar-like system are very long and complex and do have not to be considered unidirectional, but rather as subdivisions designed to simplify a very complicated system to deal with as a whole entity. It has been seen that thickening processes of matter can be triggered from a nebula of gas and dust in hydrostatic equilibrium, facts that through gravitational attraction lead, starting from a *Pre-stellar core* and passing through a *Protostellar envelope*, a *Protoplanetary disk* and a *Planetesimal formation*, to the *Planet formation*, the last step of a path through which the increase in structural complexity is accompanied by a chemical diversification that fits into the various passages. First of all, it has been seen that water, an essential factor for the proliferation of life as it is known to us, is said to come mainly from regions far away from that in which our planet is located and that it is came here only later [24]; the same comets, ambassadors and carriers of distant regions, intervened in the chemical enrichment of our atmosphere by bringing the aforementioned substance. Moreover, various carbonaceous molecules have been identified: think of methane and ethane, hydrogen sulphide, formaldehyde and acetonitrile, ammonia and methanol, just to name a few. The last two, to which the water is added, are by the way the most abundant ingredients of the KBOs. Moving on to meteorites, specifically carbonaceous chondrites, we find even more complex forms. Here the organic part is even categorized into insoluble and soluble, the former characterized respectively by the presence of aromatic elements held together by short aliphatic chains [28], the latter by carboxylic acids, aliphatic and aromatic hydrocarbons and amino-acids [34]. Without necessarily considering the Murchson meteorite there are therefore many molecules of prebiotic interest.

But it is through the isotopic abundances that it is possible to trace the temporal differences that occur in the synthesis of one species rather than another, a fact that allows us to theorize from where certain objects originate. For example, precisely due to the abnormalities in the abundances of deuterium in comets, the idea of their formation [36] and the linearity of temperatures in the Solar Nebula have been questioned [37], as has also been hypothesized that the Sun, observing this time even nitrogen and oxygen anomalies, actually born from a large cluster of stars [28]. By observing objects such as L1544 in the Taurus Molecular Cloud Complex, it is possible to get an idea of the diversification that is taking place in these systems and how different species are segregating in these macro objects because of the differences in the conditions in which molecules, and before these even individual atoms, are in. For example, in the external area of L1544 the chemistry of the carbon-ion reactions and the neutral-neutral reactions lead to the formation of N_2, CO, NH_3 and N_2H^+, while in the internal area the lower temperatures and higher pressures cause the molecules previously in the gas phase to freeze-out onto the surface of dust grains.

The latter, secondarily affected by cosmic rays and FUV, assume the role of catalyst substrate which in addition to fixing oxygen in H_2O also becomes the theater of the synthesis of complex organic compounds that potentially could results in the amino acids synthesis [51]. But the whole thing is far from stopping at this: once the balance of the system has ceased, it will begin to collapse again until reaching temperatures sufficiently high to allow in the densest and consequently warmest point the triggering of those reactions of nuclear fusion which, with the constraint of the mass, will lead the star to convert hydrogen into heavier elements [45]. The formation of the envelope will therefore be observed around the star; new conditions, new chemistry. Here, exceeding 25 K, the sublimation of CH_4 leads to the destruction of carbon radicals with the consequent formation of long carbon chains while, exceeding 100 K, it is accompanied by the release of the compounds imprisoned in the icy dust mantle giving way to the processes of complex chemistry of *hot cores* and *hot corinos*. Thus methyl formate and dimethyl ether are produced, but also compounds which incorporate nitrogen and sulfur atoms; molecules such as methanol, ethanol, formic acid and methyl cyanide have for example been identified in the outflows of L1157-B1 [99]. This ends with the formation of what is defined as planetary disk, a phase in which dust grains and simple molecular species in the midplane region placed from about 1 AU onwards start to coagulate. Just above this plane, but still shielded from external ionizing radiation by peripheral dusts, more complex species such as those of aromatic aliphatic hydrocarbons are found. These leading players in organic and prebiotic chemistry, reacting with other species, will then enrich the basket of complex organic products [134]. It is in this sense that it is possible to insert the pieces of the puzzle that come from theoretical models and laboratory tests, and in this context the observation of molecular species assumes their importance. To date, molecules with a skeleton made by three carbon and one nitrogen atoms such as methanimine have been observed in the giant molecular cloud Sgr B2 [158] and in the center of others [159], in translucent clouds [160] and other galaxies such as Arp220 [161] and NGC 253 [162]; 3-imino-1,2-propadienylidene has been observed in TMC 1 [163] and the isomers of ethanimine and ketemine [163] have been still identified in the molecular Sgr B2 complex [164]. Therefore, possibly among these same clouds of gas, the three carbon and one nitrogen molecule 2-Propene-1-Imine could be some day revealed.

Specifically, the latter has been the object on which the work of this thesis focused, constituting of the spectral lines measurement of 2-Propen-1-Imine (CH_2CHCNH) in the microwave frequency from ~85 GHz to ~350 GHz. The molecule, obtained by pyrolysis of diallylamine, had been previously investigated by Robert E. Penn in 1978 [169] but in his work the insufficient resolutions made not possible to reached the detail required to accurately determine the distortion constants; these constants allow to reliably model the overall rotational spectra of this molecule. Starting from the results of Penn and from ab initio calculations, the use of the CASAC frequency modulation spectrometer of the Max Planck für extraterrestrische Physik of Garching (Germany) has therefore made it possible to achieve the resolution necessary to obtain up to sextical and octic distortion constants and quadrupole constants. The transition frequencies of the TA and TS rotamers (*trans anti* and *trans syn*, respectively; see chapter 5 for further information) have been in parallel fitted through an iterative non-linear least squares fitting procedure (software used Spfit, part of the CALPGM program suite [46]) with the use of the Watson S-reduced Hamiltonian

[45] It must be considered that fusion reactions that produce elements heavier than iron consume energy rather than produce it [195].

[46] https://spec.jpl.nasa.gov/ftp/pub/calpgm/calpgm.pdf

for asymmetric-top molecules [179]. With the use of Spcat (another program of the CALPGM software suite) the constants obtained by means of the thoroughly rotational analysis carried out in the present work have been then used to produce a complete catalog of the transitions of the two rotamers.

The importance of this molecule derives from the fact that starting from methylamine (C_3NH_2) it has been seen that it is possible to arrive, combining a solid phase reaction with CO_2 followed by VUV irradiation, to glycine (NH_2CH_2COOH), the simplest amino-acid. Likewise, it has been observed that methanimine (CH_2NH) can be hydrogenated returning methylamine [150]. The same glycine is then also produced starting from aminoacetonitrile -observed in Sgr B2 [151]-, the latter also liable to hydrogenation. If we now take into account that in the Strecker synthesis (see figure 1.12B), considered the main way that lead to ammonia formation in the Urey-Miller experiment, the reaction between imines and hydrogen cyanide [47]the latter among other things is the same that leads to aminoacetonitrile) leads to the production of the relative aminonitrile which once hydrolyzed returns the relative amino-acid even at 20 K [152], the importance of 2-Propene-1-imine becomes clear. In fact, if this molecule were observed there would not only be further confirmation in support of the feasibility of the amino-acids synthesis in the interstellar medium, that as we have seen has already been confirmed, but could brings to much more complex forms than the simple glycine only. This would in primis lead to demolish the current idea according to which, excluding glycine, the amino-acid synthesis took place onto the surface of our planet and in secundis inevitably to review, if the synthesis of more complex amino-acids could take place in the interstellar medium, the timing of a subsequent biological development in its complexity. If things would then be this way it would certainly be interesting to see the enantiomeric abundances repartition, element that could eventually lead to a further discriminant in the selection of habitable areas, and an entire new research vein could then develop in that direction.

The subsequent coagulation of the rocky bodies finally leads to the formation of planets and comets made up of what goes to be incorporated into them. If the first ones were to be formed by the right molecular pool [48] and the same conditions in which our own planet found itself, no need to add to what it could lead to. In the end, it's just a matter of conditions and times: the state function will tend to a minimum. In the meantime, the thermonuclear reactions in the star would lead to the extinction of hydrogen combustion in the nucleus, which would bring to a further gravitational collapse of the body causing an increase in temperature such as to trigger the fusion of the hydrogen in the most external layers. Limited to our Sun, since conditions similar to our Solar system are being surveyed, it will expand over five billion years to reach beyond the orbit of Mercury; once the hydrogen of the outer layers will be almost converted into helium, externals regions will follow a further gravitational collapse. Temperatures will then reach about 10^8 K [196] and the fusion of helium will be triggered in the core, leading to the synthesis of carbon and oxygen [197]. Once the second most light element will run out a further contraction will follow and leading to the triggering of the fusion reactions of helium and hydrogen in the outermost regions not yet exhausted it will cause another expansion of the Sun that due to very high temperatures will cause the evaporation of the entire terrestrial biosphere. The same atoms that starting thickening in the *Prestellar core* had begun the process that had led them to become the support for the development of

[47](

[48]Right with respect to what? It is clear that what we are looking for is what we know. Life as we know it has developed using carbon, and around its chemistry we identify the conditions for life.

the biologically complex world such as that of the planet that hosts us, will finally return where that path had begun, in that equilibrium of gas and dust that gave rise to our own Solar system born from a third generation star, the Sun, partially consisting of those ashes remained from the explosion of one or more supernovae near the molecular cloud of the Orion Arm ([198]; [199]) in order to start for the umpteenth time what appears to be in all respects a complex and elegant cosmic dance.

Appendix A

TA lines list and relative errors

TABLE A.1: Transitions of TA 2-Propen-1-Imine rotamer.

Quantum number	EXP.FREQ.	CALC.FREQ.	DIFF.
1 0 1 0 1 0 0 0 0 0	8709.07000	8709.17622	-0.10622
2 0 2 0 2 1 0 1 0 1	17415.61000	17415.24675	0.36325
3 0 3 0 3 2 0 2 0 2	26115.22000	26115.10729	0.11271
2 1 2 0 2 1 1 1 0 1	17006.05000	17005.68133	0.36867
2 1 1 0 2 1 1 0 0 1	17831.31000	17831.04019	0.26981
3 1 3 0 3 2 1 2 0 2	25506.68000	25506.55353	0.12647
3 1 2 0 3 2 1 1 0 2	26744.78000	26744.56455	0.21545
6 1 5 0 6 6 1 6 0 6	8664.28000	8664.75270	-0.47270
3 2 1 0 3 2 2 0 0 2	26139.98000	26139.95571	0.02429
3 2 2 0 3 2 2 1 0 2	26127.80000	26127.62281	0.17719
7 1 6 0 7 7 1 7 0 7	11551.33000	11551.42550	-0.09550
8 1 7 0 8 8 1 8 0 8	14848.31000	14848.82464	-0.51464
9 1 8 0 9 9 1 9 0 9	18555.63000	18555.70377	-0.07377
16 2 14 0 16 16 2 15 0 16	8993.62000	8993.73436	-0.11436
6 0 6 0 6 5 1 5 0 5	13736.34000	13736.13260	0.20740
7 0 7 0 7 6 1 6 0 6	23535.14000	23534.87869	0.26131
14 1 13 0 14 13 2 12 0 13	18509.83000	18509.99469	-0.16469
1 1 1 0 1 2 0 2 0 2	23797.65000	23797.17506	0.47494
10 2 9 0 10 11 1 10 0 11	15172.36000	15172.00678	0.35322
9 2 8 0 9 10 1 9 0 10	26052.42000	26051.90894	0.51106
13 2 11 0 13 14 1 14 0 14	28750.13000	28750.77384	-0.64384
14 2 12 0 14 15 1 15 0 15	24630.67000	24630.71528	-0.04528
10 0 10 0 10 9 0 9 0 9	86586.26900	86586.28153	-0.01253
11 0 11 0 11 10 0 10 0 10	95131.06800	95131.07688	-0.00888
12 0 12 0 12 11 0 11 0 11	103646.15500	103646.14567	0.00933
13 0 13 0 13 12 0 12 0 12	112130.55100	112130.55671	-0.00571
14 0 14 0 14 13 0 13 0 13	120584.03400	120584.03721	-0.00321
10 1 10 0 10 9 1 9 0 9	84907.62600	84907.61739	0.00861
10 1 9 0 10 9 1 8 0 9	89022.21000	89022.21190	-0.00190
11 1 11 0 11 10 1 10 0 10	93370.87800	93370.88762	-0.00962
11 1 10 0 11 10 1 9 0 10	97890.79400	97890.78972	0.00428
12 1 12 0 12 11 1 11 0 11	101826.98200	101826.98962	-0.00762
12 1 11 0 12 11 1 10 0 11	106749.00000	106749.01221	-0.01221
13 1 13 0 13 12 1 12 0 12	110275.56700	110275.56954	-0.00254
13 1 12 0 13 12 1 11 0 12	115595.59600	115595.60035	-0.00435

Continued on next page

Table A.1 – continued from previous page

Quantum number	EXP.FREQ.	CALC.FREQ.	DIFF.
14 1 14 0 14 13 1 13 0 13	118716.34100	118716.34183	-0.00083
14 1 13 0 14 13 1 12 0 13	124429.19300	124429.18978	0.00322
10 2 9 0 10 9 2 8 0 9	87010.88500	87010.88757	-0.00257
10 2 8 0 10 9 2 7 0 9	87512.66500	87512.62366	0.04134
11 2 10 0 11 10 2 9 0 10	95691.40000	95691.40048	-0.00048
11 2 9 0 11 10 2 8 0 10	96356.20100	96356.20565	-0.00465
12 2 10 0 12 11 2 9 0 11	105223.35200	105223.34383	0.00817
12 2 11 0 12 11 2 10 0 11	104366.04600	104366.05779	-0.01179
13 2 12 0 13 12 2 11 0 12	113034.34000	113034.34261	-0.00261
13 2 11 0 13 12 2 10 0 12	114114.38900	114114.39082	-0.00182
14 2 13 0 14 13 2 12 0 13	121695.74000	121695.74498	-0.00498
14 2 12 0 14 13 2 11 0 13	123029.01100	123029.03200	-0.02100
10 3 8 0 10 9 3 7 0 9	87153.26000	87153.25869	0.00131
10 3 7 0 10 9 3 6 0 9	87164.64700	87164.63500	0.01200
11 3 9 0 11 10 3 8 0 10	95879.65600	95879.65817	-0.00217
11 3 8 0 11 10 3 7 0 10	95898.11900	95898.12539	-0.00639
12 3 10 0 12 11 3 9 0 11	104608.53400	104608.53718	-0.00318
12 3 9 0 12 11 3 8 0 11	104637.22200	104637.22518	-0.00318
13 3 11 0 13 12 3 10 0 12	113339.83800	113339.82422	0.01378
14 3 12 0 14 13 3 11 0 13	122073.38500	122073.37972	0.00528
14 3 11 0 14 13 3 10 0 13	122135.72200	122135.72995	-0.00795
10 4 7 0 10 9 4 6 0 9	87129.95800	87129.91705	0.04095
10 4 6 0 10 9 4 5 0 9	87129.95800	87130.01265	-0.05465
11 4 8 0 11 10 4 7 0 10	95850.03000	95849.93864	0.09136
11 4 7 0 11 10 4 6 0 10	95850.03000	95850.12977	-0.09977
10 5 6 0 10 9 5 5 0 9	87118.47000	87118.46970	0.00030
10 5 5 0 10 9 5 4 0 9	87118.47000	87118.47009	-0.00009
11 5 7 0 11 10 5 6 0 10	95834.41600	95834.41805	-0.00205
11 5 6 0 11 10 5 5 0 10	95834.41600	95834.41903	-0.00303
12 5 8 0 12 11 5 7 0 11	104551.52600	104551.53783	-0.01183
12 5 7 0 12 11 5 6 0 11	104551.52600	104551.54006	-0.01406
13 5 9 0 13 12 5 8 0 12	113269.91300	113269.93539	-0.02239
13 5 8 0 13 12 5 7 0 12	113269.91300	113269.94013	-0.02713
14 5 10 0 14 13 5 9 0 13	121989.72200	121989.71706	0.00494
14 5 9 0 14 13 5 8 0 13	121989.72200	121989.72654	-0.00454
10 6 4 0 10 9 6 3 0 9	87113.39600	87113.39583	0.00017
10 6 5 0 10 9 6 4 0 9	87113.39600	87113.39583	0.00017
11 6 5 0 11 10 6 4 0 10	95827.27800	95827.28248	-0.00448
11 6 6 0 11 10 6 5 0 10	95827.27800	95827.28248	-0.00448
12 6 6 0 12 11 6 5 0 11	104541.90100	104541.89648	0.00452
12 6 7 0 12 11 6 6 0 11	104541.90100	104541.89647	0.00453
13 6 8 0 13 12 6 7 0 12	113257.31300	113257.30382	0.00918
13 6 7 0 13 12 6 6 0 12	113257.31300	113257.30384	0.00916
14 6 8 0 14 13 6 7 0 13	121973.57200	121973.57058	0.00142
14 6 9 0 14 13 6 8 0 13	121973.57200	121973.57054	0.00146
13 0 13 1 12 12 1 12 1 11	84472.22600	84472.19420	0.03180
13 0 13 1 14 12 1 12 1 13	84472.22600	84472.26667	-0.04067

Continued on next page

Table A.1 – continued from previous page

Quantum number	EXP.FREQ.	CALC.FREQ.	DIFF.
13 0 13 1 13 12 1 12 1 12	84473.08300	84473.09128	-0.00828
14 0 14 1 13 13 1 13 1 12	94780.71700	94780.68755	0.02945
14 0 14 1 15 13 1 13 1 14	94780.71700	94780.75026	-0.03326
14 0 14 1 14 13 1 13 1 13	94781.51400	94781.51852	-0.00452
15 0 15 1 14 14 1 14 1 13	105071.41100	105071.39542	0.01558
15 0 15 1 16 14 1 14 1 15	105071.41100	105071.44965	-0.03865
15 0 15 1 15 14 1 14 1 14	105072.14600	105072.15990	-0.01390
16 0 16 1 15 15 1 15 1 14	115323.02900	115323.00435	0.02465
16 0 16 1 17 15 1 15 1 16	115323.02900	115323.05117	-0.02217
16 0 16 1 16 15 1 15 1 15	115323.70100	115323.70266	-0.00166
17 0 17 1 16 16 1 16 1 15	125516.18300	125516.18189	0.00111
17 0 17 1 18 16 1 16 1 17	125516.18300	125516.22223	-0.03923
17 0 17 1 17 16 1 16 1 16	125516.79300	125516.81513	-0.02213
18 1 17 1 17 18 0 18 1 17	86537.32300	86537.26729	0.05571
18 1 17 1 19 18 0 18 1 19	86537.32300	86537.37329	-0.05029
18 1 17 1 18 18 0 18 1 18	86539.27000	86539.27984	-0.00984
19 1 18 1 18 19 0 19 1 18	92458.75800	92458.69869	0.05931
19 1 18 1 20 19 0 19 1 20	92458.75800	92458.80121	-0.04321
19 1 18 1 19 19 0 19 1 19	92460.74000	92460.74740	-0.00740
20 1 19 1 19 20 0 20 1 19	98802.45500	98802.38858	0.06642
20 1 19 1 21 20 0 20 1 21	98802.45500	98802.48762	-0.03262
20 1 19 1 20 20 0 20 1 20	98804.47100	98804.46777	0.00323
21 1 20 1 20 21 0 21 1 20	105559.33500	105559.27437	0.06063
21 1 20 1 22 21 0 21 1 22	105559.33500	105559.36989	-0.03489
21 1 20 1 21 21 0 21 1 21	105561.37500	105561.37767	-0.00267
22 1 21 1 21 22 0 22 1 21	112715.27200	112715.21618	0.05582
22 1 21 1 23 22 0 22 1 23	112715.27200	112715.30882	-0.03682
22 1 21 1 22 22 0 22 1 22	112717.32900	112717.33672	-0.00772
23 1 22 1 22 23 0 23 1 22	120251.31000	120251.25052	0.05948
23 1 22 1 24 23 0 23 1 24	120251.31000	120251.33945	-0.02945
23 1 22 1 23 23 0 23 1 23	120253.38100	120253.38088	0.00012
8 1 8 1 8 7 0 7 1 7	103904.95700	103904.94874	0.00826
8 1 8 1 9 7 0 7 1 8	103906.13500	103906.07020	0.06480
8 1 8 1 7 7 0 7 1 6	103906.13500	103906.20843	-0.07343
9 1 9 1 9 8 0 8 1 8	110928.56800	110928.55105	0.01695
9 1 9 1 10 8 0 8 1 9	110929.71400	110929.64262	0.07138
9 1 9 1 8 8 0 8 1 7	110929.71400	110929.76161	-0.04761
10 1 10 1 10 9 0 9 1 9	117822.92500	117822.92901	-0.00401
10 1 10 1 11 9 0 9 1 10	117824.03000	117823.98495	0.04505
10 1 10 1 9 9 0 9 1 8	117824.03000	117824.08803	-0.05803
11 1 11 1 11 10 0 10 1 10	124607.57500	124607.56615	0.00885
11 1 11 1 12 10 0 10 1 11	124608.63000	124608.58124	0.04876
11 1 11 1 10 10 0 10 1 9	124608.63000	124608.67096	-0.04096
7 2 6 1 7 6 1 5 1 6	180882.97100	180882.98976	-0.01876
7 2 6 1 8 6 1 5 1 7	180884.32000	180884.20334	0.11666
7 2 6 1 6 6 1 5 1 5	180884.32000	180884.40772	-0.08772
20 0 20 0 20 19 0 19 0 19	170726.58600	170726.57638	0.00962

Continued on next page

Table A.1 – continued from previous page

Quantum number	EXP.FREQ.	CALC.FREQ.	DIFF.
20 1 19 0 20 19 1 18 0 19	177070.27500	177070.27511	-0.00011
20 1 20 1 20 19 0 19 1 19	184324.32700	184324.35171	-0.02471
20 1 20 1 21 19 0 19 1 20	184324.88800	184324.87769	0.01031
20 1 20 1 19 19 0 19 1 18	184324.88800	184324.90138	-0.01338
20 2 19 0 20 19 2 18 0 19	173492.44200	173492.43683	0.00517
20 2 18 0 20 19 2 17 0 19	176906.49000	176906.46632	0.02368
20 3 18 0 20 19 3 17 0 19	174505.84600	174505.86815	-0.02215
20 6 14 0 20 19 6 13 0 19	174292.90600	174292.92124	-0.01524
20 7 14 0 20 19 7 13 0 19	174265.05100	174265.01152	0.03948
20 8 13 0 20 19 8 12 0 19	174249.12500	174249.13076	-0.00576
20 11 10 0 20 19 11 9 0 19	174235.23000	174235.21622	0.01378
21 0 21 0 21 20 0 20 0 20	179010.63200	179010.62921	0.00279
21 1 20 0 21 20 1 19 0 20	185767.52800	185767.52166	0.00634
21 1 21 0 21 20 1 20 0 20	177573.59600	177573.59513	0.00087
21 2 20 0 21 20 2 19 0 20	182092.39100	182092.39489	-0.00389
21 2 19 0 21 20 2 18 0 20	185921.36900	185921.38710	-0.01810
21 3 19 0 21 20 3 18 0 20	183245.70200	183245.69110	0.01090
21 3 18 0 21 20 3 17 0 20	183709.76400	183709.77197	-0.00797
21 6 15 0 21 20 6 14 0 20	183017.04000	183017.05763	-0.01763
21 7 14 0 21 20 7 13 0 20	182984.32800	182984.32202	0.00598
21 8 14 0 21 20 8 13 0 20	182965.44000	182965.45324	-0.01324
21 10 12 0 21 20 10 11 0 20	182949.34400	182949.32602	0.01798
21 11 11 0 21 20 11 10 0 20	182947.55900	182947.51173	0.04727
21 12 10 0 21 20 12 9 0 20	182948.36900	182948.34919	0.01981
21 13 9 0 21 20 13 8 0 20	182951.23900	182951.23235	0.00665
24 3 21 1 24 24 2 22 1 24	184336.33300	184336.33804	-0.00504
24 3 21 1 25 24 2 22 1 25	184337.04100	184337.01319	0.02781
24 3 21 1 23 24 2 22 1 23	184337.04100	184337.04135	-0.00035
25 3 22 1 25 25 2 23 1 25	181644.39600	181644.38913	0.00687
25 3 22 1 25 25 2 23 1 25	181645.09800	181645.05286	0.04514
25 3 22 1 24 25 2 23 1 24	181645.09800	181645.07943	0.01857
22 0 22 0 22 21 0 21 0 21	187282.14300	187282.13552	0.00748
22 1 22 0 22 21 1 21 0 21	185949.75300	185949.75096	0.00204
22 2 21 0 22 21 2 20 0 21	190681.91300	190681.90093	0.01207
26 0 26 0 26 25 0 25 0 25	220298.32500	220298.33959	-0.01459
26 1 26 0 26 25 1 25 0 25	219382.99100	219382.98185	0.00915
26 1 25 0 26 25 1 24 0 25	228819.58000	228819.56765	0.01235
26 2 25 0 26 25 2 24 0 25	224929.10600	224929.11197	-0.00597
26 2 24 0 26 25 2 23 0 25	230920.39800	230920.38875	0.00925
26 8 19 0 26 25 8 18 0 25	226556.06800	226556.06754	0.00046
26 19 8 0 26 25 19 7 0 25	226553.38300	226553.37364	0.00936
27 0 27 0 27 26 0 26 0 26	228545.69800	228545.70401	-0.00601
27 2 26 0 27 26 2 25 0 26	233461.95300	233461.96805	-0.01505
27 1 26 0 27 26 1 25 0 26	237333.00000	237332.99740	0.00260
27 2 25 0 27 26 2 24 0 26	239882.20900	239882.19424	0.01476
27 8 19 0 27 26 8 18 0 26	235276.18200	235276.17783	0.00417
28 13 15 0 28 27 13 14 0 27	243929.15100	243929.17703	-0.02603

Continued on next page

Table A.1 – continued from previous page

Quantum number	EXP.FREQ.	CALC.FREQ.	DIFF.
28 12 16 0 28 27 12 15 0 27	243930.44600	243930.45675	-0.01075
28 14 15 0 28 27 14 14 0 27	243931.13300	243931.16500	-0.03200
28 15 14 0 28 27 15 13 0 27	243935.86800	243935.79329	0.07471
28 11 18 0 28 27 11 17 0 27	243935.86800	243935.93906	-0.07106
28 16 13 0 28 27 16 12 0 27	243942.40800	243942.63050	-0.22250
28 17 12 0 28 27 17 11 0 27	243950.96600	243951.37502	-0.40902
39 2 37 1 38 39 1 38 1 38	181437.93300	181437.90981	0.02319
39 2 37 1 40 39 1 38 1 40	181437.93300	181437.94435	-0.01135
39 2 37 1 39 39 1 38 1 39	181439.28200	181439.29002	-0.00802
47 3 44 1 46 47 2 45 1 46	180959.94900	180959.93858	0.01042
47 3 44 1 48 47 2 45 1 48	180959.94900	180959.95283	-0.00383
47 3 44 1 47 47 2 45 1 47	180960.63400	180960.62174	0.01226
47 8 40 0 47 48 7 41 0 48	198879.02700	198879.00574	0.02126
47 8 39 0 47 48 7 42 0 48	198887.51500	198887.51309	0.00191
48 8 40 0 48 49 7 43 0 49	189852.18000	189852.09175	0.08825
38 4 34 1 38 38 3 35 1 38	253690.88800	253690.91769	-0.02969
38 4 34 1 39 38 3 35 1 39	253691.49100	253691.50480	-0.01380
38 4 34 1 37 38 3 35 1 37	253691.49100	253691.52025	-0.02925
50 3 47 1 49 49 4 46 1 48	265195.88200	265195.88786	-0.00586
50 3 47 1 51 49 4 46 1 50	265195.88200	265195.90618	-0.02418
50 3 47 1 50 49 4 46 1 49	265196.83700	265196.82651	0.01049
30 7 24 0 30 31 6 25 0 31	266997.88400	266997.91777	-0.03377
30 7 23 0 30 31 6 26 0 31	266999.05800	266999.09866	-0.04066
38 2 37 1 37 38 1 38 1 37	278498.84900	278498.84051	0.00849
38 2 37 1 39 38 1 38 1 39	278498.84900	278498.87233	-0.02333
38 2 37 1 38 38 1 38 1 38	278500.09500	278500.08113	0.01387
51 3 48 1 50 50 4 47 1 49	281319.80600	281319.80595	0.00005
51 3 48 1 52 50 4 47 1 51	281319.80600	281319.82372	-0.01772
51 3 48 1 51 50 4 47 1 50	281320.73500	281320.73428	0.00072
42 3 40 1 41 42 2 41 1 41	282262.56000	282262.54671	0.01329
42 3 40 1 43 42 2 41 1 43	282262.56000	282262.56590	-0.00590
42 3 40 1 42 42 2 41 1 42	282263.36900	282263.37163	-0.00263
47 9 38 0 47 48 8 41 0 48	282856.68800	282856.80243	-0.11443
46 9 38 0 46 47 8 39 0 47	291766.80000	291766.71164	0.08836
27 7 21 0 27 28 6 22 0 28	293491.44200	293491.32487	0.11713
71 4 67 1 70 71 3 68 1 70	293647.20300	293647.21744	-0.01444
71 4 67 1 72 71 3 68 1 72	293647.20300	293647.22977	-0.02677
71 4 67 1 71 71 3 68 1 71	293648.12800	293648.10650	0.02150
55 10 45 0 55 56 9 48 0 56	295153.14700	295153.14268	0.00432
39 4 36 0 39 39 3 37 0 39	296866.49100	296866.52696	-0.03596
24 2 23 1 24 23 1 22 1 23	280220.90700	280220.89670	0.01030
24 2 23 1 25 23 1 22 1 24	280221.99200	280221.93709	0.05491
24 2 23 1 23 23 1 22 1 22	280221.99200	280221.98185	0.01015
28 4 24 0 28 28 3 25 0 28	280242.85800	280242.79739	0.06061
19 6 14 0 19 20 5 15 0 20	280850.81200	280850.84161	-0.02961
19 6 13 0 19 20 5 16 0 20	280851.47900	280851.47964	-0.00064
66 11 55 0 66 67 10 58 0 67	280562.80500	280562.81048	-0.00548

Continued on next page

Table A.1 – continued from previous page

Quantum number	EXP.FREQ.	CALC.FREQ.	DIFF.
29 7 22 0 29 28 7 21 0 28	252774.23800	252774.26799	-0.02999
31 2 29 0 31 30 2 28 0 30	275521.36000	275521.36678	-0.00678
32 0 32 0 32 31 0 31 0 31	269800.43000	269800.41913	0.01087
32 1 32 0 32 31 1 31 0 31	269356.53300	269356.52176	0.01124
32 2 31 0 32 31 2 30 0 31	275946.21700	275946.21488	0.00212
32 3 30 0 32 31 3 29 0 31	279144.80100	279144.74712	0.05388
32 4 29 0 32 31 4 28 0 31	279573.40800	279573.40061	0.00739
32 4 28 0 32 31 4 27 0 31	279921.65300	279921.64231	0.01069
32 5 28 0 32 31 5 27 0 31	279299.31400	279299.32402	-0.01002
32 7 26 0 32 31 7 25 0 31	278964.58100	278964.56840	0.01260
32 9 23 0 32 31 9 22 0 31	278839.54700	278839.52797	0.01903
33 0 33 0 33 32 0 32 0 32	278057.77300	278057.76424	0.00876
33 1 33 0 33 32 1 32 0 32	277669.46700	277669.46462	0.00238
33 4 29 0 33 32 4 28 0 32	288775.13800	288775.14161	-0.00361
33 7 27 0 33 32 7 26 0 32	287697.33500	287697.32899	0.00601
33 9 25 0 33 32 9 24 0 32	287559.16300	287559.14972	0.01328
33 11 22 0 33 32 11 21 0 32	287502.08800	287502.06919	0.01881
34 0 34 0 34 33 0 33 0 33	286317.41900	286317.40690	0.01210
34 1 34 0 34 33 1 33 0 33	285978.73400	285978.72887	0.00513
34 2 33 0 34 33 2 32 0 33	292856.25800	292856.26032	-0.00232
34 5 29 0 34 33 5 28 0 33	296862.20000	296862.20497	-0.00497
34 11 23 0 34 33 11 22 0 33	296215.65400	296215.63505	0.01895
34 13 21 0 34 33 13 20 0 33	296192.00800	296192.00772	0.00028
34 17 17 0 34 33 17 16 0 33	296202.38200	296202.89712	-0.51512
35 0 35 0 35 34 0 34 0 34	294579.21700	294579.22133	-0.00433
35 1 34 0 35 34 1 33 0 34	304270.40800	304270.39582	0.01218
35 2 34 0 35 34 2 33 0 34	301293.89300	301293.88467	0.00833
36 0 36 0 36 35 0 35 0 35	302843.03200	302843.03465	-0.00265
36 2 35 0 36 35 2 34 0 35	309720.22600	309720.22881	-0.00281
36 3 33 0 36 35 3 32 0 35	318626.60500	318626.62402	-0.01902
37 7 30 0 37 36 7 29 0 36	322642.88800	322642.93002	-0.04202
38 0 38 0 38 37 0 37 0 37	319375.84800	319375.83871	0.00929
38 1 38 0 38 37 1 37 0 37	319184.58100	319184.58282	-0.00182
38 4 34 0 38 37 4 33 0 37	333284.28000	333284.27381	0.00619
38 7 31 0 38 37 7 30 0 37	331383.16600	331383.19123	-0.02523
38 11 28 0 38 37 11 27 0 37	331071.18000	331071.13917	0.04083
38 13 25 0 38 37 13 24 0 37	331031.40600	331031.40495	0.00105
38 17 22 0 38 37 17 21 0 37	331029.16700	331029.69794	-0.53094
39 0 39 0 39 38 0 38 0 38	327644.41700	327644.39471	0.02229
39 2 38 0 39 38 2 37 0 38	334934.69100	334934.69062	0.00038
39 3 37 0 39 38 3 36 0 38	339658.74000	339658.75556	-0.01556
39 9 30 0 39 38 9 29 0 38	339888.82900	339888.82109	0.00791
39 11 28 0 39 38 11 27 0 38	339785.35500	339785.34137	0.01363
39 13 26 0 39 38 13 25 0 38	339740.89800	339740.90580	-0.00780
39 17 22 0 39 38 17 21 0 38	339734.75500	339735.34919	-0.59419
40 0 40 0 40 39 0 39 0 39	335914.10600	335914.09781	0.00819
40 1 40 0 40 39 1 39 0 39	335772.11100	335772.11033	0.00067

Continued on next page

Table A.1 – continued from previous page

Quantum number	EXP.FREQ.	CALC.FREQ.	DIFF.
40 2 39 0 40 39 2 38 0 39	343319.18900	343319.19798	-0.00898
40 4 37 0 40 39 4 36 0 39	349734.00300	349733.99526	0.00774
40 7 33 0 40 39 7 32 0 39	348868.58300	348868.69339	-0.11039
40 9 31 0 40 39 9 30 0 39	348612.57500	348612.57733	-0.00233
40 11 30 0 40 39 11 29 0 39	348499.70200	348499.68042	0.02158
40 13 27 0 40 39 13 26 0 39	348450.24200	348450.25901	-0.01701
40 17 24 0 40 39 17 23 0 39	348439.93400	348440.55774	-0.62374
41 0 41 0 41 40 0 40 0 40	344184.74700	344184.74067	0.00633

Registered TA rotamer lines and relative errors between regestered and calculated frequencies returned by Spfit in the .fit file.

Appendix B

TS lines list and relative errors

TABLE B.1: Transitions of TS 2-Propen-1-Imine rotamer.

Quantum number	EXP.FREQ.	CALC.FREQ.	DIFF.
1 0 1 0 1 0 0 0 0 0	8699.38000	8698.99912	0.38088
2 0 2 0 2 1 0 1 0 1	17394.41000	17394.45508	-0.04508
2 1 2 0 2 1 1 1 0 1	16968.57000	16967.93214	0.63786
2 1 1 0 2 1 1 0 0 1	17828.46000	17828.07941	0.38059
3 0 3 0 3 2 0 2 0 2	26082.94000	26082.82654	0.11346
3 1 3 0 3 2 1 2 0 2	25449.80000	25449.65674	0.14326
3 1 2 0 3 2 1 1 0 2	26740.40000	26739.84585	0.55415
3 2 2 0 3 2 2 1 0 2	26097.89000	26097.08878	0.80122
3 2 1 0 3 2 2 0 0 2	26111.19000	26111.16717	0.02283
7 0 7 0 7 6 1 6 0 6	25610.92000	25610.75463	0.16537
10 0 10 0 10 9 0 9 0 9	86414.84000	86414.82705	0.01295
11 0 11 0 11 10 0 10 0 10	94927.66100	94927.67164	-0.01064
12 0 12 0 12 11 0 11 0 11	103407.52100	103407.51219	0.00881
13 0 13 0 13 12 0 12 0 12	111853.68700	111853.68076	0.00624
14 0 14 0 14 13 0 13 0 13	120266.33800	120266.33517	0.00283
20 0 20 0 20 19 0 19 0 19	170147.04900	170147.04010	0.00890
21 0 21 0 21 20 0 20 0 20	178390.85400	178390.85021	0.00379
22 0 22 0 22 21 0 21 0 21	186624.24500	186624.23957	0.00543
23 0 23 0 23 22 0 22 0 22	194850.32500	194850.31961	0.00539
24 0 24 0 24 23 0 23 0 23	203071.77000	203071.76187	0.00813
25 0 25 0 25 24 0 24 0 24	211290.75900	211290.76374	-0.00474
26 0 26 0 26 25 0 25 0 25	219509.04900	219509.05482	-0.00582
27 0 27 0 27 26 0 26 0 26	227727.92300	227727.93257	-0.00957
28 0 28 0 28 27 0 27 0 27	235948.30700	235948.31582	-0.00882
29 0 29 0 29 28 0 28 0 28	244170.79300	244170.80624	-0.01324
10 1 9 0 10 9 1 8 0 9	88988.32500	88988.31970	0.00530
10 1 10 0 10 9 1 9 0 9	84702.67700	84702.68536	-0.00836
11 1 11 0 11 10 1 10 0 10	93141.94800	93141.95261	-0.00461
11 1 10 0 11 10 1 9 0 10	97848.50100	97848.50066	0.00034
12 1 12 0 12 11 1 11 0 11	101573.22900	101573.21368	0.01532
12 1 11 0 12 11 1 10 0 11	106696.70400	106696.70888	-0.00488
13 1 13 0 13 12 1 12 0 12	109996.11800	109996.10785	0.01015
13 1 12 0 13 12 1 11 0 12	115531.44800	115531.43485	0.01315
14 1 14 0 14 13 1 13 0 13	118410.36100	118410.35701	0.00399
14 1 13 0 14 13 1 12 0 13	124351.08200	124351.06436	0.01764

Continued on next page

Table B.1 – continued from previous page

Quantum number	EXP.FREQ.	CALC.FREQ.	DIFF.
20 1 19 0 20 19 1 18 0 19	176848.41800	176848.41346	0.00454
21 1 21 0 21 20 1 20 0 20	177061.76500	177061.76424	0.00076
22 1 22 0 22 21 1 21 0 21	185406.37900	185406.37672	0.00228
28 1 28 0 28 27 1 27 0 27	235324.86700	235324.88055	-0.01355
27 1 26 0 27 26 1 25 0 26	236763.89100	236763.88933	0.00167
29 1 29 0 29 28 1 28 0 28	243623.59000	243623.58881	0.00119
28 1 27 0 28 27 1 26 0 27	245178.04500	245178.05366	-0.00866
10 2 9 0 10 9 2 8 0 9	86897.95500	86897.94556	0.00944
11 2 10 0 11 10 2 9 0 10	95564.34000	95564.34176	-0.00176
11 2 9 0 11 10 2 8 0 10	96320.31800	96320.31528	0.00272
12 2 11 0 12 11 2 10 0 11	104224.09200	104224.08381	0.00819
12 2 10 0 12 11 2 9 0 11	105197.45300	105197.46217	-0.00917
13 2 12 0 13 12 2 11 0 12	112876.57900	112876.58755	-0.00855
13 2 11 0 13 12 2 10 0 12	114100.62700	114100.61339	0.01361
14 2 13 0 14 13 2 12 0 13	121521.28300	121521.27824	0.00476
20 2 19 0 20 19 2 18 0 19	173195.00500	173195.00840	-0.00340
20 2 18 0 20 19 2 17 0 19	176978.77900	176978.75458	0.02442
21 2 20 0 21 20 2 19 0 20	181770.27300	181770.27937	-0.00637
21 2 19 0 21 20 2 18 0 20	185996.83400	185996.83194	0.00206
27 2 26 0 27 26 2 25 0 26	232965.10100	232965.10141	-0.00041
27 2 25 0 27 26 2 24 0 26	239885.64500	239885.64703	-0.00203
28 2 27 0 28 27 2 26 0 27	241452.66200	241452.65198	0.01002
28 2 26 0 28 27 2 25 0 27	248800.97200	248800.97641	-0.00441
10 3 8 0 10 9 3 7 0 9	87059.76800	87059.75807	0.00993
10 3 7 0 10 9 3 6 0 9	87073.98100	87073.97764	0.00336
11 3 9 0 11 10 3 8 0 10	95778.15400	95778.14978	0.00422
11 3 8 0 11 10 3 7 0 10	95801.23100	95801.22802	0.00298
12 3 10 0 12 11 3 9 0 11	104499.23700	104499.23996	-0.00296
12 3 9 0 12 11 3 8 0 11	104535.10100	104535.08184	0.01916
13 3 10 0 13 12 3 9 0 12	113276.50100	113276.56073	-0.05973
13 3 11 0 13 12 3 10 0 12	113222.89100	113222.90785	-0.01685
14 3 12 0 14 13 3 11 0 13	121948.95000	121948.95032	-0.00032
14 3 11 0 14 13 3 10 0 13	122026.80300	122026.79069	0.01231
20 3 18 0 20 19 3 17 0 19	174333.43200	174333.42740	0.00460
20 3 17 0 20 19 3 16 0 19	174787.89900	174787.89261	0.00639
21 3 19 0 21 20 3 18 0 20	183063.67400	183063.69266	-0.01866
21 3 18 0 21 20 3 17 0 20	183639.01200	183639.00338	0.00862
10 4 7 0 10 9 4 6 0 9	87033.62000	87033.56164	0.05836
10 4 6 0 10 9 4 5 0 9	87033.62000	87033.69257	-0.07257
12 4 9 0 12 11 4 8 0 11	104458.74400	104458.75500	-0.01100
12 4 8 0 12 11 4 7 0 11	104459.19800	104459.24548	-0.04748
13 4 10 0 13 12 4 9 0 12	113174.96300	113174.96680	-0.00380
13 4 9 0 13 12 4 8 0 12	113175.81500	113175.83812	-0.02312
14 4 11 0 14 13 4 10 0 13	121893.84000	121893.82992	0.01008
14 4 10 0 14 13 4 9 0 13	121895.30500	121895.30983	-0.00483
20 4 17 0 20 19 4 16 0 19	174270.86400	174270.86287	0.00113
20 4 16 0 20 19 4 15 0 19	174289.32100	174289.32555	-0.00455

Continued on next page

Table B.1 – continued from previous page

Quantum number	EXP.FREQ.	CALC.FREQ.	DIFF.
21 4 18 0 21 20 4 17 0 20	183011.91900	183011.93442	-0.01542
21 4 17 0 21 20 4 16 0 20	183037.94200	183037.92486	0.01714
27 4 24 0 27 26 4 23 0 26	235526.48100	235526.48503	-0.00403
27 4 23 0 27 26 4 22 0 26	235675.16800	235675.16724	0.00076
28 4 25 0 28 27 4 24 0 27	244288.70100	244288.69332	0.00768
28 4 24 0 28 27 4 23 0 27	244479.40200	244479.41490	-0.01290
10 5 6 0 10 9 5 5 0 9	87020.33900	87020.32195	0.01705
10 5 5 0 10 9 5 4 0 9	87020.33900	87020.32253	0.01647
11 5 7 0 11 10 5 6 0 10	95727.11600	95727.11780	-0.00180
11 5 6 0 11 10 5 5 0 10	95727.11600	95727.11927	-0.00327
12 5 8 0 12 11 5 7 0 11	104435.28600	104435.27428	0.01172
12 5 7 0 12 11 5 6 0 11	104435.28600	104435.27762	0.00838
13 5 9 0 13 12 5 8 0 12	113144.90700	113144.91493	-0.00793
13 5 8 0 13 12 5 7 0 12	113144.90700	113144.92204	-0.01504
14 5 10 0 14 13 5 9 0 13	121856.17500	121856.16324	0.01176
14 5 9 0 14 13 5 8 0 13	121856.17500	121856.17745	-0.00245
21 5 17 0 21 20 5 16 0 20	182890.22900	182890.22954	-0.00054
21 5 16 0 21 20 5 15 0 20	182890.79800	182890.82260	-0.02460
22 5 18 0 22 21 5 17 0 21	191618.74500	191618.73677	0.00823
22 5 17 0 22 21 5 16 0 21	191619.63100	191619.64238	-0.01138
27 5 23 0 27 26 5 22 0 26	235303.74000	235303.73223	0.00777
27 5 22 0 27 26 5 21 0 26	235309.50200	235309.50963	-0.00763
28 5 24 0 28 27 5 23 0 27	244049.90300	244049.90692	-0.00392
28 5 23 0 28 27 5 22 0 27	244057.92200	244057.92032	0.00168
11 6 5 0 11 10 6 4 0 10	95718.75200	95718.72923	0.02277
11 6 6 0 11 10 6 5 0 10	95718.75200	95718.72923	0.02277
13 6 7 0 13 12 6 6 0 12	113130.20800	113130.20809	-0.00009
13 6 8 0 13 12 6 7 0 12	113130.20800	113130.20805	-0.00005
14 6 9 0 14 13 6 8 0 13	121837.42300	121837.42170	0.00130
14 6 8 0 14 13 6 7 0 13	121837.42300	121837.42178	0.00122
20 6 15 0 20 19 6 14 0 19	174106.22100	174106.23346	-0.01246
20 6 14 0 20 19 6 13 0 19	174106.22100	174106.23814	-0.01714
21 6 16 0 21 20 6 15 0 20	182822.69500	182822.68415	0.01085
21 6 15 0 21 20 6 14 0 20	182822.69500	182822.69225	0.00275
27 6 22 0 27 26 6 21 0 26	235158.49800	235158.43240	0.06560
27 6 21 0 27 26 6 20 0 26	235158.49800	235158.56648	-0.06848
28 6 23 0 28 27 6 22 0 27	243888.07500	243887.97262	0.10238
28 6 22 0 28 27 6 21 0 27	243888.07500	243888.17337	-0.09837
13 7 6 0 13 12 7 5 0 12	113122.81500	113122.79891	0.01609
13 7 7 0 13 12 7 6 0 12	113122.81500	113122.79891	0.01609
14 7 7 0 14 13 7 6 0 13	121827.73200	121827.72703	0.00497
14 7 8 0 14 13 7 7 0 13	121827.73200	121827.72702	0.00498
20 7 14 0 20 19 7 13 0 19	174073.84300	174073.85158	-0.00858
20 7 13 0 20 19 7 12 0 19	174073.84300	174073.85162	-0.00862
21 7 14 0 21 20 7 13 0 20	182784.76500	182784.76702	-0.00202
21 7 15 0 21 20 7 14 0 20	182784.76500	182784.76695	-0.00195
27 7 21 0 27 26 7 20 0 26	235074.20100	235074.21598	-0.01498

Continued on next page

Table B.1 – continued from previous page

Quantum number	EXP.FREQ.	CALC.FREQ.	DIFF.
27 7 20 0 27 26 7 19 0 26	235074.20100	235074.21804	-0.01704
28 7 22 0 28 27 7 21 0 27	243793.58300	243793.59197	-0.00897
28 7 21 0 28 27 7 20 0 27	243793.58300	243793.59530	-0.01230
14 8 6 0 14 13 8 5 0 13	121822.94200	121822.92627	0.01573
14 8 7 0 14 13 8 6 0 13	121822.94200	121822.92627	0.01573
20 8 12 0 20 19 8 11 0 19	174055.13600	174055.12686	0.00914
20 8 13 0 20 19 8 12 0 19	174055.13600	174055.12686	0.00914
21 8 13 0 21 20 8 12 0 20	182762.58400	182762.60073	-0.01673
21 8 14 0 21 20 8 13 0 20	182762.58400	182762.60073	-0.01673
27 8 19 0 27 26 8 18 0 26	235023.05000	235023.05675	-0.00675
27 8 20 0 27 26 8 19 0 26	235023.05000	235023.05673	-0.00673
28 8 20 0 28 27 8 19 0 27	243736.03300	243736.04029	-0.00729
28 8 21 0 28 27 8 20 0 27	243736.03300	243736.04025	-0.00725
20 9 11 0 20 19 9 10 0 19	174044.51300	174044.45443	0.05857
20 9 12 0 20 19 9 11 0 19	174044.51300	174044.45443	0.05857
21 9 12 0 21 20 9 11 0 20	182749.70200	182749.69292	0.00908
21 9 13 0 21 20 9 12 0 20	182749.70200	182749.69292	0.00908
27 9 18 0 27 26 9 17 0 26	234991.08600	234991.08595	0.00005
27 9 19 0 27 26 9 18 0 26	234991.08600	234991.08595	0.00005
28 9 19 0 28 27 9 18 0 27	243699.83300	243699.83795	-0.00495
28 9 20 0 28 27 9 19 0 27	243699.83300	243699.83795	-0.00495
21 10 11 0 21 20 10 10 0 20	182742.70600	182742.70452	0.00148
21 10 12 0 21 20 10 11 0 20	182742.70600	182742.70452	0.00148
23 10 14 0 23 22 10 13 0 22	200151.01200	200151.01297	-0.00097
27 10 17 0 27 26 10 16 0 26	234971.19700	234971.17749	0.01951
27 10 18 0 27 26 10 17 0 26	234971.19700	234971.17749	0.01951
28 10 18 0 28 27 10 17 0 27	243677.01500	243677.02876	-0.01376
28 10 19 0 28 27 10 18 0 27	243677.01500	243677.02876	-0.01376
23 12 12 0 23 22 12 11 0 22	200144.14000	200144.12974	0.01026
22 0 22 0 22 21 1 21 0 21	176324.58500	176324.57113	0.01387
23 0 23 0 23 22 1 22 0 22	185768.53200	185768.51402	0.01798
24 0 24 0 24 23 1 23 0 23	195097.06300	195097.04188	0.02112
25 0 25 0 25 24 1 24 0 24	204315.10900	204315.09842	0.01058
26 0 26 0 26 25 1 25 0 25	213428.96200	213428.96087	0.00113
27 0 27 0 27 26 1 26 0 26	222445.80900	222445.79139	0.01761
28 0 28 0 28 27 1 27 0 27	231373.25700	231373.24988	0.00712
29 0 29 0 29 28 1 28 0 28	240219.19800	240219.17557	0.02243
30 0 30 0 30 29 1 29 0 29	248991.35300	248991.33721	0.01579
21 1 21 0 21 20 0 20 0 20	188690.52700	188690.51865	0.00835
22 1 22 0 22 21 0 21 0 21	195706.04300	195706.04516	-0.00216
23 1 23 0 23 22 0 22 0 22	202825.03000	202825.03960	-0.00960
26 1 26 0 26 25 0 25 0 25	224791.19600	224791.19600	-0.00000
27 1 27 0 27 26 0 26 0 26	232302.99900	232302.99852	0.00048
28 1 28 0 28 27 0 27 0 27	239899.91600	239899.94649	-0.03049
13 0 13 1 12 12 1 12 1 11	86563.80600	86563.77023	0.03577
13 0 13 1 14 12 1 12 1 13	86563.80600	86563.80353	0.00247
13 0 13 1 13 12 1 12 1 12	86564.18400	86564.16829	0.01571

Continued on next page

Table B.1 – continued from previous page

Quantum number	EXP.FREQ.	CALC.FREQ.	DIFF.
14 0 14 1 13 13 1 13 1 12	96834.04100	96834.01005	0.03095
14 0 14 1 15 13 1 13 1 14	96834.04100	96834.03867	0.00233
14 0 14 1 14 13 1 13 1 13	96834.37600	96834.37586	0.00014
15 0 15 1 14 14 1 14 1 13	107070.18200	107070.15927	0.02273
15 0 15 1 16 14 1 14 1 15	107070.18200	107070.18384	-0.00184
15 0 15 1 15 14 1 14 1 14	107070.49600	107070.49282	0.00318
16 0 16 1 15 15 1 15 1 14	117250.43000	117250.41402	0.01598
16 0 16 1 17 15 1 15 1 16	117250.43000	117250.43509	-0.00509
16 0 16 1 16 15 1 15 1 15	117250.71200	117250.71573	-0.00373
6 1 6 1 6 5 0 5 1 5	87154.54200	87154.50477	0.03723
6 1 6 1 7 5 0 5 1 6	87155.03900	87155.03595	0.00305
6 1 6 1 5 5 0 5 1 4	87155.03900	87155.11891	-0.07991
7 1 7 1 7 6 0 6 1 6	94425.91500	94425.88913	0.02587
7 1 7 1 8 6 0 6 1 7	94426.41700	94426.41366	0.00334
7 1 7 1 6 6 0 6 1 5	94426.41700	94426.48406	-0.06706
8 1 8 1 8 7 0 7 1 7	101532.50100	101532.49327	0.00773
8 1 8 1 9 7 0 7 1 8	101533.00200	101533.00691	-0.00491
8 1 8 1 7 7 0 7 1 6	101533.00200	101533.06725	-0.06525
9 1 9 1 9 8 0 8 1 8	108491.95900	108491.96499	-0.00599
9 1 9 1 10 8 0 8 1 9	108492.45400	108492.46415	-0.01015
9 1 9 1 8 8 0 8 1 7	108492.45400	108492.51622	-0.06222
12 1 12 1 12 11 0 11 1 11	128696.96700	128696.97519	-0.00819
12 1 12 1 13 11 0 11 1 12	128697.40800	128697.41366	-0.00566
12 1 12 1 11 11 0 11 1 10	128697.40800	128697.44758	-0.03958
19 1 18 1 18 19 0 19 1 18	93434.29700	93434.28239	0.01461
19 1 18 1 20 19 0 19 1 20	93434.29700	93434.33109	-0.03409
19 1 18 1 19 19 0 19 1 19	93435.25700	93435.25538	0.00162
20 1 19 1 19 20 0 20 1 19	100135.67300	100135.65248	0.02052
20 1 19 1 21 20 0 20 1 21	100135.67300	100135.69939	-0.02639
20 1 19 1 20 20 0 20 1 20	100136.64600	100136.63733	0.00867
21 1 20 1 20 21 0 21 1 20	107253.78800	107253.77976	0.00824
21 1 20 1 22 21 0 21 1 22	107253.78800	107253.82502	-0.03702
21 1 20 1 21 21 0 21 1 21	107254.76100	107254.77297	-0.01197
22 1 21 1 21 22 0 22 1 21	114768.11400	114768.09980	0.01420
22 1 21 1 23 22 0 22 1 23	114768.11400	114768.14324	-0.02924
22 1 21 1 22 22 0 22 1 22	114769.10200	114769.09761	0.00439
23 1 22 1 22 23 0 23 1 22	122653.02000	122653.01173	0.00827
23 1 22 1 24 23 0 23 1 24	122653.02000	122653.05339	-0.03339
23 1 22 1 23 23 0 23 1 23	122654.00200	122654.01033	-0.00833
37 2 35 1 36 37 1 36 1 36	170597.38100	170597.37618	0.00482
37 2 35 1 38 37 1 36 1 38	170597.38100	170597.39309	-0.01209
37 2 35 1 37 37 1 36 1 37	170598.06600	170598.01843	0.04757
22 2 21 1 21 22 1 22 1 21	174387.72800	174387.69434	0.03366
22 2 21 1 23 22 1 22 1 23	174387.72800	174387.72284	0.00516
22 2 21 1 22 22 1 22 1 22	174388.32800	174388.34957	-0.02157
23 2 22 1 22 23 1 23 1 22	179529.74800	179529.75918	-0.01118
23 2 22 1 24 23 1 23 1 24	179529.74800	179529.78641	-0.03841

Continued on next page

Table B.1 – continued from previous page

Quantum number	EXP.FREQ.	CALC.FREQ.	DIFF.
23 2 22 1 23 23 1 23 1 23	179530.41600	179530.41216	0.00384
24 2 23 1 23 24 1 24 1 23	184881.45100	184881.44467	0.00633
24 2 23 1 25 24 1 24 1 25	184881.45100	184881.47070	-0.01970
24 2 23 1 24 24 1 24 1 24	184882.10900	184882.09497	0.01403
39 2 37 1 38 39 1 38 1 38	188057.47400	188057.45743	0.01657
39 2 37 1 40 39 1 38 1 40	188057.47400	188057.47405	-0.00005
39 2 37 1 39 39 1 38 1 39	188058.12300	188058.12175	0.00125
43 2 41 1 42 43 1 42 1 42	226661.78600	226661.77565	0.01035
43 2 41 1 44 43 1 42 1 44	226661.78600	226661.79086	-0.00486
43 2 41 1 43 43 1 42 1 43	226662.58800	226662.44514	0.14286
32 2 31 1 31 32 1 32 1 31	234447.70000	234447.67833	0.02167
32 2 31 1 33 32 1 32 1 33	234447.70000	234447.69690	0.00310
32 2 31 1 32 32 1 32 1 32	234448.29500	234448.29077	0.00423
44 2 42 1 43 44 1 43 1 43	236829.85300	236829.82331	0.02969
44 2 42 1 45 44 1 43 1 45	236829.85300	236829.83806	0.01494
44 2 42 1 44 44 1 43 1 44	236830.49800	236830.48694	0.01106
33 2 32 1 32 33 1 33 1 32	241369.71400	241369.70330	0.01070
33 2 32 1 34 33 1 33 1 34	241369.71400	241369.72113	-0.00713
33 2 32 1 33 33 1 33 1 33	241370.30300	241370.30909	-0.00609
45 2 43 1 44 45 1 44 1 44	247118.50000	247118.50151	-0.00151
45 2 43 1 46 45 1 44 1 46	247118.50000	247118.51576	-0.01576
45 2 43 1 45 45 1 44 1 45	247119.17200	247119.15692	0.01508
34 2 33 1 33 34 1 34 1 33	248424.36300	248424.34447	0.01853
34 2 33 1 35 34 1 34 1 35	248424.36300	248424.36158	0.00142
34 2 33 1 34 34 1 34 1 34	248424.93900	248424.94326	-0.00426
11 2 9 1 10 10 1 10 1 9	228235.45300	228235.42944	0.02356
11 2 9 1 12 10 1 10 1 11	228235.45300	228235.50994	-0.05694
11 2 9 1 11 10 1 10 1 10	228236.32400	228236.31379	0.01021
12 2 11 1 12 11 1 10 1 11	208509.34800	208509.36516	-0.01716
12 2 11 1 13 11 1 10 1 12	208509.92300	208509.92769	-0.00469
12 2 11 1 11 11 1 10 1 10	208509.92300	208509.97764	-0.05464
13 2 12 1 13 12 1 11 1 12	214689.25600	214689.24587	0.01013
13 2 12 1 14 12 1 11 1 13	214689.79400	214689.80714	-0.01314
13 2 12 1 12 12 1 11 1 11	214689.79400	214689.85283	-0.05883
34 2 32 1 33 33 3 31 1 32	178068.70200	178068.70660	-0.00460
34 2 32 1 35 33 3 31 1 34	178068.70200	178068.72003	-0.01803
34 2 32 1 34 33 3 31 1 33	178069.15500	178069.17310	-0.01810
36 2 34 1 35 35 3 33 1 34	206756.07500	206756.08488	-0.00988
36 2 34 1 37 35 3 33 1 36	206756.07500	206756.09707	-0.02207
36 2 34 1 36 35 3 33 1 35	206756.50600	206756.53188	-0.02588
37 2 35 1 36 36 3 34 1 35	221127.31000	221127.30002	0.00998
37 2 35 1 38 36 3 34 1 37	221127.31000	221127.31157	-0.00157
37 2 35 1 37 36 3 34 1 36	221127.75100	221127.73507	0.01593
38 2 36 1 37 37 3 35 1 36	235481.44000	235481.46037	-0.02037
38 2 36 1 39 37 3 35 1 38	235481.44000	235481.47129	-0.03129
38 2 36 1 38 37 3 35 1 37	235481.86000	235481.88210	-0.02210
39 2 37 1 38 38 3 36 1 37	249791.22000	249791.21346	0.00654

Continued on next page

Table B.1 – continued from previous page

Quantum number	EXP.FREQ.	CALC.FREQ.	DIFF.
39 2 37 1 40 38 3 36 1 39	249791.22000	249791.22374	-0.00374
39 2 37 1 39 38 3 36 1 38	249791.61900	249791.62055	-0.00155
40 1 39 1 39 40 0 40 1 39	280690.59800	280690.62969	-0.03169
40 1 39 1 41 40 0 40 1 41	280690.59800	280690.64582	-0.04782
40 1 39 1 40 40 0 40 1 40	280691.31900	280691.29083	0.02817
37 4 34 0 37 37 3 35 1 37	282104.96300	282104.97371	-0.01071
42 9 34 0 42 43 8 35 0 43	293325.72200	293325.72460	-0.00260
58 4 54 0 58 58 3 55 0 58	210316.04600	210316.04089	0.00511
59 4 55 0 59 59 3 56 0 59	214551.63200	214551.62044	0.01156
60 4 56 0 60 60 3 57 0 60	219456.92400	219456.93487	-0.01087
61 4 57 0 61 61 3 58 0 61	225028.40800	225028.41009	-0.00209
62 4 58 0 62 62 3 59 0 62	231257.29400	231257.30951	-0.01551
63 4 59 0 63 63 3 60 0 63	238129.60800	238129.49221	0.11579
55 5 50 0 55 55 4 51 0 55	282919.18400	282919.15338	0.03062
65 5 60 0 65 65 4 61 0 65	246972.98300	246973.01806	-0.03506
67 5 62 0 67 67 4 63 0 67	245063.01500	245063.02004	-0.00504
68 5 63 0 68 68 4 64 0 68	245044.10400	245044.10118	0.00282
69 5 64 0 69 69 4 65 0 69	245687.39300	245687.35704	0.03596
68 11 57 0 68 69 10 60 0 69	220302.55800	220302.55673	0.00127
66 11 56 0 66 67 10 57 0 67	238365.44500	238364.90172	0.54328
22 6 16 0 22 23 5 19 0 23	232491.27700	232491.25950	0.01750
23 6 18 0 23 24 5 19 0 24	223662.03500	223662.05816	-0.02316
23 6 17 0 23 24 5 20 0 24	223667.91600	223667.91304	0.00296
24 6 18 0 24 25 5 21 0 25	214829.29800	214829.26375	0.03425
25 6 20 0 25 26 5 21 0 26	205961.22800	205961.24038	-0.01238
25 6 19 0 25 26 5 22 0 26	205974.19000	205974.18509	0.00491
26 6 21 0 26 27 5 22 0 27	197082.72300	197082.73177	-0.00877
26 6 20 0 26 27 5 23 0 27	197101.54800	197101.54203	0.00597
28 6 23 0 28 29 5 24 0 29	179260.88800	179260.90625	-0.01825
28 6 22 0 28 29 5 25 0 29	179299.03100	179299.04568	-0.01468
29 6 24 0 29 30 5 25 0 30	170313.65700	170313.67270	-0.01570
29 6 23 0 29 30 5 26 0 30	170366.99500	170366.98638	0.00862
29 11 19 0 29 28 11 18 0 28	252367.16500	252367.17799	-0.01299
29 13 17 0 29 28 13 16 0 28	252354.17700	252354.15836	0.01864
29 16 14 0 29 28 16 13 0 28	252363.05300	252363.03888	0.01412
29 17 13 0 29 28 17 12 0 28	252370.95300	252370.94096	0.01204
31 1 31 1 31 30 1 30 1 30	260206.66900	260206.66419	0.00481
31 5 26 0 31 30 5 25 0 30	270328.06000	270328.07864	-0.01864
31 12 20 0 31 30 12 19 0 30	269763.08200	269763.09672	-0.01472
31 13 19 0 31 30 13 18 0 30	269756.67800	269756.62359	0.05441
31 14 18 0 31 30 14 17 0 30	269754.84400	269754.84015	0.00385
31 15 17 0 31 30 15 16 0 30	269756.67800	269756.76153	-0.08353
31 16 16 0 31 30 16 15 0 30	269761.70200	269761.70205	-0.00005
31 17 15 0 31 30 17 14 0 30	269769.16000	269769.17164	-0.01164
32 2 31 0 32 31 2 30 0 31	275272.30300	275272.30362	-0.00062
32 3 29 0 32 31 3 28 0 31	282491.09100	282491.08134	0.00966
32 4 29 0 32 31 4 28 0 31	279353.18000	279353.20203	-0.02203

Continued on next page

Table B.1 – continued from previous page

Quantum number	EXP.FREQ.	CALC.FREQ.	DIFF.
32 5 28 0 32 31 5 27 0 31	279067.58100	279067.58122	-0.00022
32 7 26 0 32 31 7 25 0 31	278685.75000	278685.75357	-0.00357
32 8 24 0 32 31 8 23 0 31	278597.47600	278597.48918	-0.01318
32 10 22 0 32 31 10 21 0 31	278504.07600	278504.03829	0.03771
32 12 21 0 32 31 12 20 0 31	278465.65700	278465.66584	-0.00884
32 13 20 0 32 31 13 19 0 31	278457.74400	278457.75852	-0.01452
32 14 19 0 32 31 14 18 0 31	278454.93400	278454.94720	-0.01320
32 15 18 0 32 31 15 17 0 31	278456.14100	278456.14884	-0.00784
32 16 17 0 32 31 16 16 0 31	278460.60800	278460.60956	-0.00156
32 20 13 0 32 31 20 12 0 31	278502.21400	278502.18710	0.02690
33 0 33 0 33 32 0 32 0 32	277086.11200	277086.10658	0.00542
33 1 33 0 33 32 1 32 0 32	276773.15000	276773.14687	0.00313
33 2 32 0 33 32 2 31 0 32	283695.17400	283695.16936	0.00464
33 3 31 0 33 32 3 30 0 32	287430.90400	287430.89791	0.00609
33 4 29 0 33 32 4 28 0 32	288697.22800	288697.22505	0.00295
33 5 28 0 33 32 5 27 0 32	287865.21600	287865.21442	0.00158
33 7 26 0 33 32 7 25 0 32	287412.73200	287412.75027	-0.01827
33 10 24 0 33 32 10 23 0 32	287211.74100	287211.75233	-0.01133
33 18 16 0 33 32 18 15 0 32	287175.41300	287175.39710	0.01590
34 0 34 0 34 33 0 33 0 33	285321.10300	285321.09404	0.00896
34 1 34 0 34 33 1 33 0 33	285051.02300	285051.01779	0.00521
34 6 29 0 34 33 6 28 0 33	296313.97500	296313.96587	0.00913
34 6 28 0 34 33 6 27 0 33	296315.68300	296315.67851	0.00449
35 2 33 0 35 34 2 32 0 34	310396.15500	310396.14198	0.01302
35 7 28 0 35 34 7 27 0 34	304871.77100	304871.80653	-0.03553
35 18 18 0 35 34 18 17 0 34	304570.38800	304570.38269	0.00531
35 12 24 0 35 34 12 23 0 34	304573.65500	304573.66566	-0.01066
36 1 35 0 36 35 1 34 0 35	311369.73500	311369.73920	-0.00420
36 3 34 0 36 35 3 33 0 35	313311.69400	313311.67263	0.02137
36 17 20 0 36 35 17 19 0 35	313258.69300	313258.70092	-0.00792
36 13 24 0 36 35 13 23 0 35	313261.57100	313261.58903	-0.01803
36 12 25 0 36 35 12 24 0 35	313276.43600	313276.43339	0.00261
37 15 23 0 37 36 15 22 0 36	321949.38600	321949.41187	-0.02587
37 16 22 0 37 36 16 21 0 36	321950.52600	321950.52690	-0.00090
37 14 24 0 37 36 14 23 0 36	321952.94900	321952.96724	-0.01824
37 17 21 0 37 36 17 20 0 36	321955.48000	321955.48174	-0.00174
38 0 38 0 38 37 0 37 0 37	318279.76800	318279.77061	-0.00261
38 2 37 0 38 37 2 36 0 37	325630.80300	325630.79476	0.00824
38 4 34 0 38 37 4 33 0 37	333362.52700	333362.51299	0.01401
38 5 33 0 38 37 5 32 0 37	331814.24800	331814.20034	0.04766
38 7 31 0 38 37 7 30 0 37	331073.91700	331073.99838	-0.08138
38 10 28 0 38 37 10 27 0 37	330756.63700	330756.69826	-0.06126
39 1 39 0 39 38 1 38 0 38	326398.01900	326397.99861	0.02039
39 2 38 0 39 38 2 37 0 38	333984.98800	333984.98123	0.00677
39 3 36 0 39 38 3 35 0 38	346145.75700	346145.74681	0.01019
39 4 36 0 39 38 4 35 0 38	340685.19500	340685.18520	0.00980
39 5 35 0 39 38 5 34 0 38	340475.03600	340475.02991	0.00609

Continued on next page

Table B.1 – continued from previous page

Quantum number	EXP.FREQ.	CALC.FREQ.	DIFF.
39 7 33 0 39 38 7 32 0 38	339811.79700	339811.67216	0.12484
39 10 30 0 39 38 10 29 0 38	339467.04200	339467.04773	-0.00573
40 0 40 0 40 39 0 39 0 39	334766.95600	334766.95305	0.00295
40 1 40 0 40 39 1 39 0 39	334660.52100	334660.50771	0.01329
40 3 38 0 40 39 3 37 0 39	347631.41400	347631.40887	0.00513
40 4 37 0 40 39 4 36 0 39	349431.75400	349431.74359	0.01041
40 5 36 0 40 39 5 35 0 39	349259.18600	349259.17983	0.00617
40 7 34 0 40 39 7 33 0 39	348551.71500	348551.53846	0.17654
40 10 31 0 40 39 10 30 0 39	348177.85400	348177.87917	-0.02517
41 0 41 0 41 40 0 40 0 40	343011.73000	343011.71374	0.01626

Registered TS rotamer lines and relative errors between regestered and calculated frequencies returned by Spfit in the .fit file.

Bibliography

[1] Ministère de la Culture, *Lascaux*. 2019. URL: http://archeologie.culture.fr/lascaux/en.

[2] Wikipedia, *Lascaux*. 2019. URL: https://en.wikipedia.org/wiki/Lascaux.

[3] Dirk L. Hoffmann et al., "Symbolic use of marine shells and mineral pigments by Iberian Neandertals 115,000 years ago". In: *Science Advances* 4.2 (2018). DOI: 10.1126/sciadv.aar5255.

[4] *History of the world*. URL: https://en.wikipedia.org/wiki/History_of_the_world.

[5] Charles Darwin, *On the Origin of Species by Means of Natural Selection, or the Preservation of Favoured Races in the Struggle for Life*. 1859.

[6] A. S. Stodolna et al., "Hydrogen Atoms under Magnification: Direct Observation of the Nodal Structure of Stark States". In: *Phys. Rev. Lett.* 110 (21 May 2013), p. 213001. DOI: 10.1103/PhysRevLett.110.213001.

[7] Stephen Hawking, *A Brief History of Time*. Bantam editor, 2016.

[8] Isac Newton, *Philosophiae Naturalis Principia Mathematica*. 1687.

[9] *Earth*. URL: https://solarsystem.nasa.gov/planets/earth/in-depth/.

[10] *Alpha Centauri: A Triple Star System about 4 Light Years from Earth*. June 2018. URL: https://www.nasa.gov/missiodistancen_pages/chandra/images/alpha-centauri-a-triple-star-system-about-4-light-years-from-earth.html.

[11] *Hubble Uncovers the Farthest Star Ever Seen*. Apr. 2018. URL: https://www.nasa.gov/feature/goddard/2018/hubble-uncovers-the-farthest-star-ever-seen.

[12] *Milky Way*. URL: https://exoplanets.nasa.gov/milky-way-overlay/.

[13] *Observable universe contains ten times more galaxies than previoulsy thought*. Oct. 2016. URL: https://sci.esa.int/web/hubble/-/58444-observable-universe-contains-ten-times-more-galaxies-than-previously-thought-heic1620.

[14] A. Wolszczan and D. A. Frail, "A planetary system around the millisecond pulsar PSR1257 + 12". In: *Nature* 355.6356 (1992), pp. 145–147. DOI: 10.1038/355145a0.

[15] Queloz Didier Mayor Michel, "A Jupiter-mass companion to a solar-type star". In: *Nature* 378.6555 (1995), pp. 355–359. DOI: 10.1038/378355a0.

[16] *Physics Nobel goes to exoplanet and cosmology pioneers*. URL: https://www.nature.com/articles/d41586-019-02964-z.

[17] Allen P. Nutman et al., "Rapid emergence of life shown by discovery of 3,700-million-year-old microbial structures". In: *Nature* 537 (Aug. 2016), 535 EP. URL: https://doi.org/10.1038/nature19355.

[18] *Warm welcome: finding habitable planets*. URL: https://exoplanets.nasa.gov/what-is-an-exoplanet/how-do-we-find-habitable-planets/.

[19] *Flares May Threaten Planet Habitability Near Red Dwarfs*. URL: https://www.nasa.gov/feature/jpl/flares-may-threaten-planet-habitability-near-red-dwarfs.

[20] *Tarantula Nebula*. Nov. 2004. URL: http://www.esa.int/Science_Exploration/Space_Science/Extreme_space/The_Tarantula_Nebula_30_Doradus.

[21] Ewine F. van Dishoeck, "Astrochemistry of dust, ice and gas: Introduction and overview". In: *Faraday Discuss.* 168 (July 2014). DOI: 10.1039/C4FD00140K.

[22] Oct. 2019. URL: https://www.nasa.gov/feature/goddard/2019/a-dusty-lab-in-the-sky.

[23] Bernard Marty, "The origins and concentrations of water, carbon, nitrogen and noble gases on Earth". In: *Earth and Planetary Science Letters* 313-314 (2012), pp. 56–66. DOI: 10.1016/j.epsl.2011.10.040.

[24] Morbidelli A. Chambers J. Lunine J. I. Petit J. M. Robert F. Valsecchi G. B. Cyr K. E., "Source regions and timescales for the delivery of water to the Earth". In: *Meteoritics and planetary science* (2000). DOI: 10.1111/j.1945-5100.2000.tb01518.x.

[25] François Robert, "The D/H Ratio in Chondrites". In: *Space Science Reviews* 106.1 (2003), pp. 87–101. DOI: 10.1023/A:1024629402715.

[26] Raymond S. N. O' Brien D. P. Morbidelli A. Kaib N. A., "Building the terrestrial planets: Constrained accretion in the inner Solar System". In: *Icarus* 203.Issue 2 (2009), pp. 644–662. DOI: 10.1016/j.icarus.2009.05.016.

[27] Dauphas N., "The dual origin of the terrestrial atmosphere". In: *Icarus* 165 (2003), pp. 326–339. DOI: 10.1016/S0019-1035(03)00198-2.

[28] Cecilia Ceccarelli Paola Caselli, "Our astrochemical heritage". In: *The Astronomy and Astrophysics Review* (2012). DOI: https://doi.org/10.1007/s00159-012-0056-x.

[29] Steven B. Charnley Michael J. Mumma, "The Chemical Composition of Comets - Emerging Taxonomies and Natal Heritage". In: *Annual Review of Astronomy and Astrophysics* 49.1 (2011), pp. 471–524. DOI: 10.1146/annurev-astro-081309-130811.

[30] Dominique Bockelée-Morvan, "An Overview of Comet Composition". In: *Cambridge University Press* 7.S280 (June 2011), pp. 261–274. DOI: 10.1017/S1743921311025038.

[31] Jamie E. Elsila; Daniel P. Glavin; Jason P. Dworkin, "Cometary glycine detected in samples returned by Stardust". In: *Meteoritics and Planetary Science* 44.9 (2010). DOI: 10.1111/j.1945-5100.2009.tb01224.x.

[32] Fraser W. C. Brown M. E. Schaller E. L., "Water ice in the Kuiper Belt". In: *The Astrochemical Jornal* 143.6 (2012), p. 146. DOI: 10.1088/0004-6256/143/6/146.

[33] Chris J. Bennett et al., "Laboratory Studies on the Irradiation of Methane in Interstellar, Cometary, and Solar System Ices". In: *The Astrophysical Journal* 653.1 (2006), pp. 792–811. DOI: 10.1086/508561.

[34] Pizzarello Sandra; Huang Yongsong; Becker Luann; Poreda Robert J.; Nieman Ronald A.; Cooper George; Williams Michael, "The Organic Content of the Tagish Lake Meteorite". In: *Science* 293.5538 (Sept. 2001), p. 2236. DOI: 10.1126/science.1062614.

[35] Kendra A. Turk Sandra Pizzarello Michael Zolensky, "Nonracemic isovaline in the Murchison meteorite: Chiral distribution and mineral association". In: *Geochimica et Cosmochimica Acta* 67 (2003), pp. 1589–1595. DOI: doi:10.1016/S0016-7037(00)01283-8.

[36] Levison Harold F.; Duncan Martin J.; Brasser Ramon; Kaufmann David E., "Capture of the Sun's Oort Cloud from Stars in Its Birth Cluster". In: *Science* 329.5988 (July 2010), p. 187. DOI: 10.1126/science.1187535.

[37] Ciesla Fred J. Yang Le, "The effects of disk building on the distributions of refractory materials in the solar nebula". In: *Meteoritics and amp* (2012). DOI: 10.1111/j.1945-5100.2011.01315.x.

[38] Laurent Remusat et al., "Proto-planetary disk chemistry recorded by D-rich organic radicals in carbonaceous chondrites". In: *The Astrophysical Journal* 698.2 (2009), pp. 2087–2092. DOI: 10.1088/0004-637x/698/2/2087.

[39] Sandra Pizzarello and Yongsong Huang, "The deuterium enrichment of individual amino acids in carbonaceous meteorites: A case for the presolar distribution of biomolecule precursors". In: *Geochimica et Cosmochimica Acta* 69 (Feb. 2005), pp. 599–605. DOI: 10.1016/j.gca.2004.07.031.

[40] Eva Wirström et al., "Isotopic Anomalies in Primitive Solar System Matter: Spin-state Dependent Fractionation of Nitrogen and Deuterium in Interstellar Clouds". In: *Astrophysical Journal Letters* 757 (Aug. 2012). DOI: 10.1088/2041-8205/757/1/L11.

[41] Paul F. Goldsmith, "Molecular Depletion and Thermal Balance in Dark Cloud Cores". In: 557.2 (2001), pp. 736–746. DOI: 10.1086/322255.

[42] Tracy L. Lada Charles J.; Bergin Edwin A.; Alves Joao F.; Huard, "The Dynamical State of Barnard 68: A Thermally Supported, Pulsating Dark Cloud". In: *The Astrophysical Journal* 586.1 (2003), pp. 286–295. DOI: 10.1086/367610.

[43] F.; André P. Ward-Thompson D.; Motte, "The initial conditions of isolated star formation - III. Millimetre continuum mapping of pre-stellar cores". In: *Monthly Notices of the Royal Astronomical Society* 305.1 (May 1999), pp. 143–150. ISSN: 0035-8711. DOI: 10.1046/j.1365-8711.1999.02412.x.

[44] William Herbst Eric; Klemperer, "The Formation and Depletion of Molecules in Dense Interstellar Clouds". In: *Astrophysical Journal* 185 (1973), pp. 505–534. DOI: 10.1086/152436.

[45] Bergin Edwin A.; Alves João; Huard Tracy; Lada Charles J., "N2H+ and C18O Depletion in a Cold Dark Cloud". In: *The Astrochemical Jornal* 570.2 (2002), pp. L101–L104. DOI: 10.1086/340950.

[46] Caselli P.; Van der Tak F. F. S.; Ceccarelli C.; Bacmann A., "Abundant H2D+ in the pre–stellar core L1544". In: *Astronomy and Astrophysics* 403.3 (2003), pp. L37–L41. DOI: 10.1051000463612003052 6.

[47] Charnley S. B.; Tielens A. G. G. M.; Rodgers S. D., "Deuterated Methanol in the Orion Compact Ridge". In: 482.2 (1997), pp. L203–L206. DOI: 10.1086/310697.

[48] Caselli Paola; Stantcheva Tatiana; Shalabiea Osama; Shematovich Valery I; Herbst Eric, "Deuterium fractionation on interstellar grains studied with modified rate equations and a Monte Carlo approach". In: *Planetary and Space Science* 50.12 (2002), pp. 1257–1266. DOI: https://doi.org/10.1016/S0032-0633(02)00092-2.

[49] "Observations of Nitrogen Fractionation in Prestellar Cores: Nitriles Tracing Interstellar Chemistry". In: LPI Contribution No. 1659, id.2618 43rd. Lunar and Planetary Science Conference. The Woodlands, Texas, Mar. 2012.

[50] Adande G. R.; Ziurys L. M., "Millimeter-wave Observations of CN and HNC and Their 15N Isotopologues: A New Evaluation of the 14N/15N Ratio across the Galaxy." In: *The Astrophysical Journal* 744.2 (2011), p. 194. DOI: 10.1088/0004-637x/744/2/194.

[51] Max P Bernstein et al., "Racemic amino acids from the ultraviolet photolysis of interstellar ice analogues." eng. In: *Nature* 416.6879 (Mar. 2002), pp. 401–403. ISSN: 0028-0836 (Print); 0028-0836 (Linking). DOI: 10.1038/416401a.

[52] E. F. van Dishoeck K. I. Öberg and H. Linnartz, "Photodesorption of ices I: CO, N2, and CO2". In: *Astronomy and Astrophysics* 496.1 (Mar. 2009), pp. 281–293. DOI: 10.1051/0004-6361/200810207.

[53] Palumbo M.; Pendleton Yvonne; Strazzulla Giovanni, "Hydrogen Isotopic Substitution Studies of the 2165 Wavenumber (4.62 Micron) "XCN" Feature Produced by Ion Bombardment". In: *The Astrophysical Journal* 542 (Oct. 2000), pp. 890–893. DOI: 10.1086/317061.

[54] H. Ioppolo S.; Cuppen H. M.; Romanzin C.; van Dishoeck E. F.; Linnartz, "Laboratory Evidence for Efficient Water Formation in Interstellar Ices". In: *The Astrophysical Journal* 686.2 (2008), pp. 1474–1479. DOI: 10.1086/591506.

[55] G. W. Fuchs; H. M. Cuppen; S. Ioppolo; C. Romanzin; S. E. Bisschop; S. Andersson; E. F. van Dishoeck; H. Linnartz, "Hydrogenation reactions in interstellar CO ice analogues. A combined experimental/theoretical approach". In: *Astronomy and Astrophysics* 505.2 (Oct. 2009), pp. 629 –639. DOI: 10.1051/0004-6361/200810784.

[56] S. Cazaux and A. G. G. M. Tielens, "Molecular Hydrogen Formation in the Interstellar Medium". In: *The Astrophysical Journal* 575.1 (2002), pp. L29–L32. DOI: 10.1086/342607. URL: http://dx.doi.org/10.1086/342607.

[57] Koji Murakawa, Motohide Tamura, and Tetsuya Nagata, "1–4 Micron Spectrophotometry of Dust in the Taurus Dark Cloud: Water Ice Distribution in Heiles Cloud 2". In: 128.2 (2000), pp. 603–613. DOI: 10.1086/313387. URL: http://dx.doi.org/10.1086/313387.

[58] David Hollenbach et al., "Water, O2, and ice in molecular clouds". In: 690.2 (2008), pp. 1497–1521. DOI: 10.1088/0004-637x/690/2/1497.

[59] Volker Ossenkopf and Th Henning, "Dust opacities for protostellar cores". In: *Astronomy and Astrophysics* 291 (Nov. 1994), pp. 943–959.

[60] G. A. Baratta S. Ioppolo M. E. Palumbo and V. Mennella, "Formation of interstellar solid CO2 after energetic processing of icy grain mantles". In: *Astronomy and Astrophysics* 493.3 (2009), pp. 1017 –1028. DOI: 10.1051/0004-6361:200809769.

[61] Oba Yasuhiro; Watanabe Naoki; Kouchi Akira; Hama Tetsuya; Pirronello Valerio, "Experimental study of CO2 formation by surface reactions of non-energetic OH radicals with CO molecules". In: 712.2 (2010), pp. L174–L178. DOI: 10.1088/2041-8205/712/2/l174.

[62] M. Marseille S. Cazaux V. Cobut, M. Spaans, and P. Caselli, "Water formation on bare grains: When the chemistry on dust impacts interstellar gas". In: *Astronomy and Astrophysics* 522.A74 (Nov. 2010), p. 14. DOI: 10.1051/0004-6361/201014026.

[63] Kenzo Hiraoka et al., "Gas-Grain Processes for the Formation of CH4 and H2O: Reactions of H Atoms with C, O, and CO in the Solid Phase at 12 K". In: *The Astrophysical Journal* 498.2 (1998), pp. 710–715. DOI: 10.1086/305572.

[64] H. Mokrane et al., "Experimental evidence for water formation via ozone hydrogenation on dust grains at 10 K". In: *The Astrophysical Journal* 705.2 (2009), pp. L195–L198. DOI: 10.1088/0004-637x/705/2/l195.

[65] Karin I. Öberg et al., "Photodesorption of ices II. H2O AND D2O". In: *The Astrophysical Journal* 693.2 (2009), pp. 1209–1218. DOI: 10.1088/0004-637x/693/2/1209.

[66] W.-F. Thi, P. Woitke, and I. Kamp, "Warm non-equilibrium gas phase chemistry as a possible origin of high HDO/H2O ratios in hot and dense gases: application to inner protoplanetary discs". In: *Monthly Notices of the Royal Astronomical Society* 407.1 (Aug. 2010), pp. 232–246. ISSN: 0035-8711. DOI: 10.1111/j.1365-2966.2009.16162.x. eprint: http://oup.prod.sis.lan/mnras/article-pdf/407/1/232/3073674/mnras0407-0232.pdf.

[67] C. Ceccarelli V. Taquet and C. Kahane, "Multilayer modeling of porous grain surface chemistry". In: *Astronomy and Astrophysics* 538.A42 (Feb. 2011), p. 19. DOI: 10.1051/0004-6361/201117802.

[68] Nov. 2019. URL: http://www.astrochem.org/sci/Master_Residues.php.

[69] T. J. Matthews H. E.; Sears, "The detection of vinyl cyanide in TMC-1". In: *Astrophysical Journal* 272 (Sept. 1983), pp. 149–153. DOI: 10.1086/161271.

[70] Broten N. W.; MacLeod J. M.; Avery L. W.; Irvine W. M.; Hoglund B.; Friberg P.; Hjalmarson A., "The detection of interstellar methylcyanoacetylene". In: *Astrophysical Journal* 276 (Jan. 1984), pp. L25–L29. DOI: 10.1086/184181.

[71] Irvine W. M. Matthews H. E. Friberg P., "The detection of acetaldehyde in cold dust clouds". In: *Astrophysical Journal* 290 (Mar. 1985), pp. 609–614. DOI: 10.1086/163018.

[72] Irvine W. M.; Friberg P.; Kaifu N.; Kawaguchi K.; Kitamura Y.; Matthews H. E.; Minh Y.; Saito S.; Ukita N.; Yamamoto S., "Observations of some Oxygen-containing and Sulfur-containing Organic Molecules in Cold Dark Clouds". In: *Astrophysical Journal* 342 (July 1989), p. 871. DOI: 10.1086/167643.

[73] Friberg P.; Madden S. C.; Hjalmarson A.; Irvine W. M., "Methanol in dark clouds". In: *Astronomy and Astrophysics* 195 (Apr. 1988), pp. 281–289.

[74] L. E. Snyder et al., "Confirmation of Interstellar Methylcyanodiacetylene (CH3C5N)". In: *The Astrophysical Journal* 647.1 (Aug. 2006), pp. 412–417. DOI: 10.1086/505323.

[75] Anthony J. Remijan et al., "Methyltriacetylene (CH3C6H) toward TMC-1: The Largest Detected Symmetric Top". In: *The Astrophysical Journal* 643.1 (Apr. 2006), pp. L37–L40. DOI: 10.1086/504918. URL: http://dx.doi.org/10.1086/504918.

[76] N. Marcelino et al., "Discovery of Interstellar Propylene (CH2CHCH3): Missing Links in Interstellar Gas-Phase Chemistry". In: *The Astrophysical Journal* 665.2 (2007), pp. L127–L130. DOI: 10.1086/521398.

[77] Hirahara Yasuhiro; Suzuki Hiroko; Yamamoto Satoshi; Kawaguchi Kentarou; Kaifu Norio; Ohishi Masatoshi; Takano Shuro; Ishikawa Shin-Ichi; Masuda Akimasa, "Mapping Observations of Sulfur-containing Carbon-Chain Molecules in Taurus Molecular Cloud 1 (TMC-1)". In: *Astrophysical Journal* 394.539 (Aug. 1992). DOI: 10.1086/171605.

[78] Masatoshi Ohishi and Norio Kaifu, "Chemical and physical evolution of dark clouds Molecular spectral line survey toward TMC-1". In: *Faraday Discussions* 109 (1998), pp. 205–216. DOI: 10.1039/A801058G.

[79] M. C. McCarthy et al., "Laboratory and Astronomical Identification of the Negative Molecular Ion C6H-". In: *The Astrophysical Journal* 652.2 (2006), L141 –L144. DOI: 10.1086/510238. URL: http://dx.doi.org/10.1086/510238.

[80] S. Brünken et al., "Detection of the Carbon Chain Negative Ion C8H-in TMC-1". In: *The Astrophysical Journal* 664.1 (2007), pp. L43–L46. DOI: 10.1086/520703.

[81] M. A. Requena-Torres et al., "Organic Chemistry in the Dark Clouds L1448 and L183: A Unique Grain Mantle Composition". In: *The Astrochemical Jornal* 655.1 (Jan. 2007), pp. L37–L40. DOI: 10.1086/511677.

[82] A. Bacmann; V. Taquet; A. Faure; C. Kahane; C. Ceccarelli, "Detection of complex organic molecules in a prestellar core: a new challenge for astrochemical models". In: *Astronomy and Astrophysics* 541.L12 (May 2012). DOI: 10.1051/0004-6361/201219207.

[83] K. I. Öberg; R. T. Garrod; E. F. van Dishoeck; H. Linnartz, "Formation rates of complex organics in UV irradiated CH3OH-rich ices". In: *Astronomy and Astrophysics* 504.3 (July 2009), pp. 891 –913. DOI: 10.1051/0004-6361/200912559.

[84] J. E. Pineda; A. J. Maury; G. A. Fuller; L. Testi; D. García-Appadoo; A. B. Peck; E. Villard; S. A. Corder; T. A. van Kempen; J. L. Turner; K. Tachihara; W. Dent, "The first ALMA view of IRAS 16293-2422". In: *Astronomy and Astrophysics* 544.L7 (Aug. 2012), p. 6. DOI: 10.1051/0004-6361/201219589.

[85] R. Visser; L. E. Kristensen; S. Bruderer; E. F. van Dishoeck; G. J. Herczeg; C. Brinch; S. D. Doty; D. Harsono; M. G. Wolfire, "Modelling Herschel observations of hot molecular gas emission from embedded low-mass protostars". In: *Astronomy and Astrophysics* 537.A55 (Jan. 2012), p. 19. DOI: 10.1051/0004-6361/201117109.

[86] Alwyn Wootten, "The Duplicity of IRAS 16293-2422: A Protobinary Star?" In: *Astrophysical Journal* 337 (Feb. 1989), p. 858. DOI: 10.1086/167156.

[87] E. F. van Dishoeck J. K. Jørgensen F. L. Schöier, "Molecular freeze-out as a tracer of the thermal and dynamical evolution of pre- and protostellar cores". In: *Astronomy and Astrophysics* 435.1 (May 2005), pp. 177 –182. DOI: 10.1051/0004-6361:20042092.

[88] Nami Sakai et al., "Abundant Carbon-Chain Molecules toward the Low-Mass Protostar IRAS 04368+2557 in L1527". In: 672.1 (2008), pp. 371–381. DOI: 10.1086/523635. URL: http://dx.doi.org/10.1086/523635.

[89] Nami Sakai et al., "Long carbon-chain molecules and their anions in the starless core, LUPUS-1A". In: 718.2 (2010), pp. L49–L52. DOI: 10.1088/2041-8205/718/2/149.

[90] S. Cazaux et al., "The Hot Core around the Low-Mass Protostar IRAS 16293-2422: Scoundrels Rule!" In: 593.1 (2003), pp. L51–L55. DOI: 10.1086/378038. URL: http://dx.doi.org/10.1086/378038.

[91] Blake Geoffrey A.; Sutton E. C.; Masson C. R.; Phillips T. G., "Molecular Abundances in OMC-1: The Chemical Composition of Interstellar Molecular Clouds and the Influence of Massive Star Formation". In: *Astrophysical Journal* 315 (Apr. 1987), p. 621. DOI: 10.1086/165165.

[92] S. Bottinelli et al., "Complex Molecules in the Hot Core of the Low-Mass Protostar NGC 1333 IRAS 4A". In: 615.1 (2004), pp. 354–358. DOI: 10.1086/423952. URL: http://dx.doi.org/10.1086/423952.

[93] S. Bottinelli et al., "Near-Arcsecond Resolution Observations of the Hot Corino of the Solar-Type Protostar IRAS 16293-2422". In: 617.1 (2004), pp. L69–L72. DOI: 10.1086/426964.

[94] P. Székely; L. L. Kiss; R. Jackson; A. Derekas; B. Csák; K. Szatmáry, "RR Lyrae stars in the southern globular cluster NGC 362". In: *Astronomy and Astrophysics* 463.2 (Feb. 2007), pp. 589 –600. DOI: 10.1051/0004-6361:20066242.

[95] Nienke van der Marel, Lars E. Kristensen, and Ewine F. van Dishoeck, "Complex molecules toward low-mass protostars: the Serpens core". In: 740.1 (2011), p. 14. DOI: 10.1088/0004-637x/740/1/14.

[96] E. Caux; C. Kahane; A. Castets; A. Coutens; C. Ceccarelli; A. Bacmann; S. Bisschop; S. Bottinelli; C. Comito; F. P. Helmich; B. Lefloch; B. Parise; P. Schilke; A. G. G. M. Tielens; E. van Dishoeck; C. Vastel; V. Wakelam; A. Walters, "TIMASSS: the IRAS 16293-2422 millimeter and submillimeter spectral survey". In: *Astronomy and Astrophysics* 532.A23 (Aug. 2011), p. 41.

[97] J. K. Jørgensen; T. L. Bourke; Q. Nguyen Luong; S. Takakuwa, "Arcsecond resolution images of the chemical structure of the low-mass protostar IRAS 16293-2422". In: *Astronomy and Astrophysics* 534.A100 (Oct. 2011), p. 28.

[98] C. Codella; M. Benedettini; M. T. Beltrán; F. Gueth; S. Viti; R. Bachiller; M. Tafalla; S. Cabrit; A. Fuente; B. Lefloch, "Methyl cyanide as tracer of bow shocks in L1157-B1". In: *Astronomy and Astrophysics* 507.2 (Nov. 2009), pp. L25 –L28. DOI: DOI10.1051/0004-6361/200913340.

[99] R. Bachiller and M. Pérez Gutiérrez, "Shock Chemistry in the Young Bipolar Outflow L1157". In: 487.1 (1997), pp. L93–L96. DOI: 10.1086/310877. URL: http://dx.doi.org/10.1086/310877.

[100] C. Codella; B. Lefloch; C. Ceccarelli; J. Cernicharo; E. Caux; A. Lorenzani; S. Viti; P. Hily-Blant; B. Parise; S. Maret; B. Nisini; P. Caselli; S. Cabrit; L. Pagani; M. Benedettini; A. Boogert; F. Gueth; G. Melnick; D. Neufeld; S. Pacheco; M. Salez; K. Schuster; A. Bacmann; A. Baudry; T. Bell; E. A. Bergin; G. Blake; S. Bottinelli; A. Castets; C. Comito; A. Coutens; N. Crimier; C. Dominik; K. Demyk; P. Encrenaz; E. Falgarone; A. Fuente; M. Gerin; P. Goldsmith; F. Helmich; P. Hennebelle; Th. Henning; E. Herbst; T. Jacq; C. Kahane; M. Kama; A. Klotz; W. Langer; D. Lis; S. Lord; J. Pearson; T. Phillips; P. Saraceno; P. Schilke; X. Tielens; F. van der Tak; M. van der Wiel; C. Vastel; V. Wakelam; A. Walters; F. Wyrowski; H. Yorke; C. Borys; Y. Delorme; C. Kramer; B. Larsson; I. Mehdi; V. Ossenkopf; J. Stutzki, "The CHESS spectral survey of star forming regions: Peering into the protostellar shock L1157-B1". In: *Astronomy and Astrophysics* 518.L112 (July 2010), p. 5. DOI: 10.1051/0004-6361/201014582.

[101] Héctor G. Arce et al., "Complex Molecules in the L1157 Molecular Outflow". In: 681.1 (2008), pp. L21–L24. DOI: 10.1086/590110.

[102] C. Codella et al., "First detection of hydrogen chloride toward protostellar shocks". In: 744.2 (2011), p. 164. DOI: 10.1088/0004-637x/744/2/164.

[103] A Ratajczak et al., "The puzzling deuteration of methanol in low-to high-mass protostars". In: *Astronomy and Astrophysics* 528 (Apr. 2011). DOI: 10.1051/0004-6361/201016402.

[104] T. C. Peng et al., "Deuterated methanol in Orion BN/KL". In: *Astronomy and Astrophysics* 543 (July 2012). DOI: 10.1051/0004-6361/201118310.

[105] M. Wardle C. R. Braiding, "The Hall effect in star formation". In: *MNRAS* 422 (2012), pp. 261–281. DOI: 10.1111/j.1365-2966.2012.20601.x.

[106] Richard R. Mellon and Zhi-Yun Li, "Magnetic Braking and Protostellar Disk Formation: The Ideal MHD Limit". In: 681.2 (2008), pp. 1356–1376. DOI: 10.1086/587542.

[107] S. Fromang P. Hennebelle, "Magnetic processes in a collapsing dense core". In: *Astronomy and Astrophysics* 477.1 (Jan. 2008), pp. 9 –24. DOI: 10.1051/0004-6361:20078309.

[108] Tomoaki Matsumoto Masahiro N. Machida Shu-ichiro Inutsuka, "Effect of Magnetic Braking on the Circumstellar Disk Formation in a Strongly Magnetized Cloud". In: *PASJ* 63 (2011). DOI: 10.1093/pasj/63.3.555.

[109] A. Ciardi M. Joos P. Hennebelle, "Protostellar disk formation and transport of angular momentum during magnetized core collapse". In: *Astronomy and Astrophysics* 543.A128 (July 2012), p. 22. DOI: 10.1051/0004-6361/201118730.

[110] Laughlin Gregory; Bodenheimer Peter, "Nonaxisymmetric Evolution in Protostellar Disks". In: *Astrophysical Journal* 436 (Nov. 1994), p. 335. DOI: 10.1086/174909.

[111] Alan P. Boss, "Giant Planet Formation by Gravitational Instability". In: *Science* 276.5320 (June 1997), p. 1836. DOI: 10.1126/science.276.5320.1836.

[112] Aaron C. Boley, "The two modes of gas giant planet formation". In: 695.1 (2009), pp. L53–L57. DOI: 10.1088/0004-637x/695/1/l53.

[113] Brown David W.; Chandler Claire J; Carlstrom John E; Hills Richard E; Lay Oliver P, "A submillimetre survey for protostellar accretion discs using the JCMT-CSO interferometer". In: *Monthly Notices of the Royal Astronomical Society Journal* 319 (Nov. 2000), p. 154. DOI: 10.1046/j.1365-8711.2000.03805.x.

[114] Chandler Claire J.; Koerner David W.; Sargent Anneila I.; Wood Douglas O. S., "Dust Emission from Protostars: the Disk and Envelope of HH 24 MMS". In: 449.2 (1995). DOI: 10.1086/309644.

[115] Leslie W. Looney, Lee G. Mundy, and W. J. Welch, "Unveiling the Circumstellar Envelope and Disk: A Subarcsecond Survey of Circumstellar Structures". In: 529.1 (2000), pp. 477–498. DOI: 10.1086/308239.

[116] Jes K. Jorgensen et al., "PROSAC: A Submillimeter Array Survey of Low-Mass Protostars. I. Overview of Program: Envelopes, Disks, Outflows, and Hot Cores". In: 659.1 (2007), pp. 479–498. DOI: 10.1086/512230.

[117] Melissa L. Enoch et al., "Disk and envelope structure in Class 0 protostars. II. High-resolution millimetab". In: 195.2 (2011), p. 21. DOI: 10.1088/0067-0049/195/2/21.

[118] Minho Choi et al., "Ammonia Imaging of the Disks in the NGC 1333 IRAS 4A Protobinary System". In: 667.2 (2007), pp. L183–L186. DOI: 10.1086/522116.

[119] Jes K. Jørgensen and Ewine F. van Dishoeck, "Water vapor in the inner 25 AU of a young disk around a low-mass protostar". In: 710.1 (2010), pp. L72–L76. DOI: 10.1088/2041-8205/710/1/l72.

[120] Rodríguez Luis F.; Loinard Laurent; D'Alessio Paola; Wilner David J.; Ho Paul T. P., "IRAS 16293-2422B: A Compact, Possibly Isolated Protoplanetary Disk in a Class 0 Object". In: 621.2 (2005), pp. L133–L136. DOI: 10.1086/429223.

[121] Valentine Wakelam and Eric Herbst, "Polycyclic Aromatic Hydrocarbons in Dense Cloud Chemistry". In: 680.1 (2008), pp. 371–383. DOI: 10.1086/587734.

[122] John Ilee et al., "Chemistry in a gravitationally unstable protoplanetary disc". In: *Monthly Notices of The Royal Astronomical Society - MON NOTIC ROY ASTRON SOC* 417 (July 2011). DOI: 10.1111/j.1365-2966.2011.19455.x.

[123] Furuya Kenji; Aikawa Yuri; Tomida Kengo; Matsumoto Tomoaki; Saigo Kazuya; Tomisaka Kohji; Hersant Franck; Wakelam Valentine, "Chemistry in the first hydrostatic core stage by adopting three-dimensional radiation hydrodinamic simulations". In: 758.2 (2012), p. 86. DOI: 10.1088/0004-637x/758/2/86.

[124] Edwin Bergin et al., "A New Probe of the Planet-forming Region in T Tauri Disks". In: 614.2 (2004), pp. L133–L136. DOI: 10.1086/425865.

[125] Colette Salyk et al., "H2O and OH Gas in the Terrestrial Planet-forming Zones of Protoplanetary Disks". In: 676.1 (2008), pp. L49–L52. DOI: 10.1086/586894.

[126] Avi M. Mandell et al., "First detection of near-infrared line emission from organics in young circumstellar disks". In: 747.2 (2012), p. 92. DOI: 10.1088/0004-637x/747/2/92.

[127] A. Natta; T. Prusti; R. Neri; D. Wooden; V. P. Grinin; V. Mannings, "A reconsideration of disk properties in Herbig Ae stars". In: *Astronomy and Astrophysics* 371.1 (May 2001), pp. 186 –197. DOI: 10.1051/0004-6361:20010334.

[128] F. Lahuis et al., "Hot Organic Molecules toward a Young Low-Mass Star: A Look at Inner Disk Chemistry". In: 636.2 (2005), pp. L145–L148. DOI: 10.1086/500084. URL: http://dx.doi.org/10.1086/500084.

[129] C. Salyk et al., "A SPITZER Survey of mid-infrared molecular emission from protoplanetary disks. II. Correlations and local thermal equilibrium models". In: 731.2 (2011), p. 130. DOI: 10.1088/0004-637x/731/2/130.

[130] Karin I. Öberg et al., "The ionization fraction in the DM Tau protoplanetary disk". In: 743.2 (2011), p. 152. DOI: 10.1088/0004-637x/743/2/152.

[131] A. G. G. M. Tielens, *The Physics and Chemistry of the Interstellar Medium*. Cambridge University Press, Aug. 2005.

[132] I. Kamp, "Evolution of PAHs in Protoplanetary Disks". English. In: EAS Publications Series (Mar. 2011). Ed. by C Joblin and AGGM Tielens, pp. 271–283. DOI: 10.1051/eas/1146029.

[133] E. Habart; F. Boulanger; L. Verstraete; C. M. Walmsley; G. Pineau des Forêts, "Some empirical estimates of the H2 formation rate in photon-dominated regions". In: *Astronomy and Astrophysics* 414.2 (Feb. 2004), pp. 531 –544. DOI: 10.1051/0004-6361:20031659.

[134] J. Bouwman; A. L. Mattioda; H. Linnartz; L. J. Allamandola, "Photochemistry of polycyclic aromatic hydrocarbons in cosmic water ice". In: *Astronomy and Astrophysics* 525.A93 (Jan. 2011), p. 13. DOI: 10.1051/0004-6361/201015059.

[135] Anne Dutrey, Stephane Guilloteau, and Paul Ho, *Interferometric Spectroimaging of Molecular Gas in Protoplanetary Disks*. Jan. 2007.

[136] Chunhua; Ho Paul T. P.; Wilner David J.; Takakuwa Shigehisa; Hirano Naomi; Ohashi Nagayoshi; Bourke Tyler L.; Zhang Qizhou; Blake Geoffrey A.; Hogerheijde Michiel; Saito Masao; Choi Minho; Yang Ji Qi, "Imaging the Disk around TW Hydrae with the Submillimeter Array". In: 616.1 (2004), pp. L11–L14. DOI: 10.1086/421063.

[137] A. Dutrey, Stephane Guilloteau, and M. Guélin, "Chemistry of protosolar-like nebulae: The molecular content of the DM Tau and GG Tau disks". In: *Astronomy and Astrophysics* 317 (Jan. 1997), pp. L55–L58.

[138] G. J Zadelhoff et al., "Submillimeter lines from circumstellar disks around pre-main sequence stars". In: *Astronomy and Astrophysics* 377 (Aug. 2001). DOI: 10.1051/0004-6361:20011137.

[139] E. Chapillon; S. Guilloteau; A. Dutrey; V. Piétu; M. Guélin, "Chemistry in disks. VI. CN and HCN in protoplanetary disks". In: *Astronomy and Astrophysics* 537.A60 (Jan. 2012), p. 22. DOI: 10.1051/0004-6361/201116762.

[140] A. Dutrey; T. Henning; S. Guilloteau; D. Semenov; V. Piétu; K. Schreyer; A. Bacmann; R. Launhardt; J. Pety; F. Gueth, "Chemistry in disks. I. Deep search for N2H+ in the protoplanetary disks around LkCa 15, MWC 480, and DM Tauri". In: *Astronomy and Astrophysics* 464.2 (Mar. Volume, Number 2, March III 2007), pp. 615 –623. DOI: 10.1051/0004-6361:20065385.

[141] A. Fuente et al., "Molecular content of the circumstellar disk in AB Aur: First detection of SO in a circumstellar disk". In: *Astronomy and Astrophysics* 524 (Nov. 2010), p. 19. DOI: 10.1051/0004-6361/201014905.

[142] A. Dutrey; V. Wakelam; Y. Boehler; S. Guilloteau; F. Hersant; D. Semenov; E. Chapillon; T. Henning; V. Piétu; R. Launhardt; F. Gueth;K. Schreyer, "Chemistry in disks V. Sulfur-bearing molecules in the protoplanetary disks surrounding LkCa15, MWC480, DM Tauri, and GO Tauri". In: *Astronomy and Astrophysics* 535.A104 (2011), p. 8. DOI: 10.1051/0004-6361/201116931.

[143] E. F. van Dishoeck, W.-F. Thi, and G.-J. van Zadelhoff, "Detection of DCO+in a circumstellar disk". In: *Astronomy and Astrophysics* 400.1 (Feb. 2003), pp. L1–L4. ISSN: 1432-0746. DOI: 10.1051/0004-6361:20030091.

[144] C. Ceccarelli et al., "Detection of H2D+: Measuring the Midplane Degree of Ionization in the Disks of DM Tauri and TW Hydrae". In: 607.1 (2004), pp. L51–L54. DOI: 10.1086/421461. URL: http://dx.doi.org/10.1086/421461.

[145] C. Ceccarelli et al., "Discovery of Deuterated Water in a Young Protoplanetary Disk". In: 631.1 (2005), pp. L81–L84. DOI: 10.1086/497028.

[146] Edwige Chapillon et al., "Chemistry in disks. VII. First detection of HC3N in protoplanetary disks". In: *The Astrophysical Journal* 756.1 (Aug. 2012), p. 58. ISSN: 1538-4357. DOI: 10.1088/0004-637x/756/1/58.

[147] Alexander Dalgarno, "A Serendipitous Journey". In: *Annual Review of Astronomy and Astrophysics* 46 (2018), pp. 1–20. DOI: 10.1146/annurev.astro.46.060407.145216.

[148] J. M. GreenbergC. X. Mendoza-GómezV. Pirronello, *The Chemistry of Life's Origins*. Springer, Dordrecht, 1993. DOI: 10.1007/978-94-011-1936-8.

[149] S. Bari et al., "Photodissociation of protonated leucine-enkephalin in the VUV range of 8-40 eV". In: *The Journal of Chemical Physics* 134.2 (Nov. 2011), p. 024314. DOI: 10.1063/1.3515301.

[150] P. Theule; F. Borget; F. Mispelaer; G. Danger; F. Duvernay; J. C. Guillemin; T. Chiavassa, "Hydrogenation of solid hydrogen cyanide HCN and methanimine CH2NH at low temperature". In: *Annual Review of Astronomy and Astrophysics* 534.A64 (Oct. 2011), p. 6. DOI: 10.1051/0004-6361/201117494.

[151] A. Belloche; K. M. Menten; C. Comito; H. S. P. Müller; P. Schilke; J. Ott; S. Thorwirth; C. Hieret, "Detection of amino acetonitrile in Sgr B2(N)". In: *Astronomy and Astrophysics* 482.1 (Apr. 2008), pp. 179 –196. DOI: 10.1051/0004-6361:20079203.

[152] G. Danger; F. Borget; M. Chomat; F. Duvernay; P. Theulé; J.-C. Guillemin; L. Le Sergeant d'Hendecourt; T. Chiavassa, "Experimental investigation of aminoacetonitrile formation through the Strecker synthesis in astrophysical-like conditions: reactivity of methanimine (CH2NH), ammonia (NH3), and hydrogen cyanide (HCN)". In: *Astronomy and Astrophysics* 535.A47 (Nov. 2011), p. 9. DOI: 10.1051/0004-6361/201117602.

[153] Elsila Jamie E.; Dworkin Jason P.; Bernstein Max P.; Martin Mildred P.; Sandford Scott A., "Mechanisms of Amino Acid Formation in Interstellar Ice Analogs". In: *Astrophysical Journal* 660.1 (May 2007), pp. 911–918. DOI: 10.1086/513141.

[154] Stanley L. Miller, "A Production of Amino Acids Under Possible Primitive Earth Conditions". In: *Science* 117.3046 (May 1953), p. 528. DOI: 10.1126/science.117.3046.528.

[155] Albert Rimola, Mariona Sodupe, and Piero Ugliengo, "Deep-space glycine formation via Strecker-type reactions activated by ice water dust mantles. A computational approach". In: *Physical Chemistry Chemical Physics* 12.20 (2010), pp. 5285–5294. DOI: 10.1039/B923439J.

[156] Stephen P Walch et al., "On the reaction CH2O+NH3 to CH2NH+H2O". In: *Chemical Physics Letters* 333.1 (2001), pp. 6–11. DOI: 10.1016/S0009-2614(00)01341-5.

[157] Bossa J. B.; Theule P.; Duvernay F.; Chiavassa T., "NH2CH2OH thermal formation in interstellar ices contribution to the 5-8 µm region toward embedded protostar". In: 707.2 (2009), pp. 1524–1532. DOI: 10.1088/0004-637x/707/2/1524.

[158] Godfrey P.D.; Brown R.D.; Robinson B.J.; Sinclair M.W., "Discovery of Interstellar Methanimine (Formaldimine)". In: *Astrophysics Letters* 13 (Feb. 1973), p. 119.

[159] Dickens J.E.; Irvine W.M.; De Vries C.H.; Ohishi M., "Hydrogenation of interstellar molecules: a survey for methylenimine (CH2NH)". In: *Astrophysical Journal* 479 (1997), pp. 307–12. DOI: 10.1086/303884.

[160] Turner B.E.; Terzieva R.; Herbst Eric, "The Physics and Chemistry of Small Translucent Molecular Clouds. XII. More Complex Species Explainable by Gas-Phase Processes". In: *Astrophysical Journal* 518.2 (June 1999), pp. 699–732. DOI: 10.1086/307300.

[161] Salter C.J.; Ghosh T.; Catinella B.; Lebron M.; Lerner M.S.; Minchin R.; Momjian E., "The Arecibo ARP 220 Spectral Census. I. Discovery of the Pre-Biotic Molecule Methanimine and New Cm-Wavelength Transitions of Other Molecules". In: *Astrophysical Journal* 136.1 (July 2008), pp. 389–399. DOI: 10.1088/0004-6256/136/1/389.

[162] S. Martin et al., "A 2 Millimeter Spectral Line Survey of the Starburst Galaxy NGC 253". In: 164.2 (2006), pp. 450–476. DOI: 10.1086/503297.

[163] Kawaguchi K.; Ohishi M.; Ishikawa S.-I.; Kaifu N., "Detection of isocyanoacetylene HCCNC in TMC-1". In: *Astrophysical Journal* 386 (Feb. 1992), pp. L51–L53. DOI: 10.1086/186290.

[164] F. J. Lovas et al., "Detection of Ketenimine (CH2CNH) in Sagittarius B2(N) Hot Cores". In: 645.2 (2006), pp. L137–L140. DOI: 10.1086/506324. URL: http://dx.doi.org/10.1086/506324.

[165] David M. Mehringer et al., "Detection of Vibrationally Excited Ethyl Cyanide in the Interstellar Medium". In: 608.1 (2004), pp. 306–313. DOI: 10.1086/386357.

[166] Gardner F. F.; Winnewisser G., "The detection of interstellar vinyl cyanide acrylonitrile". In: *Astrophysical Journal* 195 (Feb. 1975), pp. L127–L130. DOI: 10.1016/j.heliyon.2019.e02384.

[167] B. E. Turner, "Detection of Interstellar Cyanoacetylene". In: *Astrophysical Journal* 163 (Jan. 1971), p. L35. DOI: 10.1086/180662.

[168] A. C. P. Alves, J. Christoffersen, and J. M. Hollas, "Near ultra-violet spectra of the s-trans and a second rotamer of acrolein vapour". In: *Molecular Physics* 20.4 (Jan. 1971), pp. 625–644. DOI: 10.1080/00268977100100601.

[169] Robert E. Penn, "Microwave Spectrum of 2-Propene-1-imine, CH=CHCH=NH". In: *Journal of Molecular Spectroscopy* 69 (1978), pp. 373–382. DOI: 10.1016/0022-2852(78)90230-8.

[170] Ronald D. BROWN; Peter D. GODFREY; David A. WINKLER, "Hyperfine interactions in the microwave spectrum of 2-Propen-1-imine (Vinylamine)". In: *Chemical Physics* 59 (1981), pp. 243–24. DOI: 10.1016/0301-0104(81)85167-1.

[171] Eugene Feenberg; G. E. Pake, *Notes on the quantum theory of angular momentum*. Cambridge, Mass., Addison-Wesley Pub. Co., 1953.

[172] Walter Gordy; Robert L. Cook, *Microwave molecular spectra*. John Wiley & Sons, 1984.

[173] Gilbert W. King; Arthur D. Little; R. M. Hainer; Paul C. Cross, "The Asymmetric Rotor I. Calculation and Symmetry Classification of Energy Levels". In: *J. Chem. Phys.* 11.27 (1943). DOI: 10.1063/1.1723778.

[174] Brati Sankar Ray, "About the eigenvalues of the asymmetric gyro". In: *Physics* 78.1-2 (May 1932), pp. 74–91. DOI: https://doi.org/10.1007/BF01342264.

[175] S. C. Wang, "On the Asymmetrical Top in Quantum Mechanics". In: *Phys. Rev.* 34 (2 1929), pp. 243–252. DOI: 10.1103/PhysRev.34.243.

[176] E. Bright Wilson, "The Effect of Rotational Distortion on the Thermodynamic Properties of Water and Other Polyatomic Molecules". In: *The Journal of Chemical Physics* 4.8 (1936), pp. 526–528. DOI: 10.1063/1.1749895.

[177] E. Bright Wilson and J. B. Howard, "The Vibration-Rotation Energy Levels of Polyatomic Molecules I. Mathematical Theory of Semirigid Asymmetrical Top Molecules". In: *The Journal of Chemical Physics* 4.4 (1936), pp. 260–268. DOI: 10.1063/1.1749833.

[178] Byron T. Darling and David M. Dennison, "The Water Vapor Molecule". In: *Physical Review* 57.2 (Jan. 1940), pp. 128–139. DOI: 10.1103/PhysRev.57.128.

[179] James K. G. Watson, "Determination of Centrifugal Distortion Coefficients of Asymmetric-Top Molecules". In: *The Journal of Chemical Physics* 46.5 (1967), pp. 1935–1949. DOI: 10.1063/1.1840957.

[180] James KG Watson, "Aspects of quartic and sextic centrifugal effects on rotational energy levels". In: *Vibrational spectra and structure* 6 (1977), pp. 1–89.

[181] James K. G. Watson, "Determination of Centrifugal-Distortion Coefficients of Asymmetric-Top Molecules. II. Dreizler, Dendl, and Rudolph's Results". In: *The Journal of Chemical Physics* 48.1 (1968), pp. 181–185. DOI: 10.1063/1.1667898.

[182] H.B.G. Casimir, *On the Interaction between Atomic Nuclei and Electrons*. Springer Netherlands, 2013. ISBN: 9789401760676. URL: https://books.google.it/books?id=KE7zCAAAQBAJ.

[183] Jr. L. Pauling; E. B. Wilson; Edgar B. Wilson, *Introduction to Quantum Mechanics: With Applications to Chemistry*. McGraw-Hill book Company, 1935.

[184] J. H. Van Vleck and V. F. Weisskopf, "On the Shape of Collision-Broadened Lines". In: *Rev. Mod. Phys.* 17 (2-3 1945), pp. 227–236. DOI: 10.1103/RevModPhys.17.227.

[185] L. S. Rothman et al., "AFGL trace gas compilation". In: *Applied Optics* 17.4 (1978), pp. 507–507. DOI: 10.1364/AO.17.000507.

[186] *Molecular Spectroscopy Jet Propululsion Laboratory*. URL: https://spec.jpl.nasa.gov/.

[187] Brian J. Drouin, "Practical uses of SPFIT". In: *Journal of Molecular Spectroscopy* 340 (2017), pp. 1–15. DOI: 10.1016/j.jms.2017.07.009.

[188] Stewart E. Novick, "A beginner's guide to Pickett's spcat/spfit". In: *Journal of Molecular Spectroscopy* 329 (2016), pp. 1–7. DOI: 10.1016/j.jms.2016.08.015.

[189] Novick Stewart E., *Herb and my Notes 4a.pdf*. URL: https://wesfiles.wesleyan.edu/home/snovick/Pickett%20Handout/SPCAT-SPFIT/.

[190] L. Bizzocchi; V. Lattanzi; J. Laas; S. Spezzano; B. M. Giuliano; D. Prudenzano; C. Endres; O. Sipilä; P. Caselli, "Accurate sub-millimetre rest frequencies for HOCO+ and DOCO+ ions". In: *Astronomy and Astrophysics* 602.A34 (June 2017), p. 7. DOI: 10.1051/0004-6361/201730638.

[191] Alves; Christoffersen; Hollas, "Near ultraviolet spectra of the s trans and a second rotamer of acrolein vapour". In: *Molecular Physics* 20.4 (Jan. 1971), pp. 625–644. DOI: 10.1080/00268977100100601.

[192] V. Haugen; M. Traeteberg. In: *Acta Chem. Scalld* 20.1726 (1966).

[193] G. N. Currie; D. A. Ramsay, "The 4875 Band System of cis Glyoxal". In: *Canadian Journal of Physics* 49.3 (1971), pp. 317–322. DOI: https://doi.org/10.1139/p71-037.

[194] Dore Luca, "Using Fast Fourier Transform to compute the line shape of frequency-modulated spectral profiles". In: *Journal of Molecular Spectroscopy* 221.1 (2003), pp. 93–98. DOI: 10.1016/S0022-2852(03)00203-0.

[195] NASA, *Stars*. URL: https://science.nasa.gov/astrophysics/focus-areas/how-do-stars-form-and-evolve.

[196] George Wallerstein et al., "Synthesis of the elements in stars: forty years of progress". In: *Reviews of Modern Physics* 69.4 (Oct. 1997), pp. 995–1084. DOI: 10.1103/RevModPhys.69.995.

[197] B.W. Ostlie D.A.; Carroll, *An Introduction to Modern Stellar Astrophysics*. ISBN 0-8053-0348-0. Addison Wesley, 2007.

[198] Michael Woolfson, "The origin and evolution of the solar system, Issue 1, February 2000, Pages , https://doi.org/10.1046/j.1468-4004.2000.00012.x". In: *Astronomy and Geophysics* 41.1 (Feb. 2000), pp. 1.12–1.19. DOI: 10.1046/j.1468-4004.2000.00012.x.

[199] Falk S. W.; Lattimer J. M.; Margolis S. H., "Are supernovae sources of presolar grains". In: *Nature* 270 (Dec. 1977), pp. 700, 701. DOI: 10.1038/270700a0.